Extreme sea levels around the northwestern Iberian Peninsula and their link to atmospheric forcing

Master's thesis

Faculty of Science

University of Bern

presented by

Alexander Nauels

2009

Supervisor:

Prof. Dr. Jürg Luterbacher

Institute of Geography and

Department of Geography, Justus-Liebig University, Giessen, Germany

Co-Supervisor:

Dr. Elena Xoplaki

Institute of Geography and Oeschger Centre for Climate Change Research

Advisor:

Prof. Dr. Michael Tsimplis

National Oceanography Centre, Southampton, United Kingdom

Extreme sea levels around the northwestern Iberian Peninsula and their link to atmospheric forcing

Master's thesis

Faculty of Science

University of Bern

presented by

Alexander Nauels

2009

Supervisor:

Prof. Dr. Jürg Luterbacher

Institute of Geography and

Department of Geography, Justus-Liebig University, Giessen, Germany

Co-Supervisor:

Dr. Elena Xoplaki

Institute of Geography and Oeschger Centre for Climate Change Research

Advisor:

Prof. Dr. Michael Tsimplis

National Oceanography Centre, Southampton, United Kingdom

When the winds of change blow, some people build walls and others build windmills.
Chinese proverb

For my father

Abstract

The danger of coastal flooding is primarily linked to regional extreme sea levels, thus single events superimposed on the mean sea level trend. This study aims to contribute to a better understanding of the link between extreme sea levels at the three northwestern Iberian tide gauge stations Coruna, Santander and Vigo and the large-scale atmospheric circulation over the observation period 1948-2001. The 10 largest surge events for each winter half year are extracted from quality-checked, hourly tidal residual time series for detailed analyses and the detection of potential trends. The long term mean surge heights for Vigo and Coruna show values of approximately 40 cm; around 35 cm can be observed for the long term surge mean at Santander. With a tidal residual value of 88.02 cm, the highest surge of all three stations has been recorded at Vigo in 1979. There is no evidence indicating a significant change in the extreme sea level intensity around the northwestern Iberian Peninsula over the entire observation period. Return values are calculated using a modified Peak over Threshold approach. Highest sea levels have to be expected for the coasts around Vigo with 100-year return levels of maximum 3 m above the mean sea level. For each extreme surge the corresponding large-scale sea level pressure (SLP) and wind fields are derived from the NCEP/NCAR reanalysis. Composite analyses are presented. Strong negative SLP anomalies and onshore winds prove to be the main atmospheric surge forcing factors at the selected stations. In order to detect predominant atmospheric circulation patterns linked to extreme surges in the study area, corresponding large-scale SLP field have been subject to a modified clustering process. The Greenland Anticyclone and Blocking type circulation patterns are found to prevail for extreme surges around the northwestern Iberian Peninsula. SLP outputs of the ECHAM5-OM1 atmosphere-ocean general circulation model (AOGCM) have been analyzed to detect future variations in cyclonicity with the intention to infer future changes in extreme sea levels around the study area. Storm track anomalies based on SLP for A1B and A2 scenario runs (2071-2100) and the 20C control run (1961-1990) indicate a changing cyclonicity in the Northern Atlantic region with increasing synoptic wave activity over the northern North Atlantic west of Ireland and decreasing cyclonicity for the area under investigation. Assuming a proportionality to cyclonicity, also a decrease in extreme sea levels might be observable by the end of the 21st century around the northwestern Iberian Peninsula. General aspects regarding the

coastal vulnerability of the region by the end of the 21st century are presented based on the evolution of the regional mean sea level and potentially hazardous atmospheric forcings. Although atmospherically induced surges are supposed to decrease for the study area in the future, an enhanced coastal vulnerability can be expected around the northwestern Iberian Peninsula due to the projected, continuing, global mean sea level rise. The analysis of past extreme sea levels and the potential future evolution of surges in the study area accounts for a more comprehensive picture of underlying forcing mechanisms and related potential future coastal threats. Further research would be useful, especially regarding the detection of local surge forcing factors and methodologies to improve the assessment of the future extreme sea level evolution in the study area considering ongoing anthropogenic climate change.

Zusammenfassung

Überflutungsrisiken im Zusammenhang mit global steigenden Meeresspiegeln sind primär an regionale Meeresspiegelextrema gebunden, d.h. an Einzelereignisse die den Trend des mittleren Meerespiegels überlagern. Mit dieser Arbeit soll ein Beitrag zum besseren Verständnis der Verbindung zwischen extremen Meeresspiegeln und der grossskaligen atmosphärischen Zirkulation im Gebiet der nordwestlichen Iberischen Halbinsel geleistet werden. Dazu wurden Meerespiegelmessungen der drei Pegelstationen Santander, Coruna und Vigo über den Beobachtungszeitraum 1948-2001 untersucht. Für eine detaillierte Analyse und zur Feststellung etwaiger Trends im Extrembereich, wurden die zehn höchsten Ereignisse pro Winterhalbjahr von den jeweils überprüften, stündlichen Pegelstandsmessungen extrahiert. Die Langzeitmittel extremer Meeresspiegel für Coruna und Vigo belaufen sich auf ca. 40 cm; ungefähr 35 cm wurden für Santander registriert. Mit einem Tiden Residuum von 88.02 cm verzeichnete Vigo im Jahr 1979 den höchsten Wert aller Stationen zwischen 1948 und 2001. Über den gesamten Beobachtungszeitraum liegen keine stichhaltigen Hinweise bezüglich einer signifikanten Änderung der Intensität extremer Meeresspiegel im Untersuchungsgebiet vor. Return Values wurden anhand einer modifizierten Peak Over Threshold Methode berechnet. Im Untersuchungsgebiet ist mit einem Maximalpegel von ca. 3 m über dem mittleren Meerespiegel für ein hundertjähriges Ereignis zu rechnen. Als Datengrundlage für die zu jedem extremen Pegelstand gehörigen grossskaligen Bodendruck- und Windfelder wurde der NCEP/NCAR Reanalysis Datensatz ausgewählt. Komposit Analysen der Druck- und Windfelder werden präsentiert. Starke negative Bodendruckanomalien sowie auflandige Winde können dabei als die dominierenden atmosphärischen Einflussfaktoren identifiziert werden. Um Aussagen über vorherrschende Zirkulationsmuster zum Zeitpunkt der aufgezeichneten Extremereignisse treffen zu können, sind die relevanten Bodendruckfelder zusätzlich einer modifizierten Clusteranalyse unterzogen worden. Die geographisch nah beieinander liegenden Stationen weisen zum Zeitpunkt der aufgezeichneten extremen Pegelstände ähnliche Bodendruckfelder auf. Für die nordwestliche Iberische Halbinsel können die Zirkulationsmuster Greenland Anticyclone und Blocking als vorherrschende, für extreme Meeresspiegel relevante, atmosphärische Zirkulationsmuster identifiziert werden. Um auf eine, sich in Zukunft potentiell ändernde Sturmhäu-

figkeit und -intensität im Untersuchungsgebiet rückschliessen zu können, wurden Ausgabewerte von mittlerem Bodendruck (SLP) des Atmosphere-Ocean General Circulation Klimamodells (AOGCM) ECHAM5-OM1 untersucht. Basierend auf SLP Werten der Modelloutputs für die IPCC Szenarien A1B und A2 (2071-2100) sowie für das Referenzszenario 20C (1961-1990) liefern berechnete Storm Track Anomalien Hinweise auf eine zunehmende synoptische Wellenaktivität über dem nördlichen Nordatlantik westlich von Irland und eine abnehmende Zyklonizität im Untersuchungsgebiet selbst. Eine sich wandelnde Zyklonizität dient dabei auch als Indikator für sich proportional verändernde, atmosphärisch induzierte Meeresspiegelextrema. Zusätzlich wurde, basierend auf der potentiellen Entwicklung eines andauernden regionalen Meeresspiegelanstieges und atmosphärisch induzierter extremer Meeresspiegel, eine erste Einschätzung der zukünftigen Vulnerabilität der betroffenen Küsten vorgenommen. Obwohl davon ausgegangen werden kann, dass die Anzahl der Meerespiegelextrema mit atmophärischem Ursprung gegen Ende des 21. Jahrhunderts abnehmen wird, kann für die nordwestliche Iberische Halbinsel eine erhöhte Gefährdung anfälliger Küstenregionen aufgrund des zu erwartenden globalen Meeresspiegelanstieges angenommen werden. Die vorliegende Untersuchung trägt zu einem umfassenderen Bild hinsichtlich der zugrundezulegenden Auslösemechanismen extremer Meeresspiegel sowie der mit extremen Pegelständen verbundenen, möglichen, zukünftigen Gefährdung der betroffenen Küsten im Untersuchungsgebiet bei. Weiterführende Untersuchungen wären wünschenswert, besonders hinsichtlich der Erfassung lokaler Ursachen für aussergewöhnlich hohe Tiden Residuen sowie alternativer Methoden für die Abschätzung der zukünftigen Entwicklung extremer Meeresspiegel im Gebiet der nordwestlichen Iberischen Halbinsel unter Berücksichtigung eines anhaltenden anthropogenen Klimawandels.

Acknowledgements

First of all, I would like to thank Prof. Dr. Jürg Luterbacher and Dr. Elena Xoplaki for the perfect supervision of my thesis. They permanently assisted and supported me not only regarding the topic itself and the numerous questions which arose from my side but they were also always cultivating a very personal and friendly relationship no matter how stressful the circumstances were. I am very happy and thankful to have participated in the European Geosciences Union 2009 at Vienna. The attendance of the conference would not have been possible without the absolute support and motivation of Elena and Jürg in a time where not everything was running smoothly. I also have to thank Prof. Dr. Michael Tsimplis and his group from the National Oceanography Centre in Southampton as well as Dr. Marta Marcos for providing me with the tide gauge records used in this work. Thanks also to Uwe Ulbrich and his research group from the Freie Universität Berlin for sending me SLP outputs and storm track data from the ECHAM5-OM1 climate model. Additionally, I would like to thank the Studienstiftung des deutschen Volkes for the generous scholarships which took a lot of financial pressure away from me.

For the successful completion of the first serious research work not only the supervision but also the working environment plays a crucial role. The Climate and Meteorology Research Group (KLIMET) headed by Prof. Dr. Heinz Wanner as well as the Remote Sensing Group of Dr. Stefan Wunderle and the whole 5th floor of the Institute of Geography will be hard to beat concerning the sense of well being, collegiality and fun at work. Especially I would like to thank Dr. Marcel Küttel for his help and patience regarding all my questions. Without him I would perhaps be still searching for the right clustering approach today. Thanks also to Andrea Toreti for the kind statistical advice especially concerning the dePOT extreme value analysis and to Dr. in spe Franz G. Kuglitsch for his undestroyable positivity and the very good time we have spent, especially in Vienna. Vergelt's Gott! Wiederluege miteinand!

When I came to Bern two years ago, I didn't expect my studies at and around the Graduate School of Climate Science to be that great and convenient. This is mainly due to the friends I made here in Switzerland and old friends who came from far away to see if I am still alive. Thanks to the unbeatable Bernese Climate Guerilla, to Beni 'Le grand

Stuckateur', Phillippe 'Illip aka Pipo Posi Rhymes', Flavio 'Arctic Flav' and Anil 'The Turkish Lifesaver'. Thanks to my very good friend Silvan and Naomi for always making me feel at home. Matthias, Bene, Ferdi and Martin never stopped keeping an eye on me, no matter where they were. Merci for that. For the glass of wine, the good chat, the cosy atmosphere and the staying with me at our beloved Depotstrasse 22, a big thanks also to Anna. There are many more who truly deserve to be mentioned at this point but who will hopefully forgive me for stopping here.

Above all I want to thank my mother for all what she has done for me and for never stopping to endure whatever came our way. Without her infinite support and her trust none of this would have been possible. Finally, I want to express my gratitude to my father who has spent twenty years in order to prepare me to find my own way.

Contents

List of Figures

List of Tables

Abbreviations

3DVAR	Three-dimensional Variational Scheme Cast
AR	Atlantic Ridge type WR
BL	Blocking type WR
AGCM	Atmosphere General Circulation Model
AOGCM	Atmosphere-Ocean General Circulation Model
CDAS	Climate Data Assimilation System
CDO	Climate Data Operators
COLA	Center for Ocean-Land-Atmosphere Studies
dePOT	Declustered Peak over Threshold
EBC	Eastern Boundary Current
ECHAM5	Most recent version of AGCM models developed at the MPIM
ECHAM5-OM1	Coupled state-of-the-art AOGCM
ECMWF	European Centre for Medium Range Weather Forecasts
ECV	Explained Cluster Variance
ENACW	Eastern North Atlantic Central Water
EOF	Empirical Orthogonal Function
ESEAS	European Sea Level Service
GA	Greenland Anticyclone type WR
GrADS	Grid Analysis and Display System
GEV	General Extreme Value distribution
GPD	General Pareto Distribution
GTECCA	Global Tropical and Extratropical Cyclone Climatic Atlas
HOPE	Hamburg Ocean Primitive Equation model
IB	Inverse Barometer effect
IPCC	Intergovernmental Panel on Climate Change
MK	Mann-Kendall trend test
MLE	Maximum Likelihood Estimation
MPI-OM	Ocean General Circulation Model developed in Hamburg
MPIM	Max Planck Institute for Meteorology

MRLP	Mean Residual Life Plot
MSL	Mean Sea Level
NAE	North Atlantic European sector
NAO	North Atlantic Oscillation
NCAR	National Centre for Atmospheric Research
NCDC	National Climatic Data Center of the NOAA
NCEP	National Centres of Environmental Prediction
NH	Northern Hemisphere
NOAA	National Oceanic and Atmospheric Administration
ONDJFM	October to March, extended winter season
PAM	Partitioning around Medoids
PCA	Principal Component Analysis
SANDRA	Simulated Annealing Diversified Randomization clustering technique
SLP	Sea Level Pressure
SRES	Special Report Emission Scenario
SST	Sea Surface Temperature
TIROS	Television Infrared Observation Satellite
TOVS	Television Operational Vertical Sounder
TSS	Total Sum of Squares
UTC	Coordinated Universal Time
WBL	West Blocking type WR
WR	Weather Regime
WSS	Within Cluster Sum of Squares
ZO	Zonal type WR

Chapter 1

Introduction

As an effect of global climate change, oceans are warming worldwide (Bindoff et al. 2007). Numerous studies of past climate change have clearly pointed out that oceans have interacted with global climate and its variability in a fundamental way (IPCC 2007). An ongoing increase in global mean temperature due to increased anthropogenic carbon emissions not only affects the oceans' key role as heat storage and carbon sink but also impinges on the sea level, which responds notably to a temperature rise (Bindoff et al. 2007). A changing sea level has to be considered as a highly relevant factor for human societies, most of which are located in coastal areas (Nicholls et al. 2007).

Globally, two major factors contribute to an increase in sea level: 1.) Thermal expansion of the ocean water masses and 2.) Freshwater input from melting continental ice masses (Bindoff et al. 2007). The rate of change is geographically non-uniform and not linear (see Figure 1.1). In addition to the global forcings, local and regional factors of oceanic, atmospheric or land origin also affect sea level on a local scale (e.g. Tsimplis et al. 2006; Bindoff et al. 2007). From the end of the last ice age until a phase of sea level stabilization 2000 to 3000 years ago the global sea level rose by 120 m due to deglaciation processes of inland ice-masses (Bindoff et al. 2007). Since the beginning of instrumental sea level measurements in the nineteenth century, an ongoing global mean sea level rise can be observed (Bindoff et al. 2007 and references therein). Best estimates for the rate of change in the twentieth century assume a global increase of around +1.7 mm per year (Holgate and Woodworth 2004; Bindoff et al. 2007). Satellite measurements have provided a better accuracy since the 1990s. This data indicate a global sea level rise of at least 3 mm per year for the period 1993-2003 (Cazenave and Nerem 2004; Bindoff et al. 2007). For the global sea level, calculations based on the IPCC Special Report Emission Scenarios (SRES) yield a rise of 0.18 to 0.76 m above the level of the 1990s by the end of the 21st century (IPCC 2007). The wide range of model outputs can be mainly explained by the varying projected surface temperature changes and uncertainties regarding the quantification of water masses

added to the oceans through inland ice sheet melting, especially in Greenland (Bindoff et al. 2007). Rahmstorf (2007) applied a semi-empirical approach projecting a global sea level rise of 0.5 to 1.4 m by the end of the 21st century. According to Siddall et al. (2009) the range of global sea level rise could be larger than the latest IPCC projections; their models predict a global mean sea level rise of 0.07 to 0.82 m by 2100 depending on the constraints of the different SRES.

Several studies dealing with coastal management and process studies have pointed out that ongoing global warming will result in increased coastal vulnerability (e.g. Klein et al. 1998; Nicholls and Mimura 1998; Nicholls et al. 2007). If the potential threat of an ongoing sea level rise is to be analyzed for low-lying coastal areas there is a variety of aspects which have to be included in the assessment. According to Betts et al. (2004) the sensitivity of a coastal system is assessable through its susceptibility and resilience. Susceptibility is a measure of the physical forcing on a coast as a function of sea level change over different temporal scales; resilience accounts for the ability of the coastal system to absorb the incident forcing and return to the pre-forcing state (Betts et al. 2004). The long-term risk of flooding is expected to increase through a loss in land elevation due to an ongoing global sea level rise (Pirazzoli 2000). This effect of increasing coastal susceptibility would be enhanced by an acceleration of the global sea level rise which is predicted by state-of-the-art climate models (Nicholls et al. 2007). Low-lying coastal areas and islands, e.g. the pacific archipelagos, are already facing an altered risk of flooding caused by rising sea levels (Nicholls et al. 2007).

Dealing with increasing coastal flood risks through rising sea levels and as a stimulus for the work at hand it is very important to stress that the danger of flooding is primarily linked to regional extreme sea levels, meaning single events superimposed on the mean sea level trend. Coastal flooding does not appear gradually and in line with a mean sea level rise but it is rather connected to major storms which produce overwash and erosion phenomena at the affected coasts (Pirazzoli et al. 2006). This aspect clearly pertains to the above mentioned coastal resilience measure (Betts et al. 2004). The majority of extreme sea levels worldwide are caused by tropical or extra-tropical cyclonic activity (Bindoff et al. 2007). Thus, the single surge events investigated in this work, generally defined as the measurable difference between observed sea level and local tidal signal, are mainly the response of sea level to meteorological forcings, namely atmospheric pressure and winds (Pirazzoli 2000). Besides storm surges which represent the most prominent cause for sea level anomalies due to atmospheric forcing, extreme sea levels can also be the result of so-called 'meteo-tsunamis' generated on a local scale by strong small-scale atmospheric disturbances (pressure jumps, atmospheric waves) in connection with specific resonance properties of the affected region (e.g. Monserrat et al. 2006). The danger of coastal flooding is particularly high with a surge taking place at high tide. Therefore the local

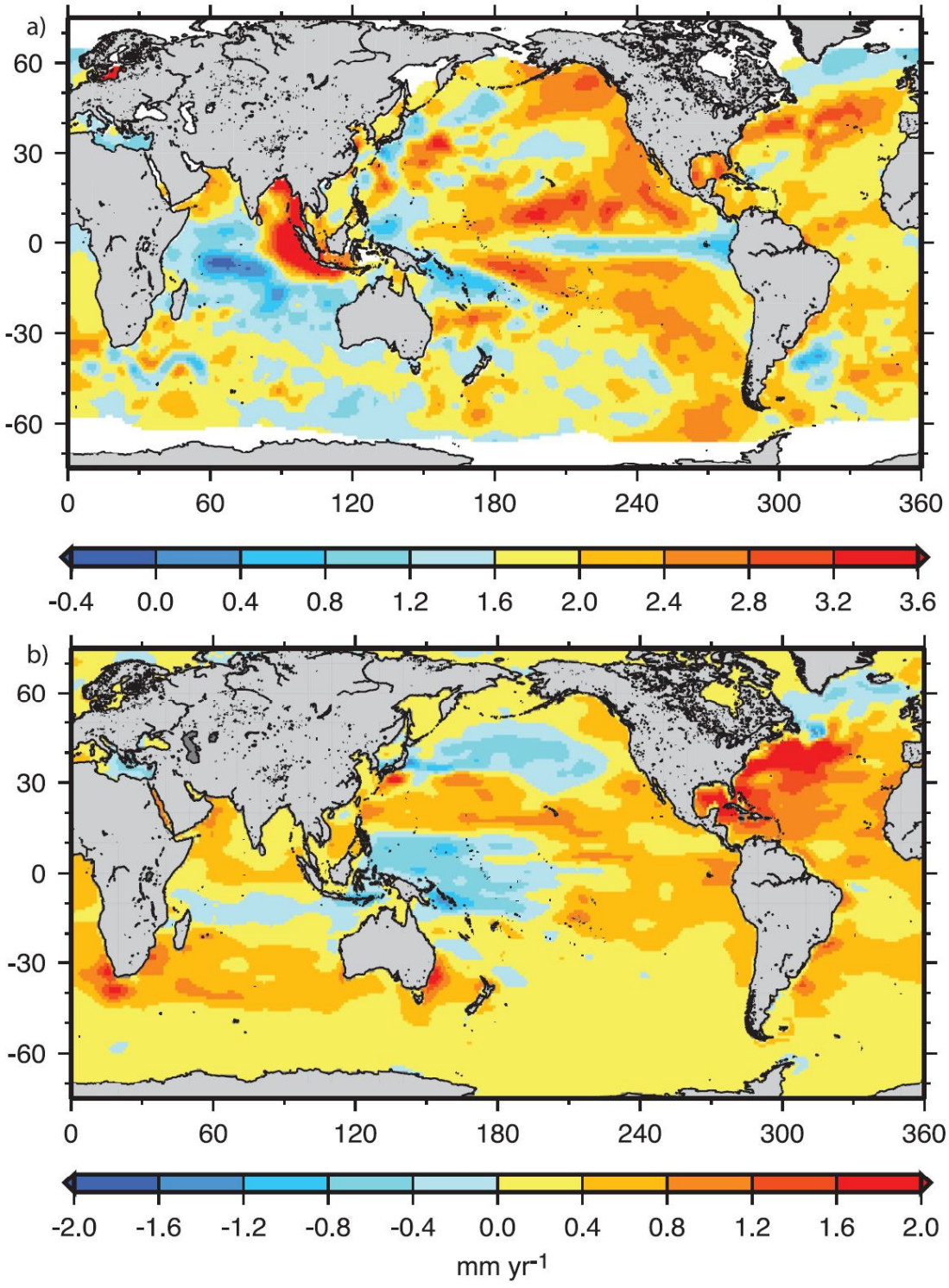

Figure 1.1: *Geographic distribution of long-term linear trends in (a) mean sea level (mm* yr^{-1}*) for 1955 to 2003 based on past sea level reconstructions with tide gauges and altimetry data and (b) thermal expansion (mm* yr^{-1}*) for 1955 to 2003 (Bindoff et al. 2007).*

tidal signal is of great importance as a high tide would amplify the atmospheric effects in macrotidal areas (Bindoff et al. 2007).

If a proper risk assessment of a specific coastal region should be carried out at some point, a sufficiently high spatial resolution has to be applied. Furthermore, the temporal resolution of the available dataset plays a crucial role. The higher the temporal resolution, the more distinct the conclusions that can be drawn with respect to single atmospheric forcing events. A comprehensive picture of the consequences of extreme sea levels and related potential threats for a specific coastal region can only be achieved if the temporal evolution of the mean sea level height plus the tidal residual signal will be analyzed together with a potential change in regional storminess. Tide gauge records provide information about the temporal evolution and magnitude of observed extreme sea levels and can therefore serve as an indicator of potentially dangerous sea level high stands.

1.1 Cyclonicity and surges - towards a regional focus

There is scientific agreement on the dominant forcing of sea level variability on timescales less than one year which can be attributed to atmospheric variations (Tsimplis and Josey 2001; Trigo and Davies 2002; Wakelin et al. 2003; Tsimplis et al. 2005).

As stated above, the decrease in atmospheric pressure caused by pervading perturbations is one of the most important forcing factors of extreme sea levels besides strong onshore winds which pile up water against the coasts. High extreme sea levels are strongly correlated with a local atmospheric pressure decrease and cyclonic activity (Tsimplis et al. 2006). The pressure drop causes the water column to rise in order to achieve hydrostatic balance of the water plus air column (e.g. Pirazzoli 2000). A pressure decrease of 1 hPa is reported to yield around 1 cm increase in local sea level; a phenomenon which is referred to as the Inverse Barometer (IB) effect (e.g. Ullmann et al. 2008). Lozano et al. (2004) have pointed out that the significance of coastal storminess has also to be linked to wind wave action: Deep water wave heights may reach values of more than 20 m (Hmax) under severe storm conditions around the exposed western coasts of Europe; In the more sheltered seas, the waves may still be able to reach Hmax values of 8 to 15 m which can be considered as a highly relevant factor for coastal protection.

On longer than seasonal timescales, changing climatic conditions not only affect oceanic thermal expansion and freshwater input but they also feedback on oceanic circulation patterns by causing temperature and salinity variations (e.g. Bindoff et al. 2007). Modified circulation patterns can also have an effect on regional sea level and on sea level anomalies (Vigo et al. 2005). Although this phenomenon is of great importance regarding the analysis of sea level anomaly trends which can also feedback on extreme sea levels (Tsimplis

et al. 2006), in the work at hand this aspect will be restricted to a short overview of the oceanographic properties of the study area in Section 1.1.3.

1.1.1 North Atlantic large-scale circulation and storminess

The Northern Hemispheric mid-latitudes are characterized by major atmospheric eddies and the alternation of migratory low pressure systems and anticyclones, also determining the climate of the Atlantic seaboard of Europe (Betts et al. 2004). According to Betts et al. (2004) the sea level pressure (SLP) over the North Atlantic Ocean shows a 'tripartite zonation' of subpolar low pressure, subtropical high pressure and equatorial trough: In winter, minimum seasonal mean SLP values of <1000 hPa are observable for the area southwest of Iceland as a result of depressions travelling eastwards and reaching their maximum intensities in this region; SLP increases to the south, reaching values of around 1015 hPa in the vicinity of Brest, France; The Azores anticyclonic field yields winter mean values of >1020 hPa. In general, this large-scale mean surface pressure pattern favors a dominant west to southwest airflow over the central North Atlantic Ocean in winter. For the North Atlantic sector, cyclones which advect precipitation and storms towards Western Europe principally originate in the western North Atlantic Ocean Basin (Betts et al. 2004). In general, mid-latitude winters show predominant lower atmospheric pressure and potentially more storminess than in the summer months (e.g. Barnston and Livezey 1987). Previous works on North Atlantic storm patterns detected a notable degree of interannual variability regarding the occurrence, location and intensity of storms hitting the western European coasts (e.g. Hayden 1981; Dolan et al. 1988; Schmith et al. 1998 and Dawson et al. 2002). Lambert (1996) observed an increase of intense cyclones in the Northern Hemisphere after 1970 using SLP data. Similar results were shown by Schinke (1993) applying cyclone central pressure as key parameter. Findings based on long-term SLP records show an overall stationarity in storm statistics over the North Atlantic during the last 100 years with significant decadal variability (e.g. Schmith 1995). Only during the last four decades of the twentieth century there are indications of a minor intensifying of the North Atlantic storm climate which would be in line with the findings of Lambert (1996) (Schmith et al. 1998). According to several other studies (e.g Alexander et al. 2005; Bärring and Fortuniak 2009; Miller 2003; Pryor et al. 2006; Wang et al. 2008 and Weisse et al. 2009) there is evidence for a changing cyclonic activity in the Northern Atlantic area throughout the whole second half of the twentieth century: Storms show a northward shift of track location and increased intensity whereas the total number of storms has been decreasing. Contrasting these results, station pressure data over the North Atlantic European sector (NAE, defined as the region between 25°N - 70°N and 75°W - 20°E) yield a decline in storminess from high levels between the late nineteenth century to lower intensities, fol-

lowed by an increase to maximum levels around 1990 and dropping thereafter (Trigo et al. 2008). Jones et al. (1999) reported an increase of severe gales in the UK since the 1960s being in line with the increasing number of extreme wind events around the North Sea. For the French coasts, Pirazzoli (2000) argues that changes in regional meteorological factors indicate a decrease in the frequency of atmospheric depressions and strong surge winds.

For the Iberian Peninsula, Trigo et al. (2008) show a decline of both cyclonic activity and wind speeds throughout the extended winter period from October to March (ONDJFM) from 1960 to 2000 with a monthly average of two to four cyclone counts. The decrease in cyclonic activity for this period is especially striking for February and March with a significant decline of around 20 % per decade corresponding to more than a 60 % decrease between the first and last decade of the record (Trigo et al. 2008). However, the ONDJFM-period is generally characterized by an increase in wind speed and cyclonic activity in several other sectors over the North Atlantic (Trigo et al. 2008). Regionally different oceanographic and atmospheric properties could be the reasons for varying study outcomes. Furthermore, causes of divergent results regarding regional storminess in the North Atlantic may also be assigned to inhomogeneities of the underlying datasets (Lozano et al. 2004) and or to the storm tracking methodology (Trigo et al. 2008).

1.1.2 Extreme sea levels at western European coasts

There are recent studies which have analyzed extreme sea levels worldwide. Through an analysis of 99th percentiles of hourly sea level data from almost 150 stations around the globe, Woodworth and Blackman (2004) showed that there is evidence for a positive trend in extremely high sea levels. This trend is analyzed to be mostly in line with the observed global mean sea level rise and is closely related to regional climatic properties (Woodworth and Blackman 2004).

Contrasting this observed trend on a global scale and following the findings regarding past North Atlantic storminess pointed out above, also the analyses of regional extreme sea level trends show different results. The findings are dependent on the geographical location of a coastal region with its relevant specific oceanographic and atmospheric properties and the statistical methods used (Bindoff et al. 2007). At Liverpool, Woodworth and Blackman (2002) observed larger values for the annual maximum surge-at-high-water level in the eighteenth, late nineteenth and late twentieth century than in most of the twentieth century for a tide gauge dataset covering the period 1768 to 1999. However, values for annual maximum high waters and surges at annual maximum high waters show considerable interannual variability but no long-term change (Woodworth and Blackman 2002). For the English Channel, Pirazzoli et al. (2006) identified storms from north-west or south-west to be mainly responsible for major surges by pushing Atlantic waters into the Channel;

highest surges of almost 3 m have been recorded at Sheerness (UK). For the southern Channel stations in France, surge-related winds were found to show mainly decreasing tendencies in frequency and wind, whereas the stations at the northern side of the Channel indicate variable trends being more exposed to southerly winds (Pirazzoli et al. 2006). In a previous study, Bouligand and Pirazzoli (1999) analyzed tide gauge records from Brest for the period between 1860 and 1994 and found an increasing trend in annual maxima and 99th percentile of surges, with a decreasing trend during the period between 1953 and 1994 and the 1960s showing an exceptionally high number of surges. The annual maximum surge level is a common measure to describe extreme sea levels. It can be defined as the largest positive anomaly measured per year with respect to the estimated sea level evolution including mean sea level and tidal signal (Bindoff et al. 2007; see also Chapter 3). Highest surges for the French Atlantic coasts have been recorded at Saint Nazaire with peak values higher than 173 cm; however, none of the detected twenty highest surges coincided with an astronomical tide level larger than the 95th percentile (Pirazzoli 2000). Based on the observed decrease in the frequency of atmospheric depressions and strong surge winds around Brest, in his study Pirazzoli (2000) argues that this trend of climate variability would also dampen the frequency of coastal flooding around the study area.

1.1.3 Oceanographic and coastal properties of the northwestern Iberian Peninsula

The area covered by the observational data which will be presented in the subsequent Chapter 2 belongs to the regions Galicia, Asturias, Cantabria and the Basque Country (Spain) and extends from roughly 42°N to 44°N and 9°W to 2°W. Somewhat less than half of the Atlantic coastline of the whole Iberian Peninsula, covering 1,653 km in total, can be associated with this selected region of interest.

From an oceanographic point of view, there are several properties which have to be pointed out for this region: The continental shelf along the coast shows varying widths from 15 km to nearly 400 km dropping off to a depth of around 1000 m at the 500 m isobath (GOA 2004). The coastal region of interest, especially Galicia, is affected by the North Atlantic Eastern Boundary Current (EBC) which is highly influenced by the seasonality of winds with the large-scale circulation forcing determined by the location of the Azores High (Ruiz-Villarreal et al. 2006).

According to Wooster et al. (1976) the prevailing geostrophic winds define in large parts the circulation within the EBC area with upwelling from April to September and downwelling from October to March. Additionally, there is evidence of a poleward subsurface countercurrent transporting warm and very salty Eastern North Atlantic Central Waters

(ENACWs) to the North (Ruiz-Villarreal et al. 2006 and references therein). Following Oliveira et al. (2004) the poleward current flows over the slope during autumn and winter being surface intensified with magnitudes in the order of 20 cm/s. The reversal of the prevailing winds in autumn favors the development of this poleward current on the slope (see Figure 1.2).

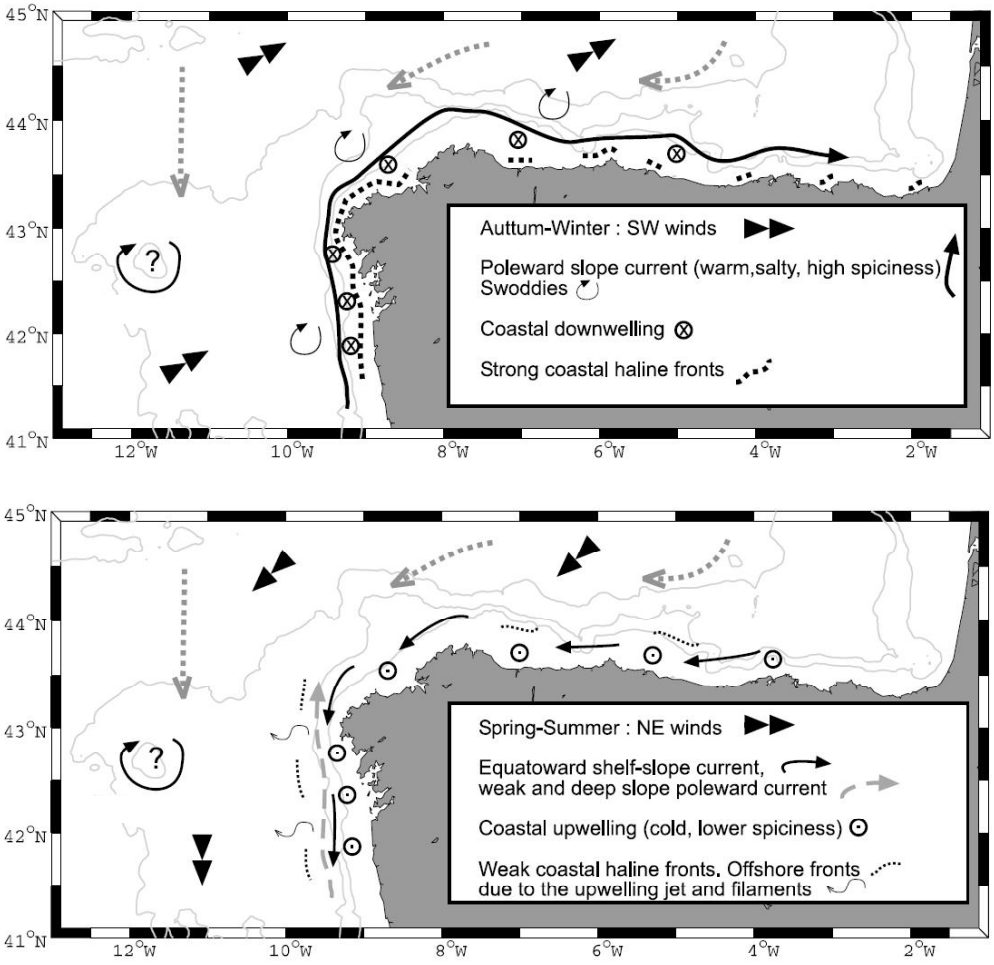

Figure 1.2: *Schematic circulation during typical autumn-winter (top) and spring-summer (bottom) seasons; offshore current is dominated by the EBC (grey dotted arrows)(Ruiz-Villareal et al. 2006).*

The penetration of the ENACWs into the Cantabrian Sea in the southern Bay of Biscay can be observed usually around Christmas (Pingree and Le Cann 1992). This so-called 'Navidad'-phenomenon can be characterized by anomalously high Sea Surface Temperatures (SSTs) (Garcia-Soto et al. 2002). The changing wind regime in spring again triggers the upwelling of central waters (Ruiz-Villarreal et al. 2006). Main freshwater inputs around the northwestern Iberian Peninsula are the Minho River south of Vigo, local rivers

in the Galician Rias Baixas and some local rivers with small catchment areas along the Cantabrian coasts.

1.2 Motivation & Objectives

Up to now, research on extreme sea levels along the Atlantic European coasts has focused more on northerly regions, i.e. north-western France, the Channel area and the British and Irish coasts (Betts et al. 2004; Bouligand and Pirazzoli 1999; Holt 1999; Pirazzoli 2000; Pirazzoli et al. 2006; Woodworth and Blackman 2004). With this study the investigated Western European coastal area will be extended to the south.

Sea level data analysis connected to the detection of relevant atmospheric causes around the northwestern Iberian Peninsula will contribute to a better understanding of underlying physical mechanisms and forcings of atmospheric origin. The analysis will follow a bottom up approach, with observational tide gauge data forming the basis of the work and providing the points in time which will then be examined regarding their large-scale atmospheric circulation structure. Furthermore, derived frequencies and trends of regional extreme sea levels might help to draw a more conclusive picture also of the oceanographic properties of the Galician and Cantabrian Sea. A first picture of potential future changes in regional extreme sea levels will be drawn with the analysis of climate model data. Simulated SLP is going to serve as the key parameter to investigate the evolution of cyclonicity over the Northern Atlantic influencing also atmospherically induced surges around the northwestern Iberian Peninsula. This in turn will support the assessment of oceanic and coastal changes triggered by ongoing climate change.

The following research questions are addressed in this study:

- *What is the connection between large-scale atmospheric circulation patterns and sea level extremes around the northwestern Iberian Peninsula for the period 1948-2001?*
- *Is it possible to detect a change in the intensity of extreme sea levels over the observation period?*
- *Do changes in observed extreme sea level trends have to be attributed to changes in storm strength and frequency or to changes in mean sea level?*
- *Are there areas around the northwestern Iberian coasts which could be affected by enhanced extreme sea level threats in the future?*

Chapter 2 provides information about the data used in this study, followed by the methodologies that have been applied in Chapter 3. The results will be presented, analyzed and discussed in Chapter 4. Finally, the conclusions and an outlook on potential future work will be presented in Chapter 5.

Chapter 2

Data

The datasets used can be separated into three parts: i) 54-year long, hourly tide gauge observation time series (1948-2001) providing date and magnitude of extremely high surges at selected sites around the northwestern Iberian Peninsula (Marcos et al. 2009); ii) 6-hourly large-scale atmospheric circulation data, related to recorded surges and taken from the NCEP/NCAR reanalysis (Kalnay et al. 1996; Kistler et al. 2001); iii) model data outputs from the ECHAM5-OM1 climate model (Roeckner et al. 2003; Marsland et al. 2003).

2.1 Tide gauge measurements

The analysis of hourly tide gauge measurements around the northwestern Iberian Peninsula is based on previous research carried out by Marcos et al. (2009). From the originally eight available records for the Atlantic region the three longest records were chosen as the basis for sea level analysis. Besides the length of the available observational records also the spatial coverage of the northwestern Iberian area has served as a selection criterion. The unprocessed tide gauge data is provided by the European Sea Level Service (ESEAS) and several national services (Marcos et al. 2009). The selected longest, coherent, hourly station records Coruna, Santander and Vigo span a period from 1943 to 2001 while the remaining available Atlantic stations reach back to 1985. The analysis has been restricted to the period 1948-2001 for both tide gauge and large-scale circulation data according to the starting point of the NCEP/NCAR reanalysis.

The tide gauge station data have been preprocessed and quality controlled by Marcos et al. (2009): Each record has been analyzed on a monthly basis in order to detect outliers, shifts in date and time drifts; records containing date shifts were divided into shorter periods which show consistent values; additionally, wild point editing was performed by removing

Table 2.1: *Tide gauge station details for the period 1943(1948)-2001 with location, maximum observed values and maximum derived tidal residuals.*

Station	Location	Max. Obs. [cm]	Max. Tid. Res. [cm]
Coruna	43.17°N 8.42°W	248.3	82.2
Santander	43.43°N 3.82°W	256.4	82.7
Vigo	43.22°N 8.63°W	252.7	88.0

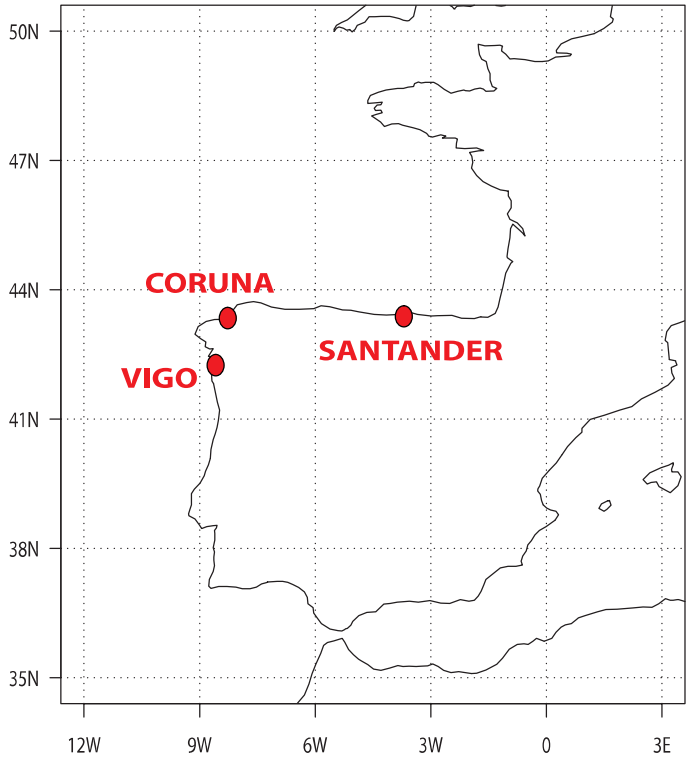

Figure 2.1: *The three tide gauge stations analyzed in this work.*

only isolated outliers which were reflected in a single hourly value (for more details see Marcos et al. 2009).

In general, the observed sea level ζ can be described as a function of the mean sea level $M_0(t)$, the tidal signal $X(t)$ and the surge level $Y(t)$ (Tsimplis and Blackman 1997):

$$\zeta = M_0(t) + X(t) + Y(t) \tag{2.1}$$

The sea level is measured with respect to a locally calibrated gauge zero which refers to the local mean sea level. In order to detect extreme sea levels the surge level $Y(t)$ has to be derived by subtracting $M_0(t)$ and $X(t)$ from the observed sea level ζ. The mean

sea level $M_0(t)$ incorporates the long term trend and a complex seasonal cycle whereas the astronomic tide $X(t)$ can be calculated for the region of interest via a fixed harmonic equation (Tsimplis and Blackman 1997). *t_tide*, a standard program for the estimation of tides through harmonic analysis (Pawlowicz et al. 2002), has been used to fit the tidal constituents to the selected time series. The derived tidal estimates have been used as a tool for identifying temporal shifts in the original sea level measurements. The observed sea level time series have been kept for the analysis if time shifts were identified, whereas faulty segments had to be removed for the analysis of the tidal residuals (Marcos et al. 2009).

Further tidal residual analysis in this work is based on the extended winter season from October to March (ONDJFM), the period when most storm surges causing extreme sea levels can be expected (Lozano et al. 2004).

The preprocessed tidal residual time series was used in order to extract the ten highest values per winter season for each station. To ensure the independence of each defined surge event, the typical regional storm length of 72 hours has been chosen as a separation criterion (Marcos et al. 2009). Furthermore, the ten highest tidal residuals within each station time series have been extracted from the seasonal extremes (see Table 2.2).

Table 2.2: *Ten highest tidal residuals (height in cm) recorded at the selected tide gauges Coruna, Santander and Vigo for the period 1948-2001.*

	CORUNA	**SANTANDER**	**VIGO**
surge rank	*tidal residual height [cm]*		
1	82.15	82.74	88.02
2	76.52	74.76	87.48
3	75.60	65.62	85.75
4	73.06	62.38	75.00
5	71.61	61.21	74.44
6	69.59	60.98	73.13
7	68.88	58.93	71.91
8	67.23	57.27	69.14
9	66.88	56.83	68.94
10	65.82	56.50	67.52

2.2 NCEP/NCAR reanalysis

The National Centers of Environmental Prediction (NCEP) and the National Center for Atmospheric Research (NCAR) have produced a gridded 4-dimensional atmospheric field data set back to 1958 (Kalnay et al. 1996) and 1948 respectively (Kistler et al. 2001). Recovered observational data have been quality checked and then assimilated with the Climate Data Assimilation System (CDAS; for more details see Kalnay et al. 1996). CDAS includes the NCEP global spectral model, including 28 "sigma" vertical levels and a triangular truncation of 62 waves (T62; 2.5° x 2.5 °), corresponding to roughly a 210 km horizontal resolution (Kistler et al. 2001). A three-dimensional variational scheme cast (3DVAR) in spectral space is used for the analysis scheme (Parrish and Derber 1992). The reanalysis data assimilation system continuously uses current real time data to update the available reanalysis products. Assimilated observations include (Kistler et al. 2001): Upper-air rawinsonde temperature, horizontal wind and specific humidity measurements; Television Infrared Observation Satellite (TIROS) and Television Operational Vertical Sounder (TOVS) temperature soundings from NOAA polar orbiters over ocean, with microwave retrievals excluded between 20°N and 20°S due to rain contamination; temperature soundings over land only above 100 hPa; cloud-tracked winds from geostationary satellites; aircraft observations of wind and temperature; land surface reports of surface pressure and Oceanic reports of surface pressure, temperature, horizontal wind and specific humidity.

Although the CDAS is maintained constant, the quality of the reanalysis data is improved through the evolution of the global observation systems. There are three major phases of the observation system which have to be distinguished: the early phase until the Geophysical Year 1957, where the first upper-air observations were established; the implementation phase of the modern rawinsonde network from 1958-1978; and the modern satellite era from 1979 to present (Kistler et al. 2001). Upper-air observations were done three hours earlier than the current synoptic times 0000, 0600, 1200 and 1800 UTC until 1 June 1957. That's why reanalysis for the first decade (1948-1957) is performed at 0300, 0900, 1500 and 2100 UTC.

The quality control and monitoring of the rawinsonde data consists of two different approaches: optimal interpolation quality control for all observations (Woollen et al. 1994) and the complex quality control for heights and temperatures (Collins 2001).

For our purpose, 6-hourly large scale reanalysis fields have been extracted for sea level pressure (SLP) covering the region 30°N - 75°N and 60°W - 40°E. Additionally, u-wind and v-wind components at the 995 hPa level have been used for a smaller area (30°N - 55°N and 35°W - 5°E). The selected reanalysis datasets cover the period 1948 to 2001. As climatological reference period we selected 1961-1990.

2.3 GTECCA

The Global Tropical and Extratropical Cyclone Climatic Atlas (GTECCA) is a product provided by the National Climatic Data Center (NCDC) of the NOAA and the U.S. Navy. It represents a compilation of all global historic tropical storm track data for five tropical storm basins going back to the 1870s. Additionally, the GTECCA includes Northern Hemispheric extratropical storm track data from 1965 to 1995. The track data comprises time, position, storm category, maximum wind and central pressure when available (NCDC 1997). It is possible to display tracks, track data for any basin or user-selected geographical region and tracks passing within a predefined radius of any point. Specific information is provided about all storms from 1980 to 1992 as well as basin-wide tropical storm climatological statistics. Observational data have mostly been collected by aircrafts, drop windsondes and buoys (NCDC 1997).

In addition to the analysis of the large-scale atmospheric patterns provided by reanalysis data, the output of the GTECCA has been included in this work with the intention to obtain specific storm track information related to extreme sea levels at the coasts of the northwestern Iberian Peninsula. The available collection of extratropical storms registered over the Northern Atlantic region from 1965 to 1995 has been filtered for those storms reaching study area, within a 1000 km radius around 42.8° N and 8.5° W.

2.4 ECHAM5-OM1

In order to investigate the future evolution of storm surges in the study area, 6-hourly SLP fields have been analyzed from the output of a state-of-the-art coupled atmosphere-ocean general circulation model (AOGCM; ECHAM5-OM1). Different model runs have been accessed from the World Data Center for Climate (WDC; http://cera-www.dkrz.de/CERA/index.html): the twentieth century (20C) control run for the period 1961 to 1990 and the IPCC Special Report Emission Scenarios (SRES) A1B and A2 runs covering the period 2071 to 2100. The A1B scenario is based on a more moderate GHG emission pathway whereas A2 conditions refer to ongoing, intensified fossil fuel burning and GHG emissions (for more details see Nakicenovic et al. 2000). Similar to the reanalysis data, the selected region of interest covers the area 30°N - 75°N and 60°W - 40°E.

The fifth generation atmospheric general circulation model (AGCM; ECHAM5) is the most recent version of a series of ECHAM models developed at the Max Planck Institute for Meteorology (MPIM) which originate from the spectral weather prediction model of the European Centre for Medium Range Weather Forecasts (ECMWF). The ECHAM5 AGCM

is based on the cycle 5.2 of the ECHAM model family, provides a T63 resolution (1.875° x 1.875°) and is run with 31 vertical hybrid levels (Jungclaus et al. 2006).

The Hamburg Ocean Model (MPI-OM) is an ocean general circulation model (OGCM) succeeding the Hamburg Ocean Primitive Equation (HOPE) model. The MPI-OM is based on primitive equations including a representation of thermodynamical processes. The oceanic circulation from small-scale (oceanic eddies) to large-scale processes (gyres) can be modeled in response to atmospheric forcing. The MPI-OM OGCM is run with an average horizontal grid spacing of 1.5° and a vertical structure of 40 unevenly spaced ocean levels.

Both, the ECHAM5 and MPI-OM models have undergone major improvements compared to their predecessors. Major modifications of the ECHAM5 compared to the ECHAM4 refer to new physical formulations (Advection scheme for positive definite variables; longwave radiation code; cloud cover parametrization; separate treatment of cloud water and cloud ice; cloud microphysics; subgrid scale orographic effects), major changes in land surface processes and land surface datasets, changes regarding shortwave radiation, vertical diffusion, cumulus convection, orbit calculation and technical changes as the source code transfer to Fortran 95. One of the most important changes of the MPI-OM is the treatment of horizontal discretization which changed from a staggered E-grid formulation to an orthogonal curvilinear C-grid. The technical details of these modifications can be looked up in Roeckner et al. (2003) for the ECHAM5 model and in Marsland et al. (2003) for the MPI-OM.

Chapter 3

Methods

In a first step, the tide gauge data are processed and modified in a way that the temporal evolution and intensity of extreme surges at each selected station can be accessed in a comprehensive way. In a second step and on the basis of the processed sea level measurements, the selected main atmospheric forcing parameters (SLP and wind fields) are taken from the reanalysis and AOGCM outputs and related to the surge events. Anomalies are calculated with respect to the 1961-1990 reference period for the derived large-scale atmospheric circulation patterns which correspond to the extracted surge extremes. Additionally, composites of the selected surge events were computed and plotted. Furthermore, the selected atmospheric circulation patterns which are related to the tidal residual extremes are subject to a classification process, i.e. cluster analyses for the detection of dominant atmospheric forcing patterns. For the assessment of future surge trends in the region, SLP AOGCM scenario outputs are compared to reference climatologies through the visualization of SLP storm track differences to detect changes in cyclonicity for the model grid points being closest to the selected tide gauge stations.

All analyses on the datasets described above have been performed with Climate Data Operators (CDO) and R. CDO is a collection of UNIX-based command line operators to process and analyze climate model data. CDO have been developed by the Max Planck Institute for Meteorology and are used by many research groups worldwide (http://www.mpimet.mpg.de/fileadmin/software/cdo/). R is a common language and environment for statistical computing and graphics developed at the Bell Laboratories by John Chambers and colleagues (http://www.r-project.org/). The tool for the illustration of the climate model data used in this work is the Grid Analysis and Display System (GrADS). GrADS is a UNIX-based 4-dimensional data model (latitude, longitude, level and time) which has been developed at the Center for Ocean-Land-Atmosphere Studies (COLA) in Maryland/USA by Brian E. Doty (http://www.iges.org/grads/).

3.1 Extreme sea levels

There is a wide range of methods dealing with the analysis of extreme values. Depending on the purpose of the extreme value analysis and the data structure there are different statistical approaches to be favored (Coles 2001). For the detection of tidal residual extremes in the three preprocessed station records two different methods were used: i) Calculation of simple annual percentiles to obtain a measure which provides a comprehensive picture of the distribution of the highest recorded values and furthermore simplifies the comparison of the three 54-year long station records; the derived seasonal percentiles were then subject to a trend analysis; ii) Estimation of return levels. In our case, the calculated return levels indicate the tidal residual height, which can be expected to occur within a given period, e.g. 25 years. In general, return values are estimated by modeling the tail of the upper part of the distribution of observations with the help of a known extreme value distribution function (e.g. Tawn 1988). Here a declustered Peak Over Threshold (dePOT) approach was used based on a Generalized Pareto Distribution (GPD) for the estimation of return levels (Toreti et al. 2009).

The term "surge" is introduced to serve as an equivalent term for the observed extreme tidal residual values assuming that the selected tidal residual extreme values (representing the difference between local tidal signal and observed sea level) can be connected to an external, meteorological forcing (Ullmann et al. 2007).

3.1.1 Percentiles

A sample quantile q can be taken as the equivalent of a data value exceeding a randomly chosen member of the dataset with probability $1 - p$ $(0 \leq p \leq 1)$. The quantile q can then be considered as the $[p \times 100]th$ percentile of the dataset (Wilks 2001). The percentile method is widely used for the analysis of changes in extreme sea levels (e.g. Woodworth and Blackman 2002, Woodworth and Blackman 2004).

The non-parametric percentiles method only ranks the data and focuses on the values which correspond to the predefined fraction exceeding the threshold specified by the percentile value. The ten highest tidal residual values per extended winter season separated by at least 72 hours have been chosen as an appropriate measure for extremely high values. If we consider the hourly basis of the data this would correspond to the 99.99th percentile of a six-month observation. The ten highest values per extended winter season are the basis for the analysis of the evolution of tidal residuals extremes for each station including a trend analysis. The extended winter season percentiles provided as well the input dates for the clustering of the corresponding large scale SLP fields (see subsection 3.2.2). Additionally, the ten highest recorded tidal residuals over the whole record length were extracted from

the 99.99th percentile data for each station. The corresponding dates of the derived surge events were then used for the SLP anomaly calculations and wind analysis.

3.1.2 Trend Analysis

The tidal residual extremes distribution of each station record is tested for the existence of a trend by applying a linear regression model: The relationship between the independent x and the dependent y is summarized by a straight line which holds the least error for predictions of y given observations of x (Wilks 2001). The predictor x is represented by the time values of the tidal residual observations; the predictand y embodies the 58 mean values of the seasonal tidal residual percentiles (1943/1944 - 2000/2001). The error criterion is chosen to be the minimization of the sum of squared errors, i.e.

$$\sum_{i=1}^{n}(y_i - [a + bx_i])^2 = min!, \tag{3.1}$$

with a being the least-squares intercept and b the slope (for more details see Wilks 2001). The significance of the derived linear trend is checked with the non-parametric Mann-Kendall (MK) test. In general, the MK test can be considered as a simple and robust trend test which is less affected by outliers because its statistic is based on the sign of difference and not directly on the random variable value (e.g. Onoz and Bayazit 2003). With $x_1, x_2, \ldots, x_n$ being a sequence of measurements over time, the null hypothesis H_0 is tested which assumes no monotonic trend (Hipel and McLeod 1994). The Mann-Kendall test statistic has the following form:

$$S = \sum_{k=1}^{n-1}\sum_{j=k+1}^{n} sgn(x_j - x_k), \tag{3.2}$$

where

$$\begin{aligned} sgn(x_j - x_k) &= +1 \quad \text{for} \quad x > 0 \\ sgn(x_j - x_k) &= 0 \quad \text{for} \quad x = 0 \\ sgn(x_j - x_k) &= -1 \quad \text{for} \quad x < 0. \end{aligned}$$

A positive value of S indicates an upward trend, whereas negative values of S indicate a downward trend in the measurement values over time. The standard normal variate Z, i.e.

$$Z = \frac{S}{\sqrt{Var(S)}}, \tag{3.3}$$

with $Var(S)$ being the variance of S, is needed to calculate the p-value which indicates the significance of a trend within a certain confidence interval (for more details see Hipel and McLeod 1994). The p-value has the form (Hirsch and Slack 1984):

$$p = 0.5 - \phi(|Z|), \tag{3.4}$$

with

$$\phi(|Z|) = \frac{1}{\sqrt{2\pi}} \int_0^{|Z|} e^{\frac{-t^2}{2}} dt. \tag{3.5}$$

The significance level α can be considered as the probability of rejecting the true null hypothesis (H_0: no monotonic trend). A significance level of 5% was chosen (or a 95% confidence in the trend) and set $\alpha = 0.05$. If the calculated p-value is smaller than 0.05 a statistically significant trend exists on a 95% level, whereas a p-value greater than 0.05 confirms a not significant trend (Hirsch and Slack 1984).

3.1.3 Declustered Peak Over Threshold (dePOT) approach

The most popular method for the estimation of return levels is the Block-Maxima approach based on a General Extreme Value (GEV) distribution. The GEV approach is suitable for the analysis of annual maxima and has been used for the purpose of sea level data analysis in several studies (e.g. Tawn 1992; Bernier et al. 2007). However, this approach is criticized to be inefficient because only a single maximum value per year is considered even if there is more data of extremes available (Coles 2001). The dePOT method avoids this problem by including all data above a certain threshold:

Let $X_1, X_2, \ldots, X_n$ be a set of independent and identically distributed (iid) random variables with a common distribution F. Furthermore $M_n = max\{X_1, \ldots, X_n\}$ and be F so that, for large n, $Pr\{M_n \leq z\} = G(z)$; where $G(z)$ belongs to the GEV family with μ, the shape parameter σ and the scale parameter ξ being estimated through the Maximum Likelihood Estimation (MLE) method.

Therefore, the new distribution $H(z)$ of $(X - u)$ conditional on $X > u$, with the threshold u being large enough, belongs to the General Pareto Distribution (GPD) family, i.e.

$$H(z) = 1 - (1 + \frac{\xi z}{\tilde{\sigma}})^{\frac{-1}{\xi}}, \tag{3.6}$$

with

$$\tilde{\sigma} = \sigma + \xi(u - \mu). \tag{3.7}$$

A first problem is the choice of an appropriate threshold. One possibility of deriving a convenient threshold value is the interpretation of the Mean Residual Life Plot (MRLP). In any case, the choice of the threshold remains influenced by a subjective decision (Coles 2001). In order to avoid the independence assumption which is violated for temporally highly resolved climatic series, the runs-declustering method is applied (Toreti et al. 2009). Then the m-year return level yields:

$$x_m = u + \frac{\sigma}{\xi}[(m\zeta_u\theta)^{\xi} - 1], \tag{3.8}$$

where σ and ξ are the parameters of the threshold excess GPD, ζ_u is the probability of exceedances of the threshold u, and θ is the extremal index; the number of exceedances of the threshold u is denoted by n_u; According to Coles (2001), the number of clusters above u is obtained by n_c, while ζ_u and θ are estimated with

$$\hat{\zeta_u} = n_u/n \tag{3.9}$$

and

$$\hat{\theta} = n_c/n. \tag{3.10}$$

Therefore the component $\zeta_u\theta$ in equation 3.8 can be estimated by n_c/n . A cluster c is active until r observations fall below u; then the next cluster will be opened.

Thus, if all consecutive observations with a value above the threshold u belong to the same cluster c, and the latter is filled with these values until r chosen observations fall below u, the cluster maxima are considered to be independent and a GPD can be fitted (Coles 2001).

For the return periods, m has been chosen to be 25, 50, 75 and 100 years. The extreme value calculation is based on the initial population of the three hourly tidal residual records from 1948 to 2001. For the tidal residual return levels x_m, 95% confidence intervals ($\alpha = 0.05$) are included in the analysis to account for the uncertainties of the return level estimation (for more details, see Coles 2001).

3.2 SLP and wind at the time of the recorded surges

In order to link the surge extreme events with the relevant large-scale atmospheric circulation patterns, the 6-hourly NCEP/NCAR SLP reanalysis fields which are temporally closest to the recorded date of the surge have been extracted from the reanalysis dataset. The same procedure has been applied to the u-wind and v-wind reanalysis data. In a

further step the u- and v-wind-components have been combined to a wind vector in order to facilitate the subsequent visualization. The preceding (LEAD) and succeeding (LAG) 6-hourly fields have been included in the analysis to observe the evolution of the atmospheric circulation and wind pattern at the time of the surge.

Besides analyzing atmospheric key characteristics of the selected surge samples, the pressure pattern anomalies are put in a wider context regarding their circulation pattern characteristics. Atmospheric forcing of severe surges can often be associated with typical modes of the large-scale circulation (Holt 1999). Thus, a relationship is established with the classical four "weather regimes" (WR) over the Northern Atlantic introduced by Vautard (1990) and widely used in several studies also related to sea level extremes (e.g., Plaut and Simonnet 2001; Ullmann et al. 2008). The classification used for these WR is based on the assumption that the atmosphere over the North Atlantic evolves between a limited number of states (Vautard 1990) and yields the following large-scale pressure patterns:

- Blocking (BL): typical European blocking dipole bringing easterlies over Western Europe, a pronounced anticyclone over Central to Eastern Europe and a maximum positive pressure anomaly over Scandinavia (Plaut and Simonnet 2001)
- Zonal (ZO): reverse dipole structure characterized by a low over Northern Europe extending to Greenland and a positive pressure anomaly in the southerly North Atlantic; the flow is zonally enhanced over the North-Atlantic with the jet extending across the Atlantic (Vautard 1990)
- Greenland Anticyclone (GA): common features to the North Atlantic Oscillation pattern but with a strong positive anomaly over Greenland and a southern part of the pattern which is more zonally symmetric; flow structure allows synoptic perturbations to travel across the North-Atlantic towards Europe (Vautard 1990)
- Atlantic Ridge (AR): positive anomaly in the mid-eastern Atlantic; cold, moist air advected from the Northern Atlantic transported to Europe; prominent feature is a ridge over the Eastern Atlantic inducing Northwesterlies over Western and Central Europe (Plaut and Simonnet 2001)

3.2.1 SLP anomalies with modified t-value significance

Only the specific surge date has been taken into account for the anomaly calculations for each year of the reference period 1961-1990 (daily mean composites of the corresponding month and day from 1961 to 1990). Thus, the reference period in this case consists of 30 SLP fields (30 surge dates in 30 years) but focuses on the specific seasonal 'surge' time in

the dataset. Hence, signal-loss due to the inclusion of circulation patterns before and or after the time window of interest can be avoided.

In order to indicate the significance of the anomalous SLP patterns of the surges compared to the reference period, t-values are calculated on the basis of annual scaled anomalies, applying a method introduced by Brown and Hall (1999):

For Gaussian data with a well known t-distribution, we obtain a t-value with $v = (n-1)$ degrees of freedom, i.e.

$$t = \frac{\bar{x} - \sqrt{v}}{\sigma}, \tag{3.11}$$

with $\bar{x}$ being the sample mean and σ the standard deviation of sample. The introduced t-value accounts for the associated variance, but is still susceptible to outliers, especially in small datasets. To overcome this problem the sample mean $\bar{x}$ is replaced with the sample median M and σ by a "pseudosigma" $\sigma_p = d_f/1.349$, where d_f represents the difference between the upper fourth and the lower fourth of a sorted data batch (Brown and Hall 1999). The constant 1.349 is based on the fact that a fourth corresponds to a tail area of 0.25, which for a Gaussian distribution is limited by $\mu - 0.6745\sigma$ and $\mu + 0.6745\sigma$, leading to an F spread of 1.349σ (Brown and Hall 1999). We now obtain:

$$t = \frac{M - \sqrt{v}}{\sigma_p}, \tag{3.12}$$

without accounting for a cutoff value or limiting magnitude for the choice of the key map parameter. Iglewicz (1983) could prove in his work that M and d_f serve very efficiently as a robust interval. The computed interval yields:

$$M \pm \frac{t_{n-1}(d_F)}{1.075(n)^{1/2}}, \tag{3.13}$$

with the constant 1.075 derived from simulated t-values while the ratio $t_{n-1}/1.075$ is in close agreement with the required t for a 95% confidence interval using M and d_F (Brown and Hall 1999). We know get a modified t-value in the form of:

$$t_{n-1} = \frac{M(1.075)\sqrt{n}}{d_F}, \tag{3.14}$$

for the significance illustration of calculated composites. $t_{n-1}/1.075$ provides a rule for some sort of cutoff value above or below which a t-value can be considered significant:

Using a t-distribution table from a textbook, $t_{n-1} = 2.045$ for $\alpha = 0.025$ (corresponding to a significance level of 95%) and $v = 29$ (for the 30-year reference period 1961-1990).

$t_{n-1}/1.075$ then equals 1.9023. Therefore t-values $\geq +1.902$ and ≤ -1.902 can be used as the limiting values for the indication of anomaly fields being significant in our case.

3.2.2 Simulated Annealing and Diversified Randomization Clustering

Establishing a connection between a single surge and the corresponding large-scale SLP field is crucial for the identification of individual atmospheric forcing factors (see Chapter 3.2.1). However, a comprehensive analysis of atmospheric circulation patterns being potentially decisive for surge events at a tide gauge station requires a method which is much more extensive. The key goal regarding the analysis of extracted surge SLP fields is the detection of dominant circulation patterns causing the recorded surges. Therefore an analysis is needed to detect similar surge SLP patterns which can be visualized in several significant groups. The data used for this analysis are the cumulated seasonal (ONDJFM) tidal residual percentiles, providing ten surge dates per season over 54 years for each station.

There is a variety of approaches dealing with the classification of similar atmospheric pressure patterns (e.g. Jones et al. 1997; Luterbacher et al. 2002; Jacobeit et al. 2003). A common method for the detection of circulation patterns with common characteristics is the classification of pressure patterns over a certain time period through classes of high within-class similarity and between-class dissimilarity (e.g. Küttel et al. 2009 and references therein). Well known examples of classification type approaches are the European Grosswetterlagen by Hess and Brezowsky (1977) or the Lamb weather types (Lamb 1972) which are both based on the expertise of experienced meteorologists and therefore have to be described as "subjective". More recently, different statistical methods which make use of the steadily increasing computational power are more and more frequently applied and can be considered to be more "objective" in a way that they are sorting circulation configurations based on mathematical calculations as for example correlations (e.g. Brinkmann 1999) or EOFs (e.g. Beck 2000). The latter approach has been chosen as appropriate for the purpose of our analysis since the final interpretation of the grouped pressure patterns with similar characteristics is rather straightforward.

The classification method used in this work, introduced by Philipp et al. (2007), is the Simulated Annealing Diversified Randomization (SANDRA) technique. SANDRA is a fully automated clustering approach focusing on one parameter describing the atmospheric circulation (SLP in our case). Classifying the parameter values will ideally create groups with members of highest possible similarity. The Within Cluster Sum of Squares of deviation (WSS) is the measure for the degree of dissimilarity within the resulting clusters, i.e.

$$WSS = \sum_{j=1}^{k} \sum_{i \epsilon C_j} D(X_i, \bar{X}_j)^2, \tag{3.15}$$

with k as the number of clusters C, i being the object number, $\bar{X}$ as the centroid of each cluster and D representing the Eucledian distance between objects and cluster centroids:

$$D(X_i, \bar{X}_j) = [\sum_{l=1}^{m} (X_{il} - \bar{X}_{jl})^2]^{1/2}. \tag{3.16}$$

m describes the number of parameters or grid points in our case. The Euclidean distance is used because it is able to take the absolute gradients of the selected pressure patterns into account (Philipp et al. 2007 and references therein). Furthermore, the Total Sum of Squares deviation (TSS) calculates the sum of Eucledian distances between all objects and the overall centroid which is used as the second parameter besides the WSS to calculate the so-called Explained Cluster Variance (ECV):

$$ECV = 1 - \frac{WSS}{TSS}. \tag{3.17}$$

The ECV is a measure for the quality of a cluster solution between datasets and should be maximized by the classification method used, that is the higher the values for the ECV the better the quality of the cluster analysis (Philipp et al. 2007).

Within a clustering process of a dataset with large sample size there is a point at which an unknown number of solutions cannot be improved by moving objects from one cluster to the other although the solutions may be far away from the best solution possible (Philipp et al. 2007). Solutions of less quality are called local optima while the best solution is named the global optimum. The only way to overcome the problem of converging to a local optimum would be to check every possible combination of objects which is practically impossible for large data sets.

The SANDRA technique applies a non-hierarchical k-means cluster analysis run multiple times (1000 times in our case) from different randomly created starting partitions in order to get close to the global optimum; the solution with the highest ECV is chosen in the end. Additionally, the ordering of objects and cluster numbers is randomized within the "process of checking and reassigning" (Philipp et al. 2007). Applying the simulated annealing technique assures that an object can be reassigned to a different cluster at almost any stage even if the WSS would increase during this process at first. For more information on the specifications of the selected k-means clustering principle and the simulated annealing details, the reader is referred to Philipp et al. (2007) and references therein. The different modifications of the clustering procedure lead to better results regarding within-class similarity and between-class separation than the other frequently used clustering techniques

like conventional k-means (e.g. Michelangeli et al. 1995) or Partitioning Around Medoids (PAM) (e.g. Beranova and Huth 2008).

The definition of the number of clusters is a very crucial part when applying cluster analysis. None of the methods used so far for the detection of the optimal cluster number can be considered as universally appropriate (for a detailed list see Philipp et al. 2007). Küttel et al. (2009) have calculated SANDRA solutions for different cluster numbers and compared the within-class correlation. Nine clusters have yielded highest within-class correlation values and have been selected as the optimal cluster number in their case, a value which corresponds to the findings of Philipp et al. (2007) who have also found nine clusters to be most appropriate for their analysis. Both, Küttel et al. (2009) and Philipp et al. (2007) analyze long time series of SLP large-scale pressure fields over the North Atlantic-European region. The data used in these two works show similar characteristics regarding the SLP fields relevant for this work, so that a number of nine clusters has been decided to be proper for the classification of the derived large-scale surge SLP fields of Coruna, Santander and Vigo.

As a quality measure for SANDRA clustering results the silhouette index by Kaufmann and Rousseeuw (1990) has been applied, marking cluster members that cannot be clearly attributed to one specific cluster with the so-called negative silhouette widths. The more positive the value for the silhouette width s_i, the better is the clustering of the observational record; for s_i-values of around 0, the sample member lies between two clusters; If s_i is negative the member is probably placed in the wrong cluster (for more details see Kaufmann and Rousseeuw 1990).

Scaled mean anomaly composites have been calculated for each cluster according to Brown and Hall (1999), i.e.

$$X = \frac{\mu\sqrt{n}}{\sigma}, \tag{3.18}$$

with the population mean μ, the sample size n and the standard deviation σ. The calculated scaled anomalies are dimensionless. The within-cluster stability is assessed through performing the modified t-test by Brown and Hall (1999) already described in detail in chapter 3.2. Different applications of scaled mean anomaly composites are for example introduced in Xoplaki et al. (2004), Broennimann (2007) or Esper et al. (2007).

3.3 Evolution of simulated SLP

The analysis of simulated future SLP in the North Atlantic-European region is based on the outputs of three different ECHAM5 model configurations and the reference NCEP/NCAR

reanalysis data. Long-term mean SLP fields have been calculated for each of the four 6-hourly datasets over the period 1961-1990 for NCEP and hindcast 20C ECHAM5 and for the period 2071-2100 for ECHAM5 scenario runs A1B and A2. SLP difference maps were calculated for A1B minus 20C and A2 minus 20C SLP long-term means. Mean values have been calculated on the basis of the extended winter seasons ONDJFM.

3.3.1 Simulated SLP anomalies with t-value significance

In order to analyze the significance of the differences of the ECHAM5 SLP composites, the student t-test has been applied (Wilks 2001). The student t-test checks in our case whether the model means μ_A of the A1B, A2 model runs and the hindcast mean μ_{20C} of the 20C model run of each grid cell can be considered to be equal or not:

$$\begin{aligned} H_0: &\quad \mu_A = \mu_{20C} \\ H_A: &\quad \mu_A \neq \mu_{20C} \end{aligned}$$

If H_0 can be rejected, the calculated mean values differ from each other on a predefined significance level. The sample size of A1B, A2 and 20C data is equal, so that we can set up the test variable t in the following form, with $(2n-2)$ degrees of freedom and the fulfilled assumption of variance homogeneity:

$$t = \frac{\bar{X}_A - \bar{X}_{20C}}{\sqrt{\frac{S_A^2 + S_{20C}^2}{n}}}, \tag{3.19}$$

where n is the sample size, $\bar{X}$ are the sample means and S^2 is the SLP variance within the modeled ECHAM5 periods. According to student t-value tables from textbooks, thresholds for t yield $t \approx \pm 1.68$ with a chosen 90% significance level for the two-sided test and $(2n-2) = 58$ degrees of freedom (with $n_A = n_{20C} = 30$).

3.3.2 SLP storm tracks

A simple quantification of synoptic wave activity can be based on the assessment of SLP variability over a defined period of 2 to 6 days (Ulbrich et al. 2009). The approach was originally introduced by Blackmon (1976), Blackmon et al. (1977) and defined the standard deviation of the bandpass filtered variability of 500-hPa geopotential heights as an indicator of the sequence of upper-air troughs and ridges as the tropospheric counterparts of surface cyclones and high-pressure systems (Wallace and Gutzler 1981; Blackmon et al. 1984; Wallace et al. 1988). The resulting quantity is often referred to as "storm track" and provides a rough representation of combined intensities and frequencies

of low pressure and high pressure systems (Ulbrich et al. 2009). As Ulbrich et al. (2008) did in their study, SLP has also been chosen as the key parameter in this study instead of the 500-hPa geopotential height since the IPCC model data archive does not deliver daily geopotential height data for the 500-hPa pressure level. It is worth mentioning that the storm track is not affected by changes in long-term mean SLP so that variations can be directly assigned to transient wave activity (for more detail see Ulbrich et al. 2008). Grid cells with a high mean orography >1500 m MSL, i.e. Greenland, have been excluded from further analysis completely to avoid the influence of extensive extrapolation below ground (Ulbrich et al. 2009). In the following, the introduced storm track parameter serves as an indicator for future changes in cyclonicity over the Northern Atlantic.

The results of the above described methodology are presented in the next section of this work. After starting with the analysis of the selected tide gauge observations, the work focuses on the interaction of atmospheric parameters and recorded extremes. In a next step, predominant large-scale circulation patterns at the time of recorded extreme sea levels are investigated applying the SANDRA clustering technique for each station. Finally, future SLP changes for the North Atlantic region are presented in connection with changing storm tracks in order to give an outlook on future storminess at northwestern Iberian coasts.

Chapter 4

Results & Discussion

In the first part of this chapter key features of the three selected observational records are presented and compared. The results of the extreme value analysis are presented providing return values for each station. The second part focuses on the atmospheric circulation patterns derived for the detected surges. SLP anomaly and wind fields corresponding to the five highest surge events are analyzed for Coruna, Santander and Vigo. Subsequently, the results of the cluster analysis are presented for each station. A short overview of Global Tropical and Extratropical Cyclone Climatic Atlas (GTECCA) outputs is given thereafter. The last part provides information about the ECHAM5-OM1 model outputs by displaying MSLP changes for the IPCC SRES A1B and A2 and presenting first implications regarding connected changing cyclonicity.

4.1 Extreme tide gauge observations

This section is focused on the analysis of the temporal distribution of extreme surges for each station. The assessment of the temporal evolution of the sea level observations is crucial to obtain first insights regarding exceptional years with particular surge values and possible trends.

Figure 4.1 provides an overview of the three station records. The surge values are defined as the extended winter seasonal (ONDJFM) 99.99th percentiles of the derived hourly tidal residuals. They are marked as grey dots and cover the period 1943 to 2001. In the years 1943 and 2001 only the months OND (1943) and JFM (2001) are included in the analysis. The resulting 58 seasonal percentiles are pooled to seasonal mean surge values represented by the green line. The long term mean of the tidal residual values are displayed by the blue horizontal line. Additionally, the linear regression lines serving as a trend measure are indicated by the dashed red line. The long term surge means slightly differ between the

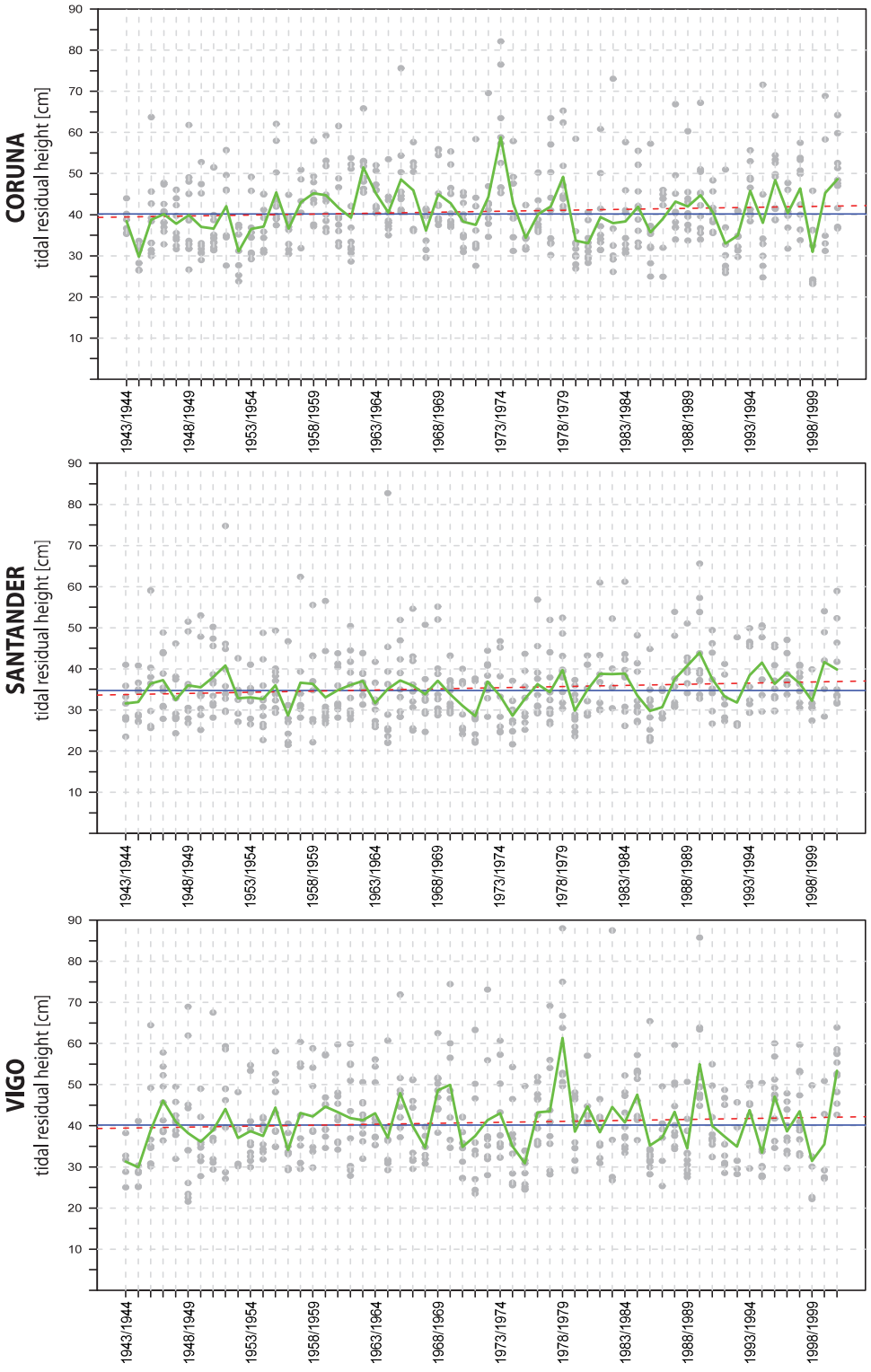

Figure 4.1: *Tidal residual records (grey dots) for the stations Coruna, Santander and Vigo* (1943 – 2001)*, with long term mean in blue, ONDJFM mean surge values (derived from seasonal 99.99th percentiles) in green and linear regressions in red (1943-2001).*

three stations. The two western tide gauges, Coruna and Vigo, show similar mean surge heights (approximately 40 cm) whereas the average for Santander is a bit lower (around 35 cm). With regards to the temporal evolution of the seasonal mean values there are some distinct features to be pointed out: the westernmost stations Coruna and Vigo exhibit a higher variability with respect to their maximum surge magnitudes than Santander, with the latter showing less pronounced positive and negative peaks. This observation is also supported on a seasonal basis with the grey dots in Figure 4.1 indicating a slightly larger spread of winter half year surges for Coruna and Vigo than for the one of Santander. When considering 2 standard deviations above the long-term mean as an indicator of exceptionally high events we obtain a tidal residual value of roughly 20 cm as an extreme surges threshold for all stations. Single events exceeding this threshold are more numerous for the two western stations. Seasons with similar mean surge height tendencies for all stations can be found e.g. in 1944/1945, 1956/1957, 1979/1980, 1998/1999 for "low extreme surge" periods and in 1951/1952, 1965/1966, 1978/1979 and 1989/1990 for "high extreme surge" periods (see Figure 4.1).

Table 4.1: *Results of the Mann-Kendall trend test: S, Kendall's tau and two-sided p-value.*

	Mann-Kendall test		
	S	*tau*	*p-value*
CORUNA	175	0.106	0.2431
SANTANDER	315	0.191	0.0352
VIGO	95	0.0575	0.5283

For all three stations the linear regression model calculated on the basis of seasonal mean values indicates an upward trend of mean surges over the observation period 1943 to 2001. However, the results of the Mann-Kendall trend test reveal that only the increase of surge heights for Santander is significant at the 95% level (see Table 4.1). As shown in Table 4.1 the p-values for the two western stations are much larger, denoting confidence levels ($(1-p)\times 100$) only at the 75% level for Coruna and at the 47% level for Vigo. Considering the 95% confidence level as the common threshold for a significantly increasing or decreasing trend (Hollander and Wolfe 1973), both tidal residual station records for Coruna and Vigo do not show a significant increase over the observation period. However, the observable positive slopes of the linear regressions calculated for all three stations may be attributed to the recorded mean sea level rise (see also Figure 1.1). Furthermore, the significant result of the trend test for Santander could have benefited from the overall smaller variability of the recorded tidal residual extremes compared to the surge observations for Coruna and Santander. Considering these aspects it does not seem reasonable to infer a true change in the intensity of extreme sea levels for the easternmost station Santander.

The ten highest surges for the period 1948-2001 are displayed in Figure 4.2. This shorter period has been chosen, so that the extracted highest tidal residual values can be directly used in combination with the NCEP/NCAR reanalysis dataset. Highest tidal residual heights are found for Vigo with a maximum height of approximately 88 cm (11 Feb 1979). Both, Coruna and Santander follow with a highest recorded tidal residual of around 82 cm (Coruna: 10 Dec 1973; Santander: 20 Jan 1965), but with Coruna showing higher values for all ten extremes and therefore holding the second rank. Santander shows the strongest decline in extreme tidal residual heights. For Vigo the highest three surges remain on a comparably high level, with, however, a decrease of as much as 10 cm towards the fourth highest recorded value and a more gentle lowering afterwards. For Coruna, the drop from the first to the tenth rank value is rather smooth and almost linear.

As can be seen in Figure 4.1, 1973/1974 is an extraordinary high surge season for Coruna which comprises three out of 10 highest tidal residual values (Figure 4.2). 1978/1979 represents a comparably intense surge season for Vigo with a seasonal mean surge value of more than 60 cm providing two of the stations' ten highest surges (Figure 4.1; Figure 4.2). For Santander no season stands out as clearly as for the two other stations. Nevertheless, 1989/1990 contributes two values to the stations top ten record being the highest surge season for this station according to seasonal percentile means (Figure 4.1; Figure 4.2).

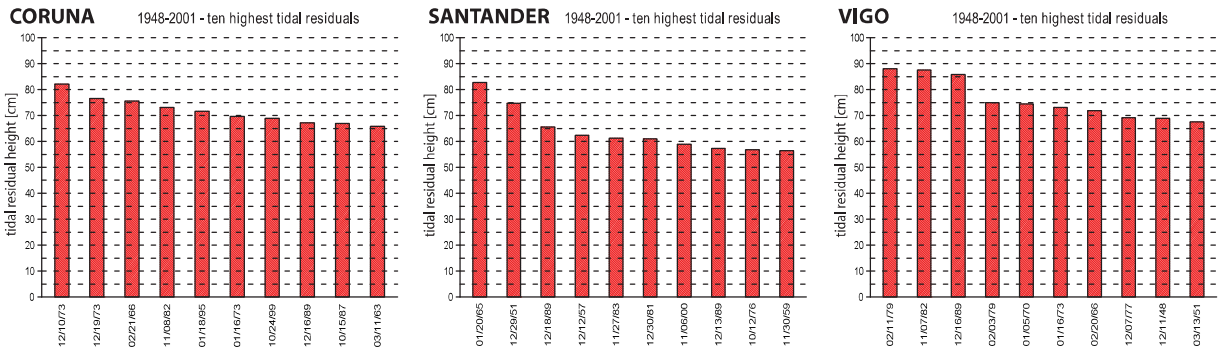

Figure 4.2: *The ten highest recorded tidal residual values for the period 1948-2001; dates are given in the form MM/DD/YY.*

According to Holt (1999) several independent studies were able to prove that changes in surge activity have so far been part of the natural variability on decadal timescales rather than a consequence of longer term climatic change due to anthropogenic influences. Looking at Figure 4.1 we can also detect a much higher interannual variability regarding surge strength compared to the not significant increase in maximum surge levels which might be induced by the global mean sea level rise. However, the future evolution of extreme sea levels in the study area does not necessarily have to show the same characteristics.

4.1.1 Return values of tidal residual extremes

The results of the return level calculations for the three stations are displayed in Table 4.2. Vigo reveals highest surge levels for each return period. For a 100-year event calculated with the dePOT approach, a tidal residual value of 86.9 cm (95% confidence interval: 80.67 cm, 99.22 cm) can be expected for Vigo, a 25-year event still yields a surge level of 79.09 cm (95% confid. int.: 74.47 cm, 87.54 cm). Coruna shows a 100-year return level of 79.77 cm (95% confid. int.: 74.89 cm, 90.26 cm). The 100-year return level for Santander yields 76.31 cm (95% confid. int.: 69.96 cm, 87.11 cm) which is lower than the 25-year return period for Vigo. As discernible in Figure 4.2, the statistically derived surge level heights for a 100-year return period are already observable in the corresponding station records between 1948 and 2001. A sea level of maximum 3 m above mean sea level for 100-year return levels is obtained at the coasts around Vigo considering tidal elevations of up to 2 m for the study area during spring tides (Marcos et al. 2009).

Table 4.2: *Results of the dePOT return level calculations for 100-, 75-, 50- and 25-year return periods; return levels a presented in cm;* 95% *confidence intervals in brackets.*

		CORUNA		
Return period [yr]	*100*	*75*	*50*	*25*
Return level [cm]	79.77	78.66	76.98	73.78
95% *confid. int.*	(74.89, 90.26)	(74.03, 88.72)	(72.70, 85.90)	(70.07, 80.85)
		SANTANDER		
Return period [yr]	*100*	*75*	*50*	*25*
Return level [cm]	76.31	74.74	72.44	68.27
95% *confid. int.*	(69.96, 87.11)	(68.80, 85.18)	(67.06, 82.36)	(63.79, 76.74)
		VIGO		
Return period [yr]	*100*	*75*	*50*	*25*
Return level [cm]	86.90	85.43	83.22	79.09
95% *confid. int.*	(80.67, 99.22)	(79.55, 97.41)	(77.82, 93.97)	(74.47, 87.54)

4.2 Surge related atmospheric circulation patterns

Extreme surges can be mainly attributed to anomalously low atmospheric pressure and strong onshore wind patterns (Bindoff et al. 2007; see also Chapter 1). In order to analyze these two relevant atmospheric parameters the five highest surges between 1948 and 2001 are selected for each station. Circulation patterns and wind fields related to the

three highest events of the station samples are displayed in Figures 4.3, 4.4 and 4.5. The fourth and fifth highest extreme events for each station can be found in the Appendix A. Additionally, the temporal evolution is displayed in the Appendix Figures A.1 - A.15 by 6-hourly absolute SLP composites of lead, surge and lag situations and corresponding wind fields. The surge SLP patterns in Figures 4.3, 4.4 and 4.5 are visualized through large scale 6-hourly SLP anomaly fields with respect to the 1961-1990 climatology, with shaded areas indicating the $\geq$ 95% significance levels (for more details see Chapter 3). The corresponding wind patterns are analyzed in vector form with shaded areas displaying wind strength.

Figure 4.3 shows the SLP anomaly and wind fields corresponding to the three highest recorded surges for Coruna between 1948 and 2001. The SLP patterns related to the highest surges present different atmospheric circulation patterns for the three events. The highest recorded surge is connected with a tripole pattern: positive SLP anomalies are located over the western North Atlantic with most positive pressure values east of Newfoundland and covering most of continental Europe. Negative anomalies have a center over the Norwegian Sea. This circulation pattern yields weak winds throughout the whole selected North-Atlantic region from 30°N - 55°N and 35°W - 5°E. Highest wind speeds can be observed at the western coasts of Ireland. For the second highest surge the large-scale circulation shows a much larger SLP range. A very strong low pressure system centered northwest of Coruna is flanked by areas of positive pressure anomalies over the whole western North Atlantic to the west and over Eastern Europe and the Eastern Mediterranean region to the east. Very strong northerly to northwesterly winds can be observed for the area around 20°W and north of approximately 40°N with highest wind speeds west of Ireland. The SLP pattern for Corunas third highest surge is dominated by anomalously low pressure, again centered northwest of Coruna. Significant positive SLP anomalies can be found over Greenland. Winds are circulating anticlockwise around the perturbation centre with highest wind speeds west of the Strait of Gibraltar and west of Ireland.

Neither SLP nor wind shows any surge forcing characteristics for the highest recorded event at Coruna on 10 Dec 1973 (Figure 4.3, top). Reanalysis even reveals the SLP anomaly to be significantly positive and wind is very weak with less than 5 m/s around the station. Two possible explanations might be responsible for this situation: The relatively coarse resolution of the available reanalysis dataset might not allow for the detection of a predominant local surge forcing. However this seems not to be very reasonable as the large-scale atmospheric circulation obtained for the 10 Dec 1973 (Figure 4, top) does not show any plausible atmospheric forcing pattern at all. The other possibility is that some inconsistency might not have been detected in the original tide gauge data although it has been preprocessed and quality checked in advance. An error in the observation process recording a tidal residual which is too high could have led to the unaccountable extreme

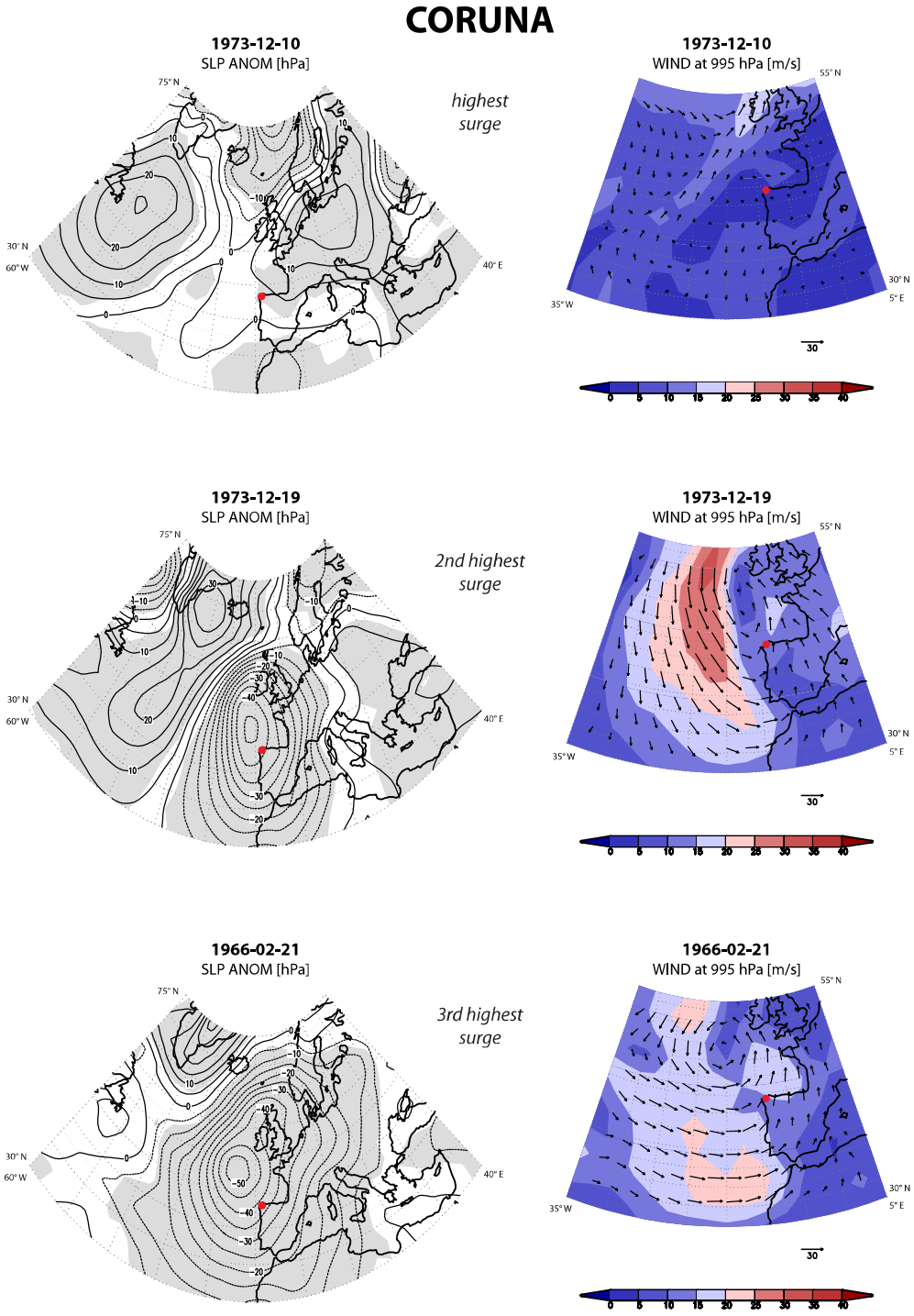

Figure 4.3: *Large-scale circulation patterns corresponding to the three highest tidal residuals for CORUNA from 1948 to 2001; left: NCEP/NCAR reanalysis SLP anomalies with respect to the 1961-1990 climatology; date in YYYY-MM-DD; shaded grey areas indicating* $\geq$ 95% *significance levels; right: NCEP/NCAR reanalysis wind fields; arrows displaying direction and strength; station location shown as red dot.*

value. The highest detected surge for Coruna is therefore excluded from further analysis. For the second (19 Dec 1973) and third highest surge event (21 Feb 1966), SLP around Coruna shows surge forcing characteristics with pressure anomalies of -40 hPa at the station itself and up to -50 hPa slightly north-northwest of it. Thus, at least 40 cm of surge height can be attributed to the IB effect directly without taking any local effects into account (e.g. Pirazzoli 2000). Southwesterly winds with an average strength of 10-15 m/s are present around Coruna in both cases which would tend to further increase the surge heights. However, the influence of a band of very strong winds on 19 Dec 1973 might be considered to be even more supportive in relation to the second highest surge by pushing water masses towards the coasts around Coruna. Strongest winds of more than 30 m/s are recorded northwest of the Iberian coasts blowing from northerly directions. Resulting winds for Corunas third highest surge are less strong than for the 1973 case with a large area indicating higher wind speeds shifted more to the south. Generally, the fraction of the surge that could be explained by the large scale pressure and wind fields is considerably high for the 1973 and 1966 events. Focussing on these remaining two surges presented in Figure 4.3 we can clearly relate the SLP pattern of the second highest surge to a Blocking type WR with anomalous high pressure over Central to Eastern Europe (see Section 3.2 for more details). The large-scale circulation for Coruna's third highest event considerably resembles the Greenland Anticyclone WR with its key features of high pressure over Greenland and a strong perturbation travelling eastwards. If we also consider the circulation for the fourth highest surge at Coruna as a substitute for the highest recorded one (Appendix Figure A.4) we can detect a structure again related to the Blocking type WR.

Large-scale circulation patterns associated with the highest three surges at Santander are displayed in Figure 4.4. The SLP pattern corresponding to the highest recorded surge in 1965 can be characterized by an extensive area of negative SLP anomalies over Europe and the Mediterranean area and a smaller perturbation of anomalous negative SLP southeast of Greenland. To the west, significantly positive SLP anomalies can be observed east of Newfoundland. Resulting strong winds are present in mainly two regions within 30°N - 55°N and 35°W - 5°E: Highest wind speeds blowing from southwesterly direction are recorded for the area around 35°W and approximately 50°N. Strong northwesterly winds are present in the Bay of Biscay, while westerly winds can be observed for the Western Mediterranean. For the second highest surge the NCEP/NCAR reanalysis also yields negative pressure anomalies over Europe, but extending further to the northeast over the North Sea than in the circulation pattern related to Santanders highest surge. To the west, two areas of positive SLP anomalies are present which are divided by a smaller perturbation with anomalous negative SLP. Besides some stronger wind fields over the North Atlantic at around 35°W and 50°N and again over the western Mediterranean, northwesterly winds are recorded to be especially strong in the Bay of Biscay. The SLP pattern for the third

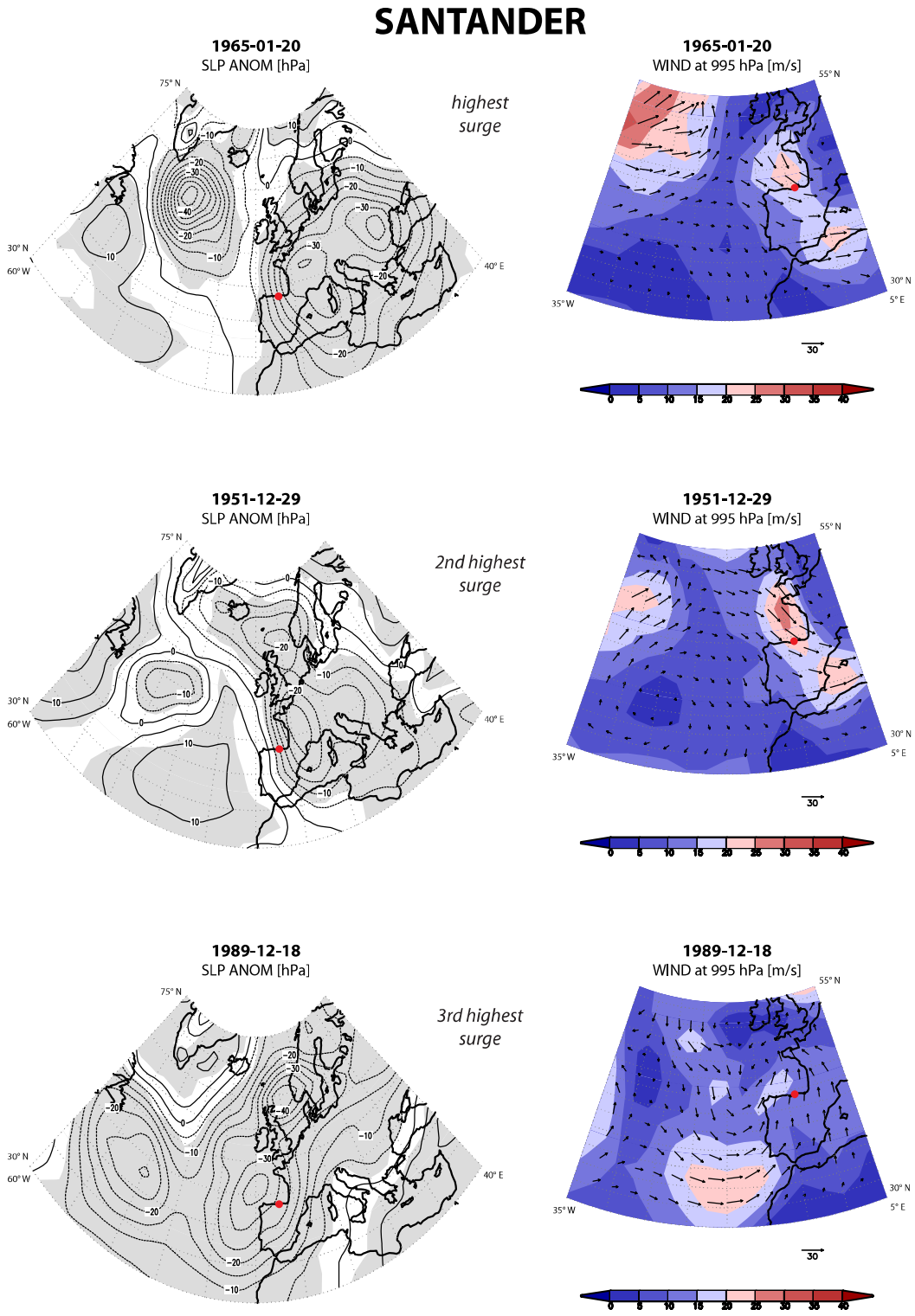

Figure 4.4: *As Figure 4.3 but for Santander.*

highest surge presents a different picture: A band of connected negative SLP anomaly fields covers almost the whole Northern Atlantic area from Newfoundland in the west to Western Norway in the northeast. Areas with slightly positive SLP anomalies are present around Greenland and in the Eastern Mediterranean region. Moderate winds are recorded for the largest part of the area under investigation, except a field of stronger westerly winds west of the Strait of Gibraltar.

Compared to Coruna, a different forcing pattern appears to be dominant for the easternmost station which is especially sensitive to northerly winds approaching from the Bay of Biscay. As can be seen, the highest two events in 1965 and 1951 are related to anomalous low pressure east of Santander with very strong onshore winds blowing from the northwest (see Figure 4.4). SLP anomalies are clearly negative with -20 hPa (20 Jan 1965) and around -10 hPa (29 Dec 1951) at the station location. The high wind speeds of more than 20 m/s caused by the strong pressure gradients have to be considered as fundamental forcings in both cases. The circulation patterns for the two highest surges at Santander resemble the Atlantic Ridge WR (see Section 3.2 for more details). The ridge is shifted far to the east in both specific cases leading to the observed strong gradient winds. For 29 Dec 1951, the well developed high pressure system over the Atlantic west of the Iberian Peninsula is an additional and distinct indicator for the Atlantic Ridge regime (Vautard 1990). If we take a look at 18 Dec 1989 being the third highest event recorded for Santander the large-scale circulation pattern features a completely differing SLP and wind field (see Figure 4.4, bottom). The negative SLP anomaly is recorded to be almost 30 hPa at the station location being part of a very pronounced band of low pressure systems reaching from the western North Atlantic to Scandinavia. A large moderately positive pressure anomaly can be observed over Greenland which relates this large-scale North Atlantic surge pattern to a Greenland Anticyclone regime. The low pressure system located over the western Bay of Biscay produces offshore winds at Santander with average speeds of 10 to 15 m/s leading to onshore winds at the western coasts of the Iberian Peninsula comparable to the 1966 situation at Coruna. This factor is clearly impeding an atmospheric surge forcing at Santander. Only the reanalysis SLP is able to induce a surge up to a certain degree in 1989; the IB effect would yield some 30 cm. However, the remaining more than 30 cm of the recorded tidal residual height of 65 cm have to be attributed to forcings which are not displayable with the NCEP/NCAR reanalysis, for example, local effects such as regional wind patterns which cannot be resolved by the 2.5° grid cells of the reanalysis data. Although the situation is not as indistinct as for the highest recorded surge at Coruna in 1973 (Figure 4.4, top) there is again one out of three atmospheric patterns related to the three highest detected surges at Santander, which cannot be fully explained by the reanalysis SLP and wind fields.

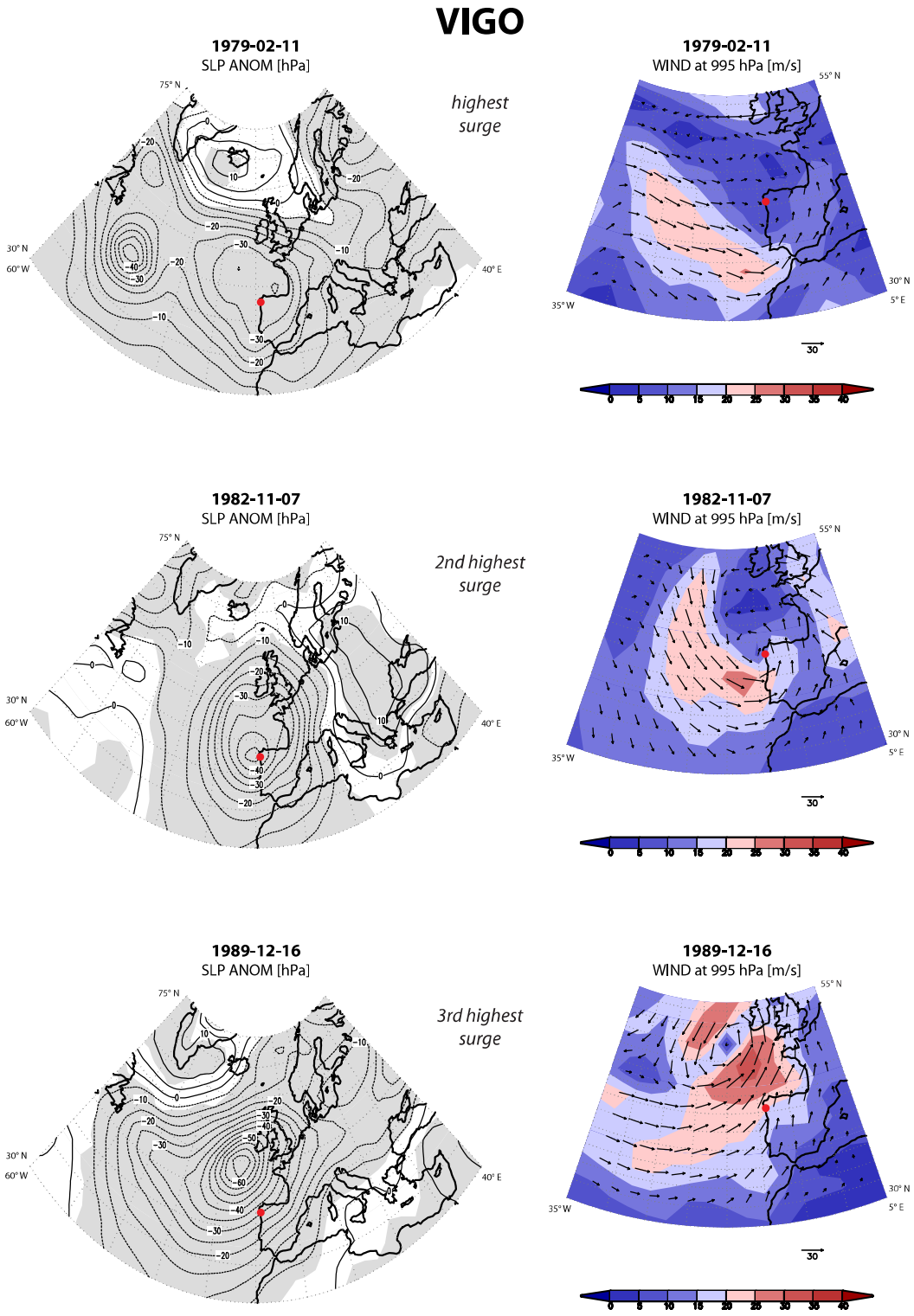

Figure 4.5: *As Figure 4.3 but for Vigo.*

In Figure 4.5, SLP anomaly and wind fields are displayed for Vigo and its highest surge of 11 Feb 1979, the second highest event recorded on 07 Nov 1982 and for the third highest surge event at 16 Dec 1989. Although all reanalysis SLP patterns show an area of negative SLP anomalies around the northwestern Iberian Peninsula, some differing features have to be distinguished for each surge event. The SLP pattern for the highest recorded surge at Vigo is characterized by three connected low pressure systems reaching from the far west close to Newfoundland to the northeast around southern Finland and Russia. A small area of positive pressure anomalies is situated over Iceland. Strong westerly winds are recorded for a large area of west of the Iberian Peninsula, spanning from around 30°W to 5°W. For the second highest surge the large-scale SLP pattern shows following key features: a pronounced low pressure system is centered slightly west the northwestern Iberian Peninsula, with an area of positive SLP anomalies over eastern Europe. In the northwest, anomalous low SLP is present in the Labrador Sea. Wind is blowing strongly from westerly direction close to the western Iberian coast, with the wind field extending far to the west. The SLP pattern which corresponds to the third highest surge is dominated by a very strong low pressure system centered southwest of Ireland. Weak positive SLP anomalies are observable around southern Greenland. Resulting wind fields are strongest for the eastern North Atlantic region west of France blowing from southwesterly directions and for an area west of Ireland blowing from the northeast.

Vigo is located around 150 km south of Coruna. A priori, the geographical closeness to Coruna suggests also similar atmospheric forcing patterns for the top surges. For the highest surge event at Vigo, which represents also the highest recorded tidal residual for all three stations, an extensive low pressure system with an SLP anomaly lower than -30 hPa is found to be centered over Vigo. However, this central position yields a strong IB effect but almost no wind for Vigo at the time of the surge (Figure 4.5, top right). For the second highest event in 1982 the atmospheric forcing pattern provided by the reanalysis is much more distinct. The centre of a strong perturbations yields a negative SLP anomaly of about 45 hPa at the station location. Wind is blowing onshore from southwesterly directions with around 15 to 20 m/s. Strong winds of more than 30 m/s are observed southwest of the station which might further amplify local surge levels at Vigo. The third highest event recorded for Vigo corresponds to a circulation pattern which provides the strongest large-scale surge forcing characteristics of reanalysis SLP and wind with respect to all three stations: A strong low pressure system with a core SLP anomaly lower than -65 hPa north of the station still accounts for around -30 hPa around Vigo; Related to this pressure pattern winds with a speed of 20 to 25 m/s are found to blow onshore from southwesterly directions.

If we position the three single events within the four predominant large-scale atmospheric patterns over the North Atlantic of Vautard (1990), we obtain the following picture: The

highest and the third highest surge for Vigo resemble the Greenland Anticyclonic (GA) atmospheric patterns. Although the positive pressure anomaly extends far to the east in the 1979 case, the GA regime remains the summarizing pattern of choice especially because of the low SLP perturbation path at around 45° N. The situation for 1989 can be considered to be a more ideal representation of the sample WR case. The circulation pattern corresponding to the second highest surge in 1982 shows a similar constellation like the Blocking situation with a high pressure system located over Eastern Europe.

Summing up some key features of the circulation patterns displayed in Figure 4.5, we can say that Vigo is much more susceptible for winds from southwesterly direction than Coruna. Coruna is located at a coastline much more exposed to northwesterly winds, but at the same time protected from southerly wind directions by Cap Finisterre. For the two stations located to the West the wind fetch contributing to sea level high stands can be very large. Thus, also wind fields which are off the coast should be taken into account for the analysis of the influence of wind on the surge level of the selected stations.

Four out of the analyzed eight large-scale circulation patterns can be attributed to the Greenland Anticyclonic WR. Two out of eight pressure fields are related to Blocking situations, whereas the remaining two out of eight circulation patterns represent the Atlantic Ridge type WR with its high surge forcing potential at northern Iberian coasts.

4.3 Clustering of surge related circulation patterns

The reanalysis dataset has so far been used for the identification of large-scale pressure and wind fields related to the five highest surge events recorded at each station from 1948-2001. The Greenland Anticyclone (GA) as well as a Blocking (BL) type patterns have been detected to form the dominating atmospheric circulation at the time of the selected maximum surges. In this section, a much bigger sample of surges is investigated without restricting the analysis to the five highest recorded surges for each station. Cumulated seasonal 99.99th percentiles over the period 1948 to 2001 yield a sample size of more than 500 surge events for each station. Again, the temporally closest 6-hourly averaged pressure patterns have been selected to represent the extreme event covering the region 30°N - 75°N and 60°W - 40°E. As mentioned in Chapter 3, the SANDRA clustering technique has been applied with a number of nine clusters to determine the most representative circulation patterns related to surges at the three selected stations.

The quality of the clustering process can be assessed in Figure 4.6 displaying the silhouette plots for each station. Only few of the obtained clusters show a considerable number of members with a negative silhouette width (Coruna: cluster 3, 5, 6 and 9; Santander:

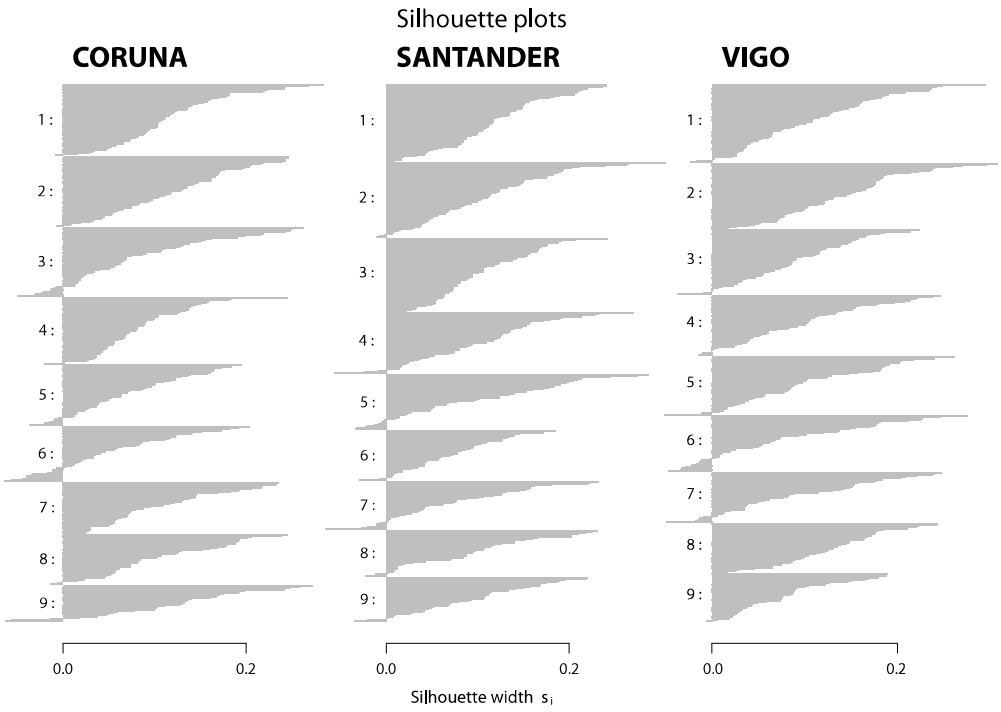

Figure 4.6: *Silhouette plots for the nine clusters of Coruna, Santander and Vigo; Silhouette width magnitude is indicated at the bottom.*

cluster 4, 5 and 7; Vigo: cluster 5, 6 and 7). Thus, the SANDRA clustering technique can be considered to yield reliable results with generally well separated clusters.

Scaled mean anomalies of the SLP clusters are presented with reference to the 1961-1990 SLP average (Figures 4.7, 4.8, 4.9). According to Brown and Hall (1999), t-values with a significance $\geq 95\%$ are displayed as shaded grey areas and are used as a stability measure for the cluster composite.

For Coruna, 13.4% of the sample members are summarized in Cluster 1, decreasing to 6.8% for Cluster 9 (see Figure 4.7). Around 14.4% of all sample members are represented in Cluster 1 for Santander; Cluster 9 still accounts for 8.4% of the sample members (Figure 4.8). The clustering results for Vigo present the following values: 14.6% of the members are grouped under Cluster 1 decreasing to 9.1% of the sample members shown by Cluster 9 (Figure 4.9). The absolute SLP outputs of the cluster analyses can be found in the Appendix Figures B.1 - B.3. In all three cases the SANDRA clustering is able to define large-scale circulation patterns which are related to well-known circulation types. In the following, a more detailed analysis is provided for each station.

The nine resulting clusters for Coruna are displayed in Figure 4.7. Except for Cluster 8 all clusters show a distinct large-scale pressure pattern which could be responsible for a surge through anomalous low atmospheric pressure and related onshore gradient winds or at least

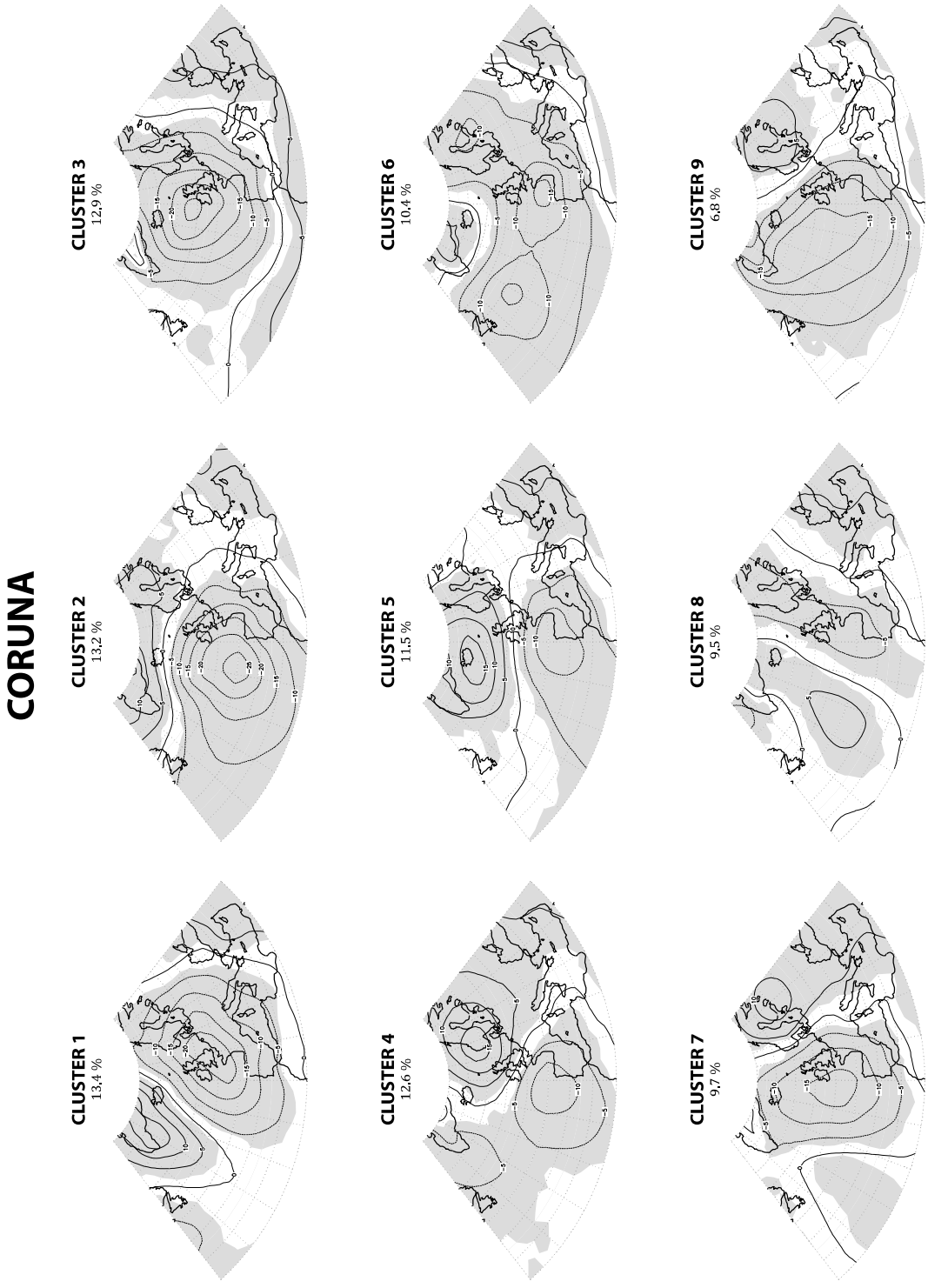

Figure 4.7: *Results of the SANDRA cluster analysis for CORUNA; Cluster composites are displayed as scaled mean SLP anomalies with reference to the 1961-1990 average; shaded grey areas indicating* $\geq 95\%$ *significance level; percentage of the included sample members for each cluster is shown below the cluster number.*

support an external (local) forcing leading to recorded tidal residual extremes at the station. The first three clusters present very strong negative anomalies. Clusters 1 and 3 show strong negative pressure anomalies centered close to or over the British Isles leading to strong westerly flow at Coruna. Cluster 2 reveals an anomalous low pressure system centered west of Coruna. Near surface winds are expected to blow from southwesterly direction in this case (absolute SLP patterns are given in the Appendix Figure B.1). All three clusters appear to represent a variation of the GA pattern. Another GA type pattern is found in Cluster 6. In this specific case a band of negative pressure anomalies is covering the typical perturbation track over the Northern Atlantic reaching as far as to Scandinavia. Clusters 4, 7 and 9 match best the characteristics of the BL pattern, with Cluster 7 representing best the sample BL case with a low located west of Ireland, blocked by an anomalous high pressure system with its center over Southern Scandinavia. Cluster 4 can be considered to be a more independent case compared to the two other clusters with its Scandinavian anomalous high pressure system extending further to the west. Still, all three clusters show key characteristics for surges at Coruna, i.e. anomalous negative pressure and onshore geostrophic wind direction. Cluster 5 shows a well defined anomalous low pressure system over the northwestern Iberian Peninsula which is located south of a strong positive pressure anomaly over Iceland. Plaut and Simonnet (2001) have introduced a circulation regime called West Blocking (WBL), with an anticyclonic cell located over Scotland extending to Eastern Europe on average and a low pressure system in the vicinity of Newfoundland. Cluster 5 seems to be combination of two WRs, the WBL and GA regime. Compared to e.g. Cluster 1 or Cluster 3, strong onshore winds caused by pronounced pressure gradients close to the station cannot be expected for Cluster 5 because pressure gradients are weak. Thus, the dominant large-scale atmospheric forcing parameter appears to be SLP in this case.

A slightly different picture is presented by the nine clusters for Santander (Figure 4.8; see also Appendix Figure B.2). Cluster 1 shows an anomalous low pressure system centered over Central Europe and a high pressure anomaly field over the Northern Atlantic Ocean. This pattern resembles the Atlantic Ridge WR rotated and shifted moderately in northwesterly direction. Anomalous low pressure over Santander and observable pressure gradients leading to onshore winds at the coasts around the station appear to favor a high tidal residual event in this case. A similar pattern can be observed for Cluster 6 with the positive pressure anomaly shifted far to the south. The characteristic 'Atlantic Ridge' is detectable west of the Iberian Peninsula causing northwesterly flow towards Santander. Blocking patterns are shown in Clusters 2, 3 and 5. The circulation characteristics for the Cluster 3 case can be considered to be one of the most distinct surge forcing patterns for Santander, although the blocking anticyclone is located far to the east. For Cluster 2 the anomalous low pressure system is surrounded by a positive pressure anomaly to the north

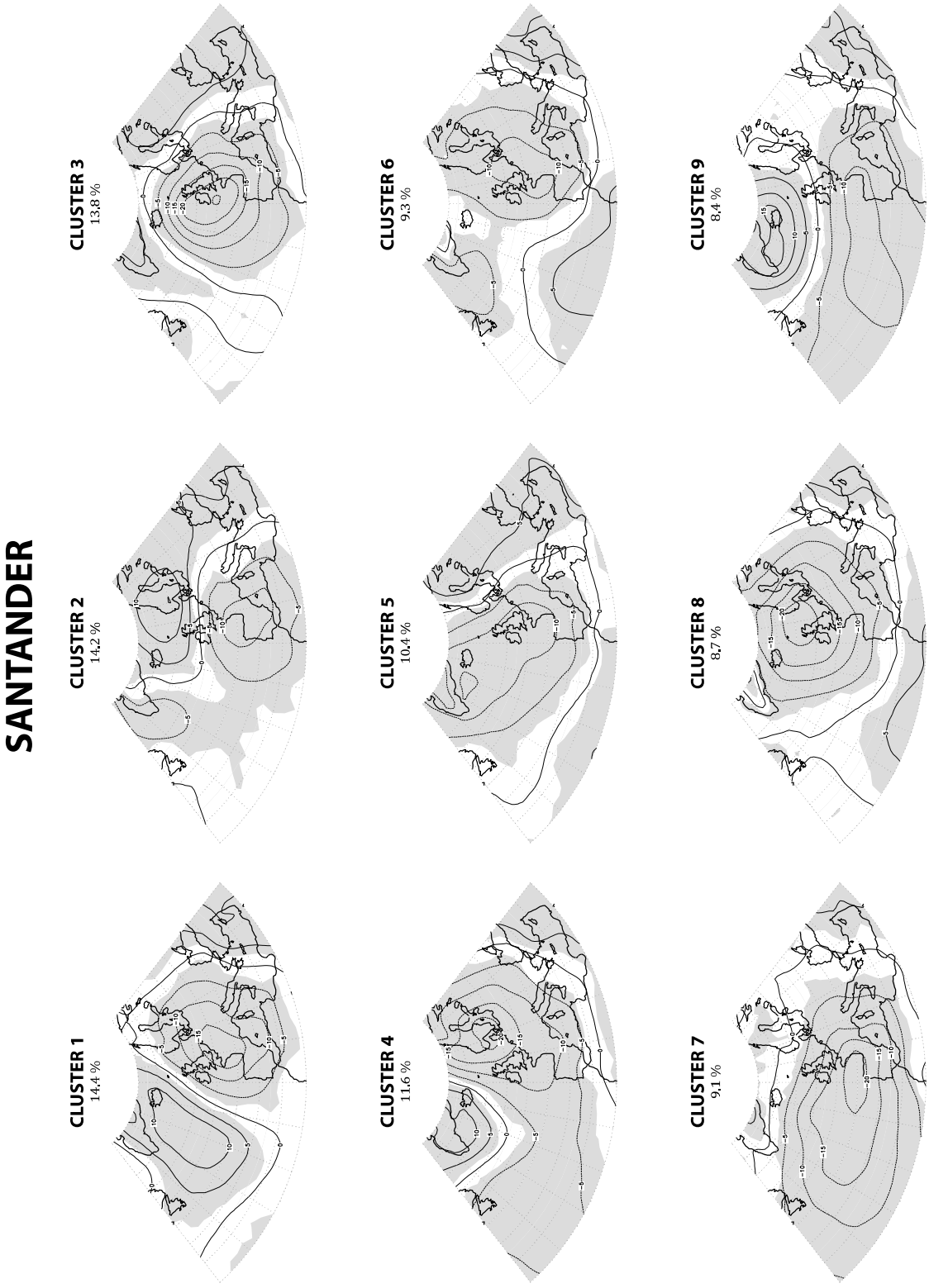

Figure 4.8: *As Figure 4.7 but for Santander.*

and west. The Cluster 5 circulation pattern is similar to the one of Cluster 3, but with the negative pressure anomaly stretched far to the northwest. Different shapes of the GA regime are found in the patterns of Cluster 4, 7 and 8. In the fourth cluster the anomalous low pressure system is located over Scandinavia being part of an anomalous low pressure band over the entire Northern Atlantic. Cluster 8 and especially Cluster 7 show extended anomalous low pressure systems over the entire Northern Atlantic (Cluster 7) and centered over the North Sea (Cluster 8). Low SLP would dominate the atmospheric surge forcing signal for Cluster 7. For Cluster 8 it seems to be the large-scale flow pushing water in the Bay of Biscay which could be the more important forcing factor. For Cluster 4 the situation is less clear, however a negative scaled SLP anomaly value of less than -10 can be observed for Santander. The last Cluster 9 provides a circulation pattern which shows similarities with the pattern identified for Coruna's Cluster 5. With its relatively large positive pressure anomaly over Iceland and a broad field of negative pressure anomaly to the south, the large-scale pattern of cluster 9 could be positioned again between the WBL pattern and the GA type 'weather regime'. In general, the cluster patterns found for Santander show more diverse circulation patterns at the expense of the significance of each cluster composite.

Figure 4.9 shows the results of the cluster analysis for Vigo (see also Appendix Figure B.3). The large-scale circulation pattern of the first Cluster is exceptional with respect to several aspects: i) With 14.6% of the sample members grouped, the first cluster for Vigo aggregates 2% more members than Cluster 2. ii) Cluster 1 represents more or less the 'ideal' large-scale atmospheric surge forcing pattern, with a very pronounced anomalous low pressure system providing a strong negative scaled SLP anomaly for Vigo with its center located northwest of the station. Additionally, a pressure gradient on the southern margin of the low indicates strong southwesterly onshore winds. Relating this pattern to the classification of Vautard (1990), it can be described best as a combination of GA and BL. Generally well-defined Blocking type regimes can be attributed to the circulation patterns of Clusters 2, 5 and 6. The latter seems to provide a lot of explanatory power regarding an atmospherically induced surge with weaker but similar characteristics as the pressure pattern of the first cluster. For Cluster 5, the anomalous low pressure area is less distinct, whereas the anticyclonic blocking system over Scandinavia shows stronger features. As far as Cluster 2 is considered, the blocking anticyclone is located much more to the south with the negative pressure anomalies reaching to the Norwegian coasts. Cluster 3 provides a pattern which is also clearly able to induce surges at Vigo being related to the GA regime: The center of the negative pressure anomaly is located over the British Isles providing negative scaled SLP anomalies of almost -15 for the area around Vigo and a wind from presumably westerly to northwesterly directions. Circulation patterns for Cluster 7 and Cluster 8 also match GA characteristics. Both show a large area of anomalous high

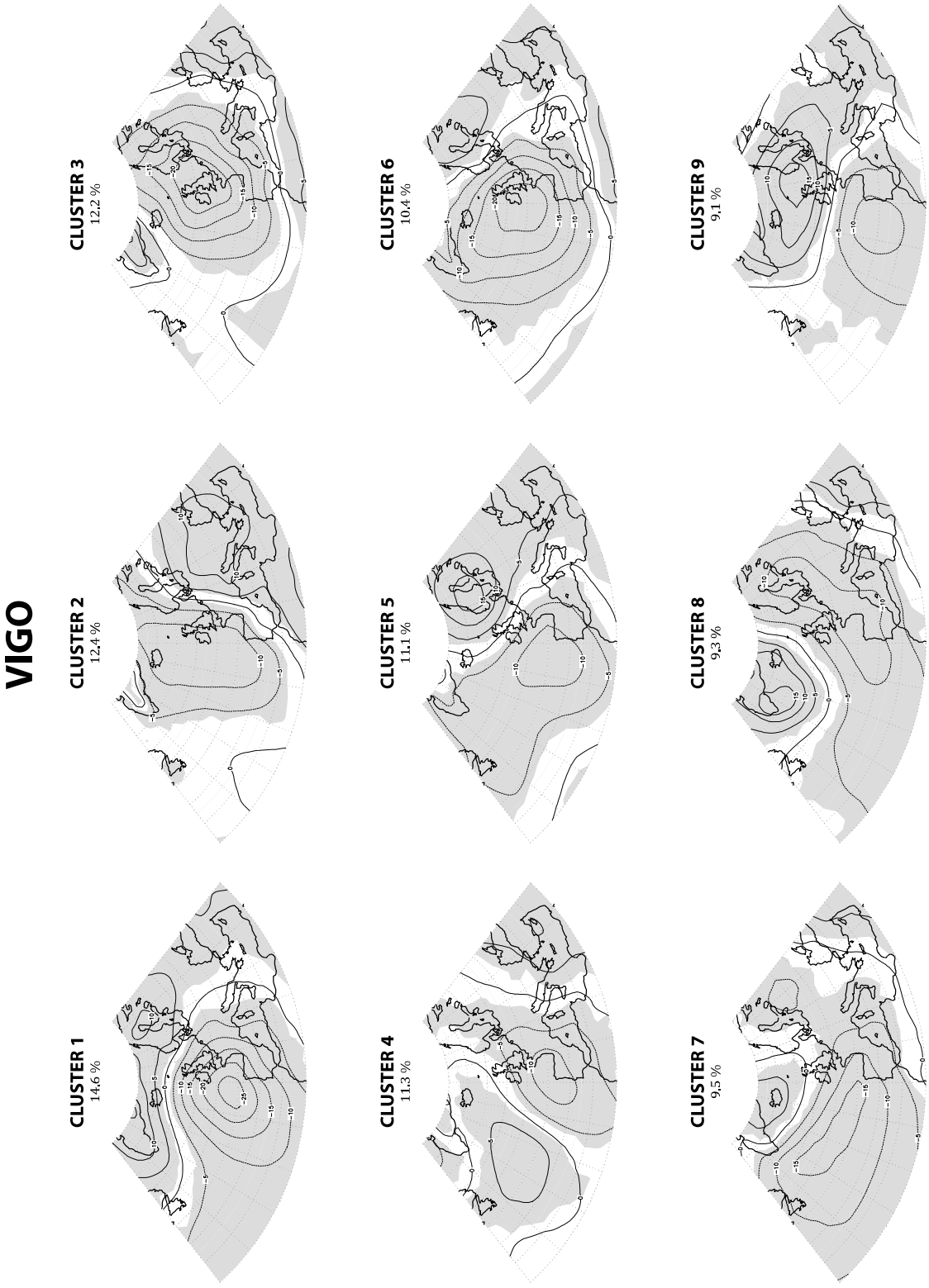

Figure 4.9: *As Figure 4.7 but for Vigo.*

pressure over Greenland extending in southwesterly and southerly directions. A broad area of anomalous low pressure is located over the Northern Atlantic for Cluster 7, whereas the negative pressure anomaly is shifted to Northern Europe for Cluster 8. However, the cluster analysis provides two outstanding circulation patterns also for Vigo. Cluster 4 shows similarities to the pattern retrieved for Santander's cluster 1, slightly less pronounced though. This time the negative pressure anomaly is located more to the south. But the structure of the 'Atlantic ridge' which is shifted and turned to the northwest is comparable to the Santander AR case. The pattern for Cluster 9 perhaps represents the best example for the additional regime introduced by Plaut and Simonnet (2001). With the centre of the anticyclonic cell located over northern Scotland it almost perfectly meets the criterion for a WBL regime. However, the atmospheric surge forcing for Vigo does not appear to be high in this situation. The same can be stated for the circulation pattern displayed for Cluster 4.

As expected, an anomalous low pressure system with its center located either at the station itself or most of the time north or northwest of it appears to be most frequently connected to the extreme events of the selected clustering sample. Approximately 37% of the presented cluster composites can be associated with a GA circulation pattern, around 33% with the Blocking WR. Consequently, around 70% of the derived clusters can be either assigned to the GA type or the BL type WR. This way, the dominance of these patterns, already detected for the five highest events at each station, can be proven by the cluster analyses based on much larger surge samples. The remaining fraction of cluster composites is related to a modified AR situation, especially conclusive for Santander, or to a mixture of intense GA and WBL.

According to Lozano et al. (2004) storms which are affecting the northwestern Iberian Peninsula are very frequent during atmospheric pressure blocking over the North Eastern Atlantic. These findings support the clustering results which have been presented above, indicating surge related BL and GA type circulation patterns to be most frequent around the study area. It has been pointed out that only very few clusters do not show a surge forcing potential at all, e.g. Corunas cluster 8.

In their study, Plaut and Simonnet (2001) show that the yearly frequencies of WRs display no significant trends over the Northern Atlantic region for the last 40 years. However, a top-down approach inferring no changes in sea level extremes which have been analyzed to appear predominantly at Greenland Above and Blocking WR in the study area is not allowed. The occurrence of a WR does not necessarily cause a surge (e.g. Ullmann and Moron 2008).

As already mentioned in Section 3.2.2, scaled pressure anomalies do not map absolute values in hPa. Thus, the actual forcing fraction which could be assigned to large-scale

atmospheric parameters cannot be quantified using this approach. However, this has not been the primary goal of the clustering process applied on the cumulated ONDJFM 99.99th percentile tidal residuals. The intention was rather to define large-scale circulation pattern composites for the clustered extreme events at each station which can be summarized by few dominating circulation regimes. Despite some minor cluster member mismatches which are acceptable for this first overview (see Figure 4.6), the SANDRA clustering technique succeeds in classifying and compiling the SLP patterns related to the recorded extreme events.

Generally, there are multiple aspects which could explain variations of the relationship between extreme sea levels and atmospheric circulation over a longer observation period according to Ullmann et al. (2008): i) Atmospheric variability, e.g. a long-term change in mean SLP fields, might be responsible for a changing relationship of the forcing circulation pattern and the surge (Wakelin et al. 2003) ii) The reliability of the sea level observations could be questioned because of inconsistent records causing differing interrelations iii) Pure stochastic processes might affect the low frequency variability (Gershunov et al. 2001) iv) Coastal erosion and shore recession close to the tide gauge station could also feedback on the correlation between sea surge and large scale circulation pattern manipulating observed sea level measurements (Suanez and Provansal 1996).

4.4 Storms registered in the GTECCA

Based on 6-hourly interval statistics, 21 storms, originating in the tropics, crossing the Northern Atlantic and reaching the study area, have been identified. Only three of these storms were experienced during the study season (ONDJFM). However, none of these registered storms is connected with the recorded extreme tidal residuals at Coruna, Santander or Vigo.

Figure 4.10 illustrates the paths of the storm tracks with tropical origin which hit the target area. Perturbations and related storms travelling from west to east in the winter season are generally expected to show different characteristics: The majority of winter cyclones are supposed to approach European coasts from westerly positions and follow a well-defined northeastwards route originating from the vicinity of Newfoundland (Lozano et al. 2004). GTECCA data can prove that most of these cyclones concentrate in the area southwest of Iceland with maximum intensities around midwinter. According to Lozano et al. (2004) and based on some further analysis of the GTECCA data, cyclones reaching the Iberian Peninsula and Bay of Biscay have the tendency to travel in a uniform easterly direction at "almost constant latitude".

The atmospheric circulation patterns which have been identified to provide surge forcing characteristics in the previous Sections 4.2 and 4.3 only show the pressure fields at the time of the surge. With the GTECCA data it is possible to obtain a general picture of the spatial and temporal evolution of perturbations travelling eastwards over the Northern Atlantic region.

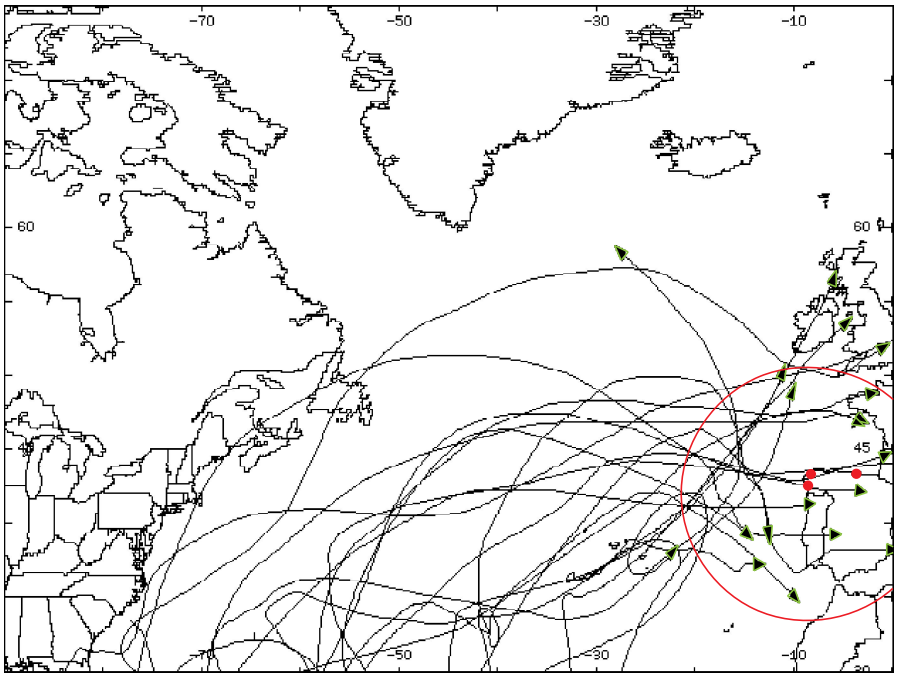

Figure 4.10: *GTECCA storms hitting a target area with 1000 km radius around 42.8° N and 8.5° W for the period 1965-1995; each black line represents one storm track; target area represented by the red circle; red dots showing station location of Coruna, Santander and Vigo.*

4.5 Future cyclonicity changes over the North Atlantic

SLP has been chosen as a first indicator of changes in the atmospheric mean state over the Northern Atlantic area. ECHAM5-OM1 SLP anomaly composites for the SRES scenarios A1B and A2 (2071-2100) referenced to the control run 20C (1961-1990) are presented in Figure 4.11. SLP anomalies have been calculated on the basis of seasonal ONDJFM mean composites (see Appendix Figure C.1). The anomaly maps show a band of positive SLP anomalies between around 35°N and 45°N for the A2 case which differs from the A1B case yielding two areas of positive SLP anomalies southeast of Newfoundland and over the Mediterranean region (see Figure 4.11). The region of negative anomalies around

Greenland is shifted slightly more to the north under the A2 than under the A1B scenario, but also extends further to the east.

The A1B pressure anomaly map indicates increasing SLP values between 0 and 1 hPa around the study area for the period 2071-2100. For A2 conditions, SLP shows values for the northwestern Iberian Peninsula which are between 1 and 2 hPa higher for 2071-2100 compared to the reference period 1961-1990. Thus, the scenario based on higher greenhouse gas emissions yields a stronger increase in SLP for the region under investigation than the moderate emission scenario A1B. However, these changes are not significant according to the applied student t-test (see Appendix Figure C.2).

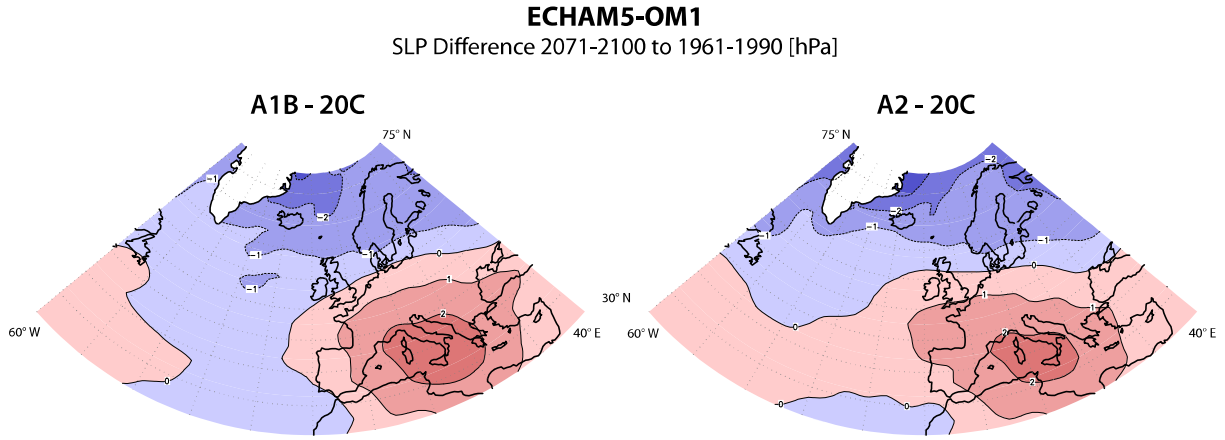

Figure 4.11: *ECHAM5-OM1 SLP anomaly fields for SRES A1B and A2 in hPa; Scenario composites cover the period 2071-2100; The 20C control run is used as reference (1961-1990); values for Greenland are excluded due to mean land elevations >1500 m.*

It is evident that the analysis of SLP is not suitable for the presentation of a comprehensive picture of resulting changes in circulation over the North Atlantic and the northwestern Iberian Peninsula. However, the SLP difference maps in Figure 4.11 visually indicate a change in the atmospheric mean states between the periods 1961-1990 and 2071-2100 which furthermore differs for the two selected IPCC emission scenarios A1B and A2.

In order to analyze future changes in storminess for the North Atlantic region, not simple SLP but the spatial distribution and intensity of SLP storm tracks is analyzed in the following (see Section 3.3.2 for more details). A changing storminess is supposed to feedback also on the occurrence and intensity of extreme sea levels around the northwestern Iberian Peninsula (e.g. Tsimplis et al. 2006). Figure 4.12 shows SLP storm track results for NCEP/NCAR reanalysis data and the 20C ECHAM5-OM1 model output both representing present-day forcing conditions (1961-1990) plus SLP storm tracks for the two scenarios A1B and A2 (2071-2100). For the period 1961-1990, NCEP/NCAR reanalysis storm track and the reference 20C ECHAM5-OM1 storm track show very similar patterns and intensities

for the Northern Atlantic region with highest wave activities over Iceland and east of Newfoundland (Figure 4.12, top). The similarity of these two datasets allows for a reliable comparison of future to present-day storm track changes based on ECHAM5-OM1 data.

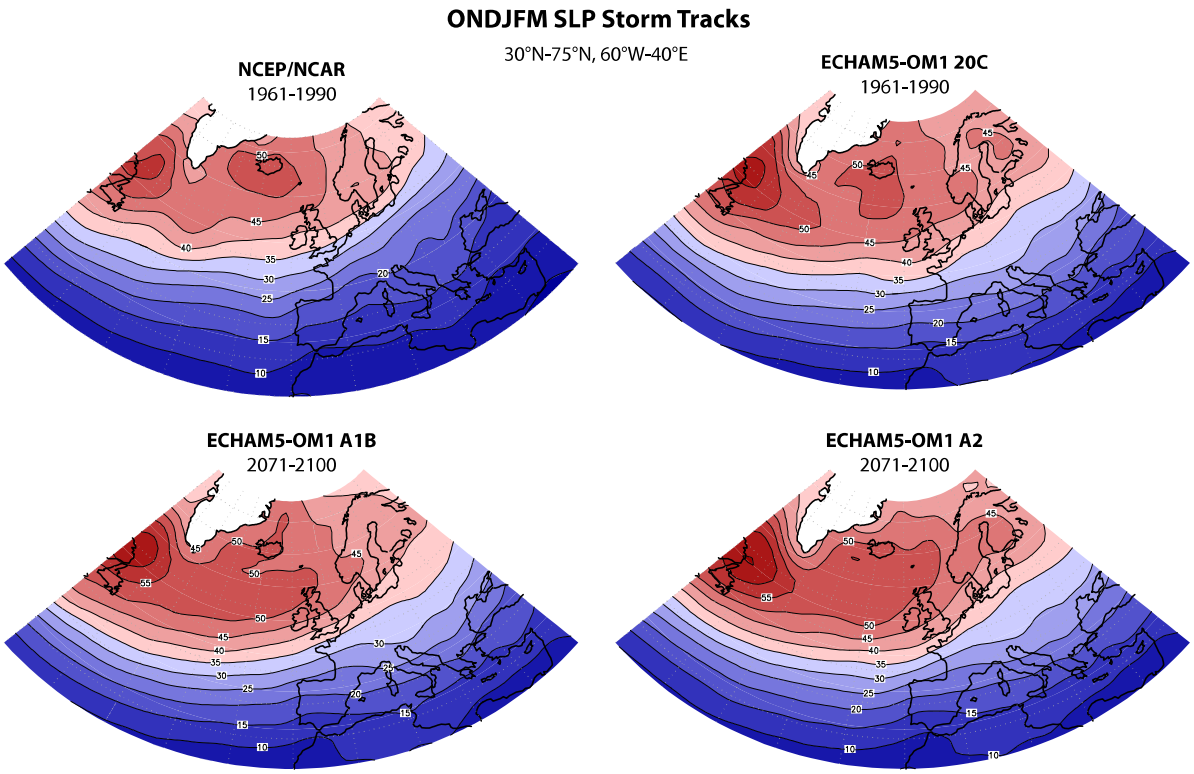

Figure 4.12: *ONDJFM mean SLP storm tracks in 1/10 hPa for NCEP/NCAR reanalysis (1961-1990) and ECHAM5-OM1 20C (1961-1990), A1B and A2 model outputs (2071-2100); values for Greenland are excluded due to mean land elevations >1500 m MSL.*

Synoptic wave activity is reported to increase for A1B conditions (Figure 4.12, bottom left) with a strengthening especially south of Greenland and a northward shift of areas with comparable storm track values in southern regions. The area with storm track values larger than 50 * 1/10 hPa is shown to even increase for the A2 scenario case (Figure 4.12, bottom right).

Figure 4.13 shows ECHAM5-OM1 SLP storm track differences for both A1B and A2 forcing conditions and the 20C reference case. Both difference maps reveal an increase in wave activity for the northern North Atlantic and a noticeable decrease for western to south-western Europe. The largest increase in cyclonicity is indicated for the area west of Ireland under A2 forcing (Figure 4.13, right). In both scenarios the region around the north-western Iberian Peninsula is reported to experience a decrease in synoptic wave activity,

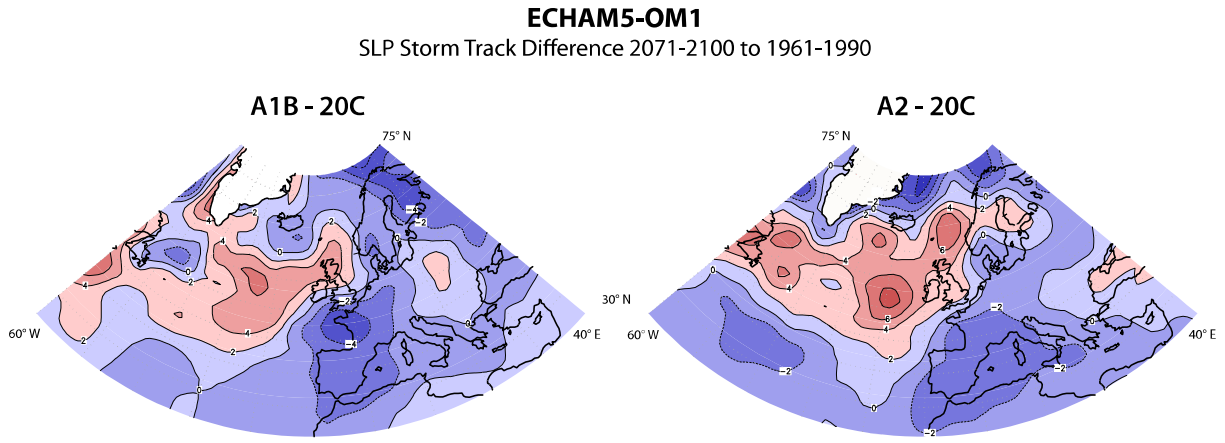

Figure 4.13: *SLP storm track differences in 1/10 hPa for ECHAM5-OM1 A1B minus 20C and A2 minus 20C conditions (2071-2100 minus 1961-1990 storm tracks); values for Greenland are excluded due to mean land elevations >1500 m MSL.*

whereas the decline is shown to be stronger under A1B conditions (Figure 4.12, left). No significance testing has been performed due to an inappropriate structure of the analyzed dataset.

Assuming a close interrelation between storminess and extreme sea levels (e.g. Bindoff et al. 2007), the following aspects should be argued for the northwestern Iberian Peninsula: The observed decline in future storminess around the study area is supposed to feedback also on the distribution of extreme sea levels. In fact, a decrease regarding the atmospherically induced extreme sea level frequency and strength around the northwestern Iberian Peninsula could be expected by the end of the 21st century if the model has skill for the future. Furthermore, the decrease in surge frequency might be more distinct for the moderate A1B scenario than for the A2 scenario conditions. Concerning future maximum extreme sea level heights triggered by atmospheric forcing, propositions are harder to be made because extreme cyclones might become more powerful than today although the frequency shows decreasing tendencies. For the period 1951-1997, Pirazzoli (2000) has observed a similar behavior for the coasts of northwestern France, where he reported the surge associated cyclones to become less frequent but slightly more powerful with stronger peak winds. Generally, a decline in storminess for the northwestern Iberian Peninsula would be in line with several studies which observe a northward shift of Northern Atlantic storm tracks with increased intensity but a decreasing overall cyclone frequency under ongoing anthropogenic climate change by the end of the 21st century (e.g. Leckebusch and Ulbrich 2004; Leckebusch et al. 2006; Jiang and Perrie 2007; Ulbrich et al. 2009).

If future changes in extreme sea levels are to be assessed for the study area, it is necessary to not only investigate the future cyclonicity in the region but to also include the changing

mean sea level in the analysis. Consequently, the following evolution of extreme sea levels might be expectable for the northwestern Iberian Peninsula: If, for the sake of simplicity, the mean sea level rise in the study area is supposed to be in line with the upper limits of the moderate IPCC SRES A1B outputs by the end of the 21st century, the ocean around the northwestern Iberian Peninsula may rise by around 40 cm (IPCC 2007). This amount of water permanently added onto the current mean sea level would dramatically increase the impact of extreme surges showing the same or slightly weaker strength and forcing characteristics as today if we assume no adaptation measures at the exposed coastlines.

Chapter 5

Conclusions & Outlook

The main goal of the study was to examine extreme sea levels and their link to corresponding large-scale atmospheric circulation patterns for the northwestern Iberian Peninsula. Quality controlled hourly tide gauge observations for the stations Coruna, Santander and Vigo were investigated for the period 1948-2001 and have been subject to an extreme value analysis. Highest sea levels have to be expected for the coasts around Vigo with 100-year return levels of around 3 m above the mean sea level taking into account the maximum tidal elevation of spring tides of 2 m in this region. Based on NCEP/NCAR SLP and wind reanalysis data the major atmospheric surge forcings have been identified and related to dominant large-scale circulation patterns over the Northern Atlantic region. In general, we can state that the NCEP/NCAR reanalysis is capable of representing the key forcing features of anomalous low SLP and onshore winds for the vast majority of derived surge events at the three tide gauge stations. Nevertheless, there are some deficiencies which must not be neglected. On the one hand, we have to notice the limited ability of the reanalysis to account for local effects due to the relatively coarse resolution. On the other hand, there remains a small insecurity concerning the quality of the sea level measurements especially regarding the highest surge recorded at the tide gauge station in Coruna. Not only SLP and wind patterns related to the highest five recorded tidal residuals have been analyzed for each station but also a much larger sample of circulation patterns corresponding to cumulated 99.99th ONDJFM surge percentiles. The intention of the classification was to detect dominant large scale atmospheric features of the selected extreme sea levels for each station. Negative SLP anomalies centered north to northwest of the northwestern Iberian Peninsula appear to be most frequent and therefore mark a key feature of the large-scale circulation pattern classification. Approximately 70% of the presented clusters can be either assigned to a Greenland Anticyclone or Blocking type WR. Data from the Global Tropical and Extratropical Cyclone Climatic Atlas (GTECCA) has been included in the analysis for further information about storms with the potential to force surges in the

study area. Furthermore, the study aimed at a first outlook regarding the future evolution of surges around the northwestern Iberian Peninsula accounting for ongoing anthropogenic climate change. In order to obtain first insights in this respect simulated SLP from the state-of-the-art ECHAM5-OM1 climate model has been investigated regarding a changing cyclonicity over Northern Atlantic. The analysis of SLP storm tracks based on A1B and A2 scenario runs (2071-2100) as well as the 20C control run (1961-1990) yields a decrease in cyclonicity for the study area. If extreme sea levels are considered to exhibit a certain proportionality to cyclonicity then a weakening of atmospherically induced extreme sea levels might be observable around the northwestern Iberian Peninsula in the future excluding the projected sea level rise due to ongoing climate change from the assessment.

Based on the results presented and discussed in Chapter 4 following answers can be given on the research questions raised in Section 1.2:

- *What is the connection between large-scale atmospheric circulation patterns and sea level extremes around the northwestern Iberian Peninsula for the period 1948-2001?*

  With the study it was possible to identify atmospheric circulation patterns related to recorded ONDJFM surges at Coruna, Santander and Vigo which show surge forcing characteristics for the largest part of selected events. Anomalous low SLP inducing the Inverse Barometer (IB) effect and strong onshore wind fields can explain major parts of recorded extreme sea levels around the northwestern Iberian Peninsula. Depending on the station location, slightly differing circulation patterns are found to dominate at analyzed surge events. For the geographically close stations Coruna and Vigo, the Greenland Anticyclone as well as the Blocking WR could be identified to dominate at the time of observed surges. These findings are in agreement with recent publications (e.g. Lozano et al. 2004). Santander which is located to the east and exposed to the north, i.e. the Bay of Biscay, reveals to be more sensitive to Atlantic Ridge type WRs producing strong onshore winds around the station.

  As already pointed out, extreme sea levels are also susceptible to local forcings. The extent to which surges can be explained by the NCEP/NCAR reanalysis is limited due to the relatively coarse resolution of the dataset. Nevertheless, it has been possible to identify key features of the large-scale circulation which show distinct surge forcing characteristics.

- *Is it possible to detect a change in the intensity of extreme sea levels over the observation period?*

  The study was not able to detect long-term changes in the intensity of extreme sea levels for the northwestern Iberian Peninsula. The records show a predominant interannual variability of winter half year 99.99th tidal residual percentiles. For

all three tide gauge stations the linear regressions show almost identical features which suggests a common origin of the observable positive slopes. As stated in Section 4.1 the mean sea level rise which has been observed for the region around the northwestern Iberian Peninsula might be responsible for this signal.

- *Do changes in observed extreme sea level trends have to be attributed to changes in storm strength or to changes in mean sea level?*

  As stated above, there are no reasonable indications which would allow for the conclusion that there have been significant changes in the extreme sea level intensity around the northwestern Iberian Peninsula from 1948-2001 due to changing cyclonicity or storm strength. As argued in Section 4.5 storm track calculations indicate a future decrease in cyclonicity for the study area which might also feedback proportionally on overall surge strength and frequency. Nevertheless, it can be expected that the magnitude of the projected global sea level rise would compensate the decrease in atmospherically induced surges. Rising mean sea levels would therefore lead to an increasing number and strength of extreme sea levels around the northwestern Iberian Peninsula.

- *Are there areas around the northwestern Iberian coasts which could be affected by enhanced extreme sea level threats in the future?*

  Projected higher mean sea levels are expected to increase the strength and impact of extreme surges as well as their frequency (e.g. Nicholls et al. 2007). Higher extreme sea levels would amplify erosion rates for the whole area under investigation. Deltaic areas, barrier-type coasts and low-lying shorelines with softer sediment structures will be particularly affected (Lozano et al. 2004). Studies are indicating that a mean sea level rise of around 1 m could lead to coastal retreats in the range of 50-100 m for these sensitive coastal environments (Fealy 2003; Smith et al. 2000). Depending on the prevention measures and specifications, e.g. freeboards, of the harbours and ports, also infrastructure might face an increasing risk of flooding through higher peak sea levels.

There is a lot of potential for ongoing research on extreme sea levels around the northwestern Iberian Peninsula although this study succeeded in addressing several key questions. Additional investigations should be carried out regarding the distribution of surges above a specific threshold over the observation period. Changes in the frequency of surge forcing, large-scale circulation patterns could be subject of further analyses. It would be very useful to include local pressure and wind data in the investigations to improve the analysis of atmospheric surge forcings and to be able to account for the fraction which was not

accessible by reanalysis data due to the coarse grid resolution. Unfortunately, the availability of records providing long timeseries of local SLP and wind has to be considered as very low. The integration of additional tide gauge stations for a more sophisticated comparison between the stations and a better identification of common forcing features might also be beneficial. Furthermore, the assessment of the future evolution of extreme sea levels around the northwestern Iberian Peninsula might be improved by establishing a more specific link between changing cyclonicity and extreme sea levels or applying a different proxy to identify the future distribution and intensity of extreme sea levels around the study area. The application of differing methods in general, a comparison between the different approaches and the integration of other study areas would further contribute to a better understanding of extreme sea levels around the northwestern Iberian Peninsula and their link to atmospheric forcing.

References

Alexander, L. V., S. F. B. Tett, and T. Jonsson (2005). Recent observed changes in severe storms over the United Kingdom and Iceland. *Geophysical Research Letters* **32** (13), L13704.

Barnston, A. G. and R. E. Livezey (1987). Classification, Seasonality and Persistence of Low-frequency Atmospheric Circulation Patterns. *Monthly Weather Review* **115** (6), 1083–1126.

Beck, C. (2000). Zirkulationsdynamische Variabilität im Bereich Nordatlantik-Europa seit 1780. *Würzburger Geographische Arbeiten* **95**.

Beranova, R. and R. Huth (2008). Time variations of the effects of circulation variability modes on European temperature and precipitation in winter. *International Journal of Climatology* **28** (2), 139–158.

Bernier, N. B., K. R. Thompson, J. Ou, and H. Ritchie (2007). Mapping the return periods of extreme sea levels: Allowing for short sea level records, seasonality, and climate change. *Global and Planetary Change* **57** (1-2), 139–150.

Betts, N. L., J. D. Orford, D. White, and C. J. Graham (2004). Storminess and surges in the South-Western Approaches of the eastern North Atlantic: the synoptic climatology of recent extreme coastal storms. *Marine Geology* **210** (1-4), 227–246.

Bindoff, N., J. Willebrand, V. Artale, A. Cazenave, J. Gregory, S. Gulev, K. Hanawa, C. Le Quéré, S. Levitus, Y. Nojiri, C. K. Shum, L. Talley, and A. Unnikrishnan (2007). *Observations: Oceanic Climate Change and Sea Level. In: Climate Change 2007: The Physical Science Basis. Contribution of Working Group I to the Fourth Assessment Report of the Intergovernmental Panel on Climate Change*. Cambridge University Press, Cambridge, United Kingdom and New York, NY, USA.

Blackmon, M. L. (1976). A Climatological Spectral Study of the 500 mb Geopotential Height of the Northern Hemisphere. *Journal of the Atmospheric Sciences* **33** (8), 1607–1623.

Blackmon, M. L., Y.-H. Lee, and J. M. Wallace (1984). Horizontal Structure of 500 mb Height Fluctuations with Long, Intermediate and Short Time Scales. *Journal of the Atmospheric Sciences* **41** (6), 961–980.

Blackmon, M. L., J. M. Wallace, N.-C. Lau, and S. L. Mullen (1977). An Observational Study of the Northern Hemisphere Wintertime Circulation. *Journal of the Atmospheric Sciences* **34** (7), 1040–1053.

Bouligand, R. and P. A. Pirazzoli (1999). Positive and negative sea surges at Brest. *Oceanologica Acta* **22** (2), 153–166.

Brinkmann, W. A. R. (1999). Application of non-hierarchically clustered circulation components to surface weather conditions: Lake Superior basin winter temperatures. *Theoretical and Applied Climatology* **63** (1-2), 41–56.

Broennimann, S. (2007). Impact of El Nino Southern Oscillation on European climate. *Reviews of Geophysics* **45** (2), RG3003.

Brown, T. J. and B. L. Hall (1999). The use of t values in climatological composite analyses. *Journal of Climate* **12** (9), 2941–2944.

Bärring, L. and K. Fortuniak (2009). Multi-indices analysis of southern Scandinavian storminess 1780-2005 and links to interdecadal variations in the NW Europe-North Sea region. *International Journal of Climatology* **29** (3), 373–384.

Cazenave, A. and R. S. Nerem (2004). Present-day sea level change: Observations and causes. *Rev. Geophys.* **42**, RG3001.

Coles, S. (2001). *An introduction to statistical modeling of extreme values*. Springer Series in Statistics, Springer-Verlag, London.

Collins, W. G. (2001). The operational complex quality control of radiosonde heights and temperatures at the National Centers for Environmental Prediction. Part I: Description of the method. *Journal of Applied Meteorology* **40** (2), 137–151.

Dawson, A. G., K. Hickey, T. Holt, L. Elliott, S. Dawson, I. D. L. Foster, P. Wadhams, I. Jonsdottir, J. Wilkinson, J. McKenna, N. R. Davis, and D. E. Smith (2002). Complex North Atlantic Oscillation (NAO) Index signal of historic North Atlantic storm-track changes. *Holocene* **12** (3), 363–369.

Dolan, R., H. Lins, and B. Hayden (1988). Mid-atlantic Coastal Storms. *Journal of Coastal Research* **4** (3), 417–433.

Esper, J., D. Frank, U. Buntgen, A. Verstege, and J. Luterbacher (2007). Long-term drought severity variations in Morocco. *Geophysical Research Letters* **34** (17), L17702.

Fealy, R. (2003). The impacts of climate change on sea level and the Irish coast. In *Sweeney, J (ed.) Climate Change: Scenarios and Impacts for Ireland*, pp. 189–222. Environmental Protection Agency, Johnstown Castle, Wexford.

Garcia-Soto, C., R. D. Pingree, and L. Valdes (2002). Navidad development in the southern Bay of Biscay: Climate change and swoddy structure from remote sensing and in situ measurements. *Journal of Geophysical Research-oceans* **107** (C8), 3118.

Gershunov, A., N. Schneider, and T. Barnett (2001). Low-Frequency Modulation of the ENSO-Indian Monsoon Rainfall Relationship: Signal or Noise? *Journal of Climate* **14** (11), 2486–2492.

GOA (2004). An Atlas of Oceanic Internal Solitary Waves. Technical report, Global Ocean Associates, Office of Naval Research.

Hayden, B. P. (1981). Secular Variation In Atlantic Coast Extratropical Cyclones. *Monthly Weather Review* **109** (1), 159–167.

Hess, P. and H. Brezowsky (1977). Katalog der Grosswetterlagen Europas 18811976. *3. verbesserte und ergaenzte Aufl. Berichte des Deutschen Wetterdienstes, Offenbach am Main* **15 (113)**.

Hipel, K. W. and A. I. McLeod (1994). *Time Series Modelling of Water Resoures and Environmental Systems*. Elsevier, Amsterdam, Netherlands.

Hirsch, R. M. and J. R. Slack (1984). A Nonparametric Trend Test For Seasonal Data With Serial Dependence. *Water Resources Research* **20** (6), 727–732.

Holgate, S. J. and P. L. Woodworth (2004). Evidence for enhanced coastal sea level rise during the 1990s. *Geophys. Res. Lett.* **31**, L07305.

Hollander, M. and D. A. Wolfe (1973). *Nonparametric Statistical Methods*. Wiley, NY.

Holt, T. (1999). A classification of ambient climatic conditions during extreme surge events off western Europe. *International Journal of Climatology* **19** (7), 725–744.

Iglewicz, B. (1983). *Robust scale estimators and confidence intervals for location. In: Understanding Robust and Exploratory Data Analysis*. Wiley, New York.

IPCC (2007). *Climate Change 2007: The Physical Science Basis. Contribution of Working Group I to the Fourth Assessment Report of the Intergovernmental Panel on Cli-*

mate Change. Cambridge University Press, Cambridge, United Kingdom and New York, NY, USA.

Jacobeit, J., H. Wanner, J. Luterbacher, C. Beck, A. Philipp, and K. Sturm (2003). Atmospheric circulation variability in the North-Atlantic-European area since the mid-seventeenth century. *Climate Dynamics* **20** (4), 341–352.

Jiang, J. and W. Perrie (2007). The impacts of climate change on autumn North Atlantic midlatitude cyclones. *Journal of Climate* **20** (7), 1174–1187.

Jones, P. D., E. B. Horton, C. K. Folland, M. Hulme, D. E. Parker, and T. A. Basnett (1999). The use of indices to identify changes in climatic extremes. *Climatic Change* **42** (1), 131–149.

Jones, P. D., T. Jonsson, and D. Wheeler (1997). Extension to the North Atlantic Oscillation using early instrumental pressure observations from Gibraltar and southwest Iceland. *International Journal of Climatology* **17** (13), 1433–1450.

Jungclaus, J. H., N. Keenlyside, M. Botzet, H. Haak, J. J. Luo, M. Latif, J. Marotzke, U. Mikolajewicz, and E. Roeckner (2006). Ocean circulation and tropical variability in the coupled model ECHAM5/MPI-OM. *Journal of Climate* **19** (16), 3952–3972.

Kalnay, E., M. Kanamitsu, R. Kistler, W. Collins, D. Deaven, L. Gandin, M. Iredell, S. Saha, G. White, J. Woollen, Y. Zhu, M. Chelliah, W. Ebisuzaki, W. Higgins, J. Janowiak, K. C. Mo, C. Ropelewski, J. Wang, A. Leetmaa, R. Reynolds, R. Jenne, and D. Joseph (1996). The NCEP/NCAR 40-year reanalysis project. *Bulletin of the American Meteorological Society* **77** (3), 437–471.

Kaufmann, L. and P. J. Rousseeuw (1990). *Finding groups in data: An introduction to cluster analysis*. Wiley, New York.

Kistler, R., E. Kalnay, W. Collins, S. Saha, G. White, J. Woollen, M. Chelliah, W. Ebisuzaki, M. Kanamitsu, V. Kousky, H. van den Dool, R. Jenne, and M. Fiorino (2001). The NCEP-NCAR 50-year reanalysis: Monthly means CD-ROM and documentation. *Bulletin of the American Meteorological Society* **82** (2), 247–267.

Klein, R. J. T., M. J. Smit, H. Goosen, and C. H. Hulsbergen (1998). Resilience and vulnerability: Coastal dynamics or Dutch dikes? *Geographical Journal* **164**, 259–268.

Küttel, M., J. Luterbacher, and H. Wanner (2009). Multidecadal changes in the circulation-climate realtionship in Europe: frequency variations, within-type modifications and long-term trends. *submitted*.

Lamb, H. H. (1972). British Isles Weather types and a register of daily sequence of circulation patterns, 1861-1971. *Geophysical Memoir, HMSO, London* **116**, 85 pp.

Lambert, S. J. (1996). Intense extratropical northern hemisphere winter cyclone events: 1899 - 1991. *J. Geophys. Res.* **101 (D16)**, 319–325.

Leckebusch, G. C., B. Koffi, U. Ulbrich, J. G. Pinto, T. Spangehl, and S. Zacharias (2006). Analysis of frequency and intensity of European winter storm events from a multi-model perspective, at synoptic and regional scales. *Climate Research* **31** (1), 59–74.

Leckebusch, G. C. and U. Ulbrich (2004). On the relationship between cyclones and extreme windstorm events over Europe under climate change. *Global and Planetary Change* **44** (1-4), 181–193.

Lozano, I., R. J. N. Devoy, W. May, and U. Andersen (2004). Storminess and vulnerability along the Atlantic coastlines of Europe: analysis of storm records and of a greenhouse gases induced climate scenario. *Marine Geology* **210** (1-4), 205–225.

Luterbacher, J., E. Xoplaki, D. Dietrich, R. Rickli, J. Jacobeit, C. Beck, D. Gyalistras, C. Schmutz, and H. Wanner (2002). Reconstruction of sea level pressure fields over the Eastern North Atlantic and Europe back to 1500. *Climate Dynamics* **18** (7), 545–561.

Marcos, M., M. N. Tsimplis, and A. G. P. Shaw (2009). Sea level extremes in southern Europe. *Journal of Geophysical Research – Oceans* **114**, C01007.

Marsland, S. J., H. Haak, J. H. Jungclaus, M. Latif, and F. Roske (2003). The Max-Planck-Institute global ocean/sea ice model with orthogonal curvilinear coordinates. *Ocean Modelling* **5** (2), 91–127.

Michelangeli, P. A., R. Vautard, and B. Legras (1995). Weather Regimes - Recurrence and Quasi Stationarity. *Journal of the Atmospheric Sciences* **52** (8), 1237–1256.

Miller, C. (2003). A once in 50-year wind speed map for Europe derived from mean sea level pressure measurements. *Journal of Wind Engineering and Industrial Aerodynamics* **91** (12-15), 1813–1826.

Monserrat, S., I. Vilibic, and A. B. Rabinovich (2006). Meteotsunamis: atmospherically induced destructive ocean waves in the tsunami frequency band. *Natural Hazards and Earth System Science* **6** (6), 1035–1051.

Nakicenovic, N., J. Alcamo, G. Davis, B. de Vries, J. Fenhann, S. Gaffin, K. Gregory, A. Grübler, J. Tae Yong, T. Kram, E. L. La Rovere, L. Michaelis, M. Shunsuke,

M. Tsuneyuki, W. Pepper, H. Pitcher, L. Price, K. Riahi, A. Roehrl, H. H. Rogner, A. Sankovski, M. Schlesinger, P. Shukla, S. Smith, R. Swart, S. van Rooijen, N. Victor, and Z. Dadi (2000). *Emission Scenarios.* Cambridge University Press, UK.

NCDC, N. C. D. C. (1997). Products and Services Guide. Technical report, U.S. Department of Commerce, NOAA, Asheville, NC.

Nicholls, R., P. P. Wong, V. R. Burkett, J. O. Codignotto, J. E. Hay, R. F. McLean, S. Ragoonaden, and C. D. Woodroffe (2007). *Coastal systems and low-lying areas. In Climate Change 2007: Impacts, Adaptation and Vulnerability. Contribution of Working Group II to the Fourth Assessment Report of the Intergovernmental Panel on Climate Change.* Cambridge University Press, Cambridge, UK.

Nicholls, R. J. and N. Mimura (1998). Regional issues raised by sea-level rise and their policy implications. *Climate Research* **11** (1), 5–18.

Oliveira, P. B., A. Peliz, J. Dubert, T. L. Rosa, and A. M. P. Santos (2004). Winter geostrophic currents and eddies in the western Iberia coastal transition zone. *Deep-sea Research Part I-oceanographic Research Papers* **51** (3), 367–381.

Onoz, B. and M. Bayazit (2003). The power of statistical tests for trend detection. *Turkish Journal of Engineering and Environmental Sciences* **27 (4)**, 247–251.

Parrish, D. F. and J. C. Derber (1992). The National-meteorological-centers Spectral Statistical-interpolation Analysis System. *Monthly Weather Review* **120** (8), 1747–1763.

Pawlowicz, R., B. Beardsley, and S. Lentz (2002). Classical tidal harmonic analysis including error estimates in MATLAB using T-TIDE. *Computers & Geosciences* **28** (8), 929–937.

Philipp, A., P. M. Della-Marta, J. Jacobeit, D. R. Fereday, P. D. Jones, A. Moberg, and H. Wanner (2007). Long-term variability of daily North Atlantic-European pressure patterns since 1850 classified by simulated annealing clustering. *Journal of Climate* **20** (16), 4065–4095.

Pingree, R. D. and B. Le Cann (1992). Anticyclonic Eddy X91 In the Southern Bay of Biscay, May 1991 To February 1992. *Journal of Geophysical Research-oceans* **97** (C9), 14353–14367.

Pirazzoli, P. A. (2000). Surges, atmospheric pressure and wind change and flooding probability on the Atlantic coast of France. *Oceanologica Acta* **23** (6), 643–661.

Pirazzoli, P. A., S. Costa, U. Dornbusch, and A. Tomasin (2006). Recent evolution of surge-related events and assessment of coastal flooding risk on the eastern coasts of the English Channel. *Ocean Dynamics* **56** (5-6), 498–512.

Plaut, G. and E. Simonnet (2001). Large-scale circulation classification, weather regimes, and local climate over France, the Alps and Western Europe. *Climate Research* **17** (3), 303–324.

Pryor, S. C., R. J. Barthelmie, and J. T. Schoof (2006). Inter-annual variability of wind indices across Europe. *Wind Energy* **9** (1-2), 27–38.

Rahmstorf, S. (2007). A Semi-Empirical Approach to Projecting Future Sea-Level Rise. *Science* **315** (5810), 368–370.

Roeckner, E., G. Baeuml, L. Bonaventura, R. Brokopf, M. Esch, M. Giorgetta, S. Hagemann, I. Kirchner, L. Kornblueh, E. Manzini, A. Rhodin, U. Schlese, U. Schulzweida, and A. Tompkins (2003). The atmospheric general circulation model ECHAM 5. PART I: Model description. Technical Report 349, MPIM, Hamburg.

Ruiz-Villarreal, M., C. Gonzalez-Pola, G. Diaz del Rio, A. Lavin, P. Otero, S. Piedracoba, and J. M. Cabanas (2006). Oceanographic conditions in North and Northwest Iberia and their influence on the Prestige oil spill. *Marine Pollution Bulletin* **53** (5-7), 220–238.

Schinke, H. (1993). On the occurrence of deep cyclones over Europe and the North Atlantic in the period 1930-1991. *Contributions to atmospheric physics* **66**, 223–237.

Schmith, T. (1995). Development of occurrence and strength of severe winds over the Northeast Atlantic during the past 100 years. *Proceedings of the Sixth International Meeting on Statistical Climatology Galway, Ireland*, 83–86.

Schmith, T., E. Kaas, and T. S. Li (1998). Northeast Atlantic winter storminess 1875-1995 re-analysed. *Climate Dynamics* **14** (7-8), 529–536.

Siddall, M., T. F. Stocker, and P. U. Clark (2009). Constraints on future sea-level rise from past sea-level change. *Nature Geosci* **2** (8), 571–575.

Smith, D. E., A. Dawson, S. Dawson, J. D. Orford, R. J. N. Devoy, I. Lozano, K. Hickey, H. Regnauld, C. Andrade, J. A. Cooper, and J. R. Vidal-Romani (2000). *Storminess and environmentally sensitive atlantic coastal areas of the European Union. Project Final Report (1997-2000)*. Commission of the European Communities, EU Contract Nr. ENV4-CT97-0488, Brussels.

Suanez, S. and M. Provansal (1996). Morphosedimentary behaviour of the deltaic fringe in comparison to the relative sea-level rise on the Rhone delta. *Quaternary Science Reviews* **15** (8-9), 811–818.

Tawn, J. A. (1988). An Extreme-value Theory Model For Dependent Observations. *Journal of Hydrology* **101** (1-4), 227–250.

Tawn, J. A. (1992). Estimating Probabilities of Extreme Sea-levels. *Applied Statistics-journal of the Royal Statistical Society Series C* **41** (1), 77–93.

Toreti, A., F. G. Kuglitsch, E. Xoplaki, and J. Luterbacher (2009). Extreme Precipitation in the Mediterranean area: an approach based on dePOT model. *Nonlinear Processes in Geophysics* **700**, revised.

Trigo, I. F. and T. D. Davies (2002). Meteorological conditions associated with sea surges in Venice: A 40 year climatology. *International Journal of Climatology* **22** (7), 787–803.

Trigo, R. M., M. A. Valente, I. F. Trigo, P. M. Miranda, A. M. Ramos, D. Paredes, and R. García-Herrera (2008). The impact of north atlantic wind and cyclone trends on European precipitation and significant wave height in the atlantic. *Ann N Y Acad Sci* **1146**, 212–34.

Tsimplis, M., V. Zervakis, S. Josey, E. Peeneva, M. Struglia, E. Stanev, P. Lionello, P. Malanotte-Rizzoli, V. Artale, A. Theocharis, E. Tragou, and T. Oguz (2006). *Chapter 4: Changes in the Oceanography of the Mediterranean Sea and their Link to Climate Variability*. Elsevier, Developments in Earth and Environmental Science, 4.

Tsimplis, M. N., E. Alvarez-Fanjul, D. Gomis, L. Fenoglio-Marc, and B. Perez (2005). Mediterranean Sea level trends: Atmospheric pressure and wind contribution. *Geophysical Research Letters* **32** (20), L20602.

Tsimplis, M. N. and D. Blackman (1997). Extreme Sea-level Distribution and Return Periods in the Aegean and Ionian Seas. *Estuarine, Coastal and Shelf Science* **44** (1), 79–89.

Tsimplis, M. N. and S. A. Josey (2001). Forcing of the Mediterranean Sea by atmospheric oscillations over the North Atlantic. *Geophysical Research Letters* **28** (5), 803–806.

Ulbrich, U., G. C. Leckebusch, and J. G. Pinto (2009). Extra-tropical cyclones in the present and future climate: a review. *Theoretical and Applied Climatology* **96** (1-2), 117–131.

Ulbrich, U., J. G. Pinto, H. Kupfer, G. C. Leckebusch, T. Spangehl, and M. Reyers (2008). Changing northern hemisphere storm tracks in an ensemble of IPCC climate change simulations. *Journal of Climate* **21** (8), 1669–1679.

Ullmann, A. and V. Moron (2008). Weather regimes and sea surge variations over the Gulf of Lions (French Mediterranean coast) during the 20th century. *International Journal of Climatology* **28** (2), 159–171.

Ullmann, A., P. Pirazzoli, and V. Moron (2008). Sea surges around the Gulf of Lions and atmospheric conditions. *Global and Planetary Change* **63** (2-3), 203–214.

Ullmann, A., P. A. Pirazzoli, and A. Tomasin (2007). Sea surges in Camargue: Trends over the 20th century. *Continental Shelf Research* **27** (7), 922–934.

Vautard, R. (1990). Multiple Weather Regimes over the North Atlantic: Analysis of Precursors and Successors. *Monthly Weather Review* **118** (10), 2056–2081.

Vigo, I., D. Garcia, and B. F. Chao (2005). Change of sea level trend in the Mediterranean and Black seas. *Journal of Marine Research* **63** (6), 1085–1100.

Wakelin, S. L., P. L. Woodworth, R. A. Flather, and J. A. Williams (2003). Sea-level dependence on the NAO over the NW European Continental Shelf. *Geophysical Research Letters* **30** (7), 1403.

Wallace, J. M. and D. S. Gutzler (1981). Teleconnections in the Geopotential Height Field during the Northern Hemisphere Winter. *Monthly Weather Review* **109** (4), 784–812.

Wallace, J. M., G.-H. Lim, and M. L. Blackmon (1988). Relationship between Cyclone Tracks, Anticyclone Tracks and Baroclinic Waveguides. *Journal of the Atmospheric Sciences* **45** (3), 439–462.

Wang, X. L., F. W. Zwiers, V. R. Swail, and Y. Feng (2008). Trends and variability of storminess in the Northeast Atlantic region, 1874-2007. *Climate Dynamics*, published online.

Weisse, R., H. von Storch, U. Callies, A. Chrastansky, F. Feser, I. Grabemann, H. Guenther, A. Pluess, T. Stoye, J. Tellkamp, J. Winterfeldt, and K. Woth (2009). Regional Meteorological-Marine Reanalyses and Climate Change Projections. *Bulletin of the American Meteorological Society* **90** (6), 849–860.

Wilks, D. S. (2001). *Statistical Methods in the Atmospheric Sciences*. Elsevier, Academic Press, International Geophysics Series, Burlington, MA.

Woodworth, P. L. and D. L. Blackman (2002). Changes in extreme high waters at Liverpool since 1768. *International Journal of Climatology* **22** (6), 697–714.

Woodworth, P. L. and D. L. Blackman (2004). Evidence for systematic changes in extreme high waters since the mid-1970s. *Journal of Climate* **17** (6), 1190–1197.

Woollen, J. S., E. Kalnay, L. Gandin, W. Collins, S. Saha, R. Kistler, M. Kanamitsu, and M. Chelliah (1994). Quality control in the reanalysis system. *Numerical Weather Prediction 10th Conference (nwp)*, 13–14.

Wooster, W. S., A. Bakun, and D. R. McLain (1976). Seasonal Upwelling Cycle Along Eastern Boundary of North-atlantic. *Journal of Marine Research* **34** (2), 131–141.

Xoplaki, E., J. F. Gonzalez-Rouco, J. Luterbacher, and H. Wanner (2004). Wet season Mediterranean precipitation variability: influence of large-scale dynamics and trends. *Climate Dynamics* **23** (1), 63–78.

Appendix A

NCEP/NCAR reanalysis

Evolution of surge related SLP and wind

CORUNA

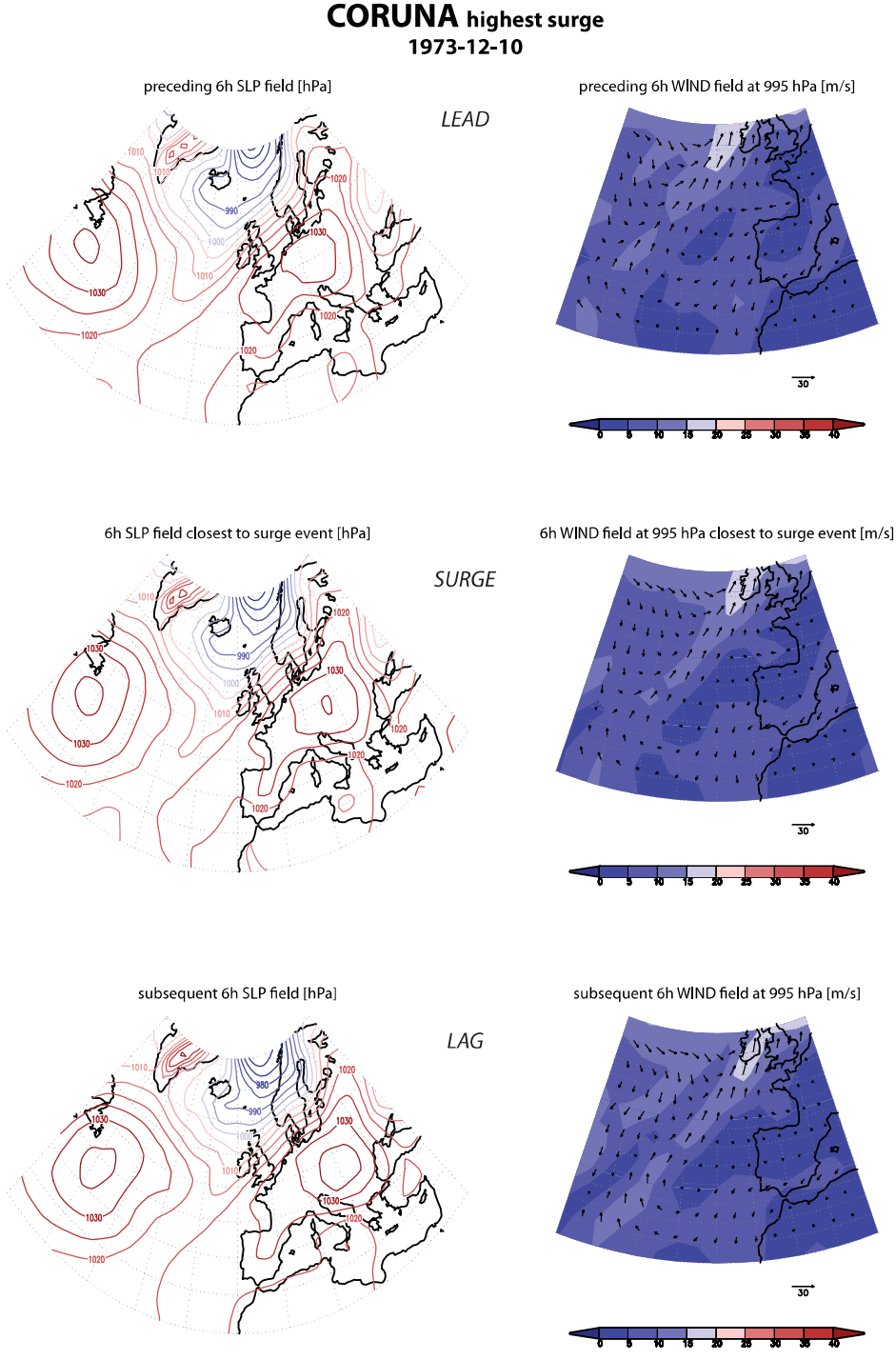

Figure A.1: *Large-scale 6h LEAD, SURGE and 6h LAG circulation patterns corresponding to the highest recorded surge at CORUNA (1948-2001); left: NCEP/NCAR reanalysis 6h absolute SLP composites in hPa; date in YYYY-MM-DD; right: NCEP/NCAR reanalysis 6h wind field composites; arrows displaying direction and strength.*

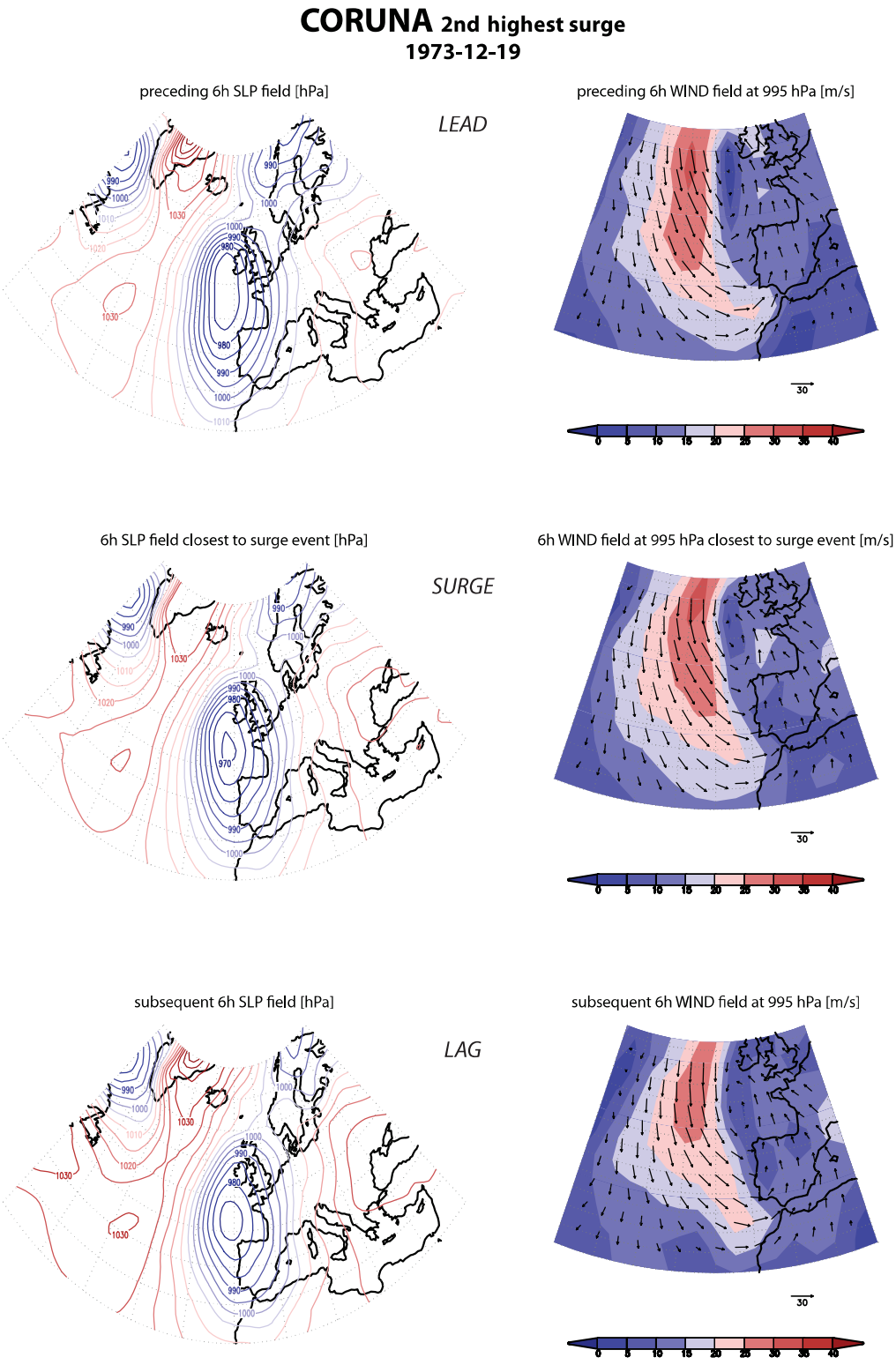

Figure A.2: *As Figure A.1 but for the second highest surge at Coruna.*

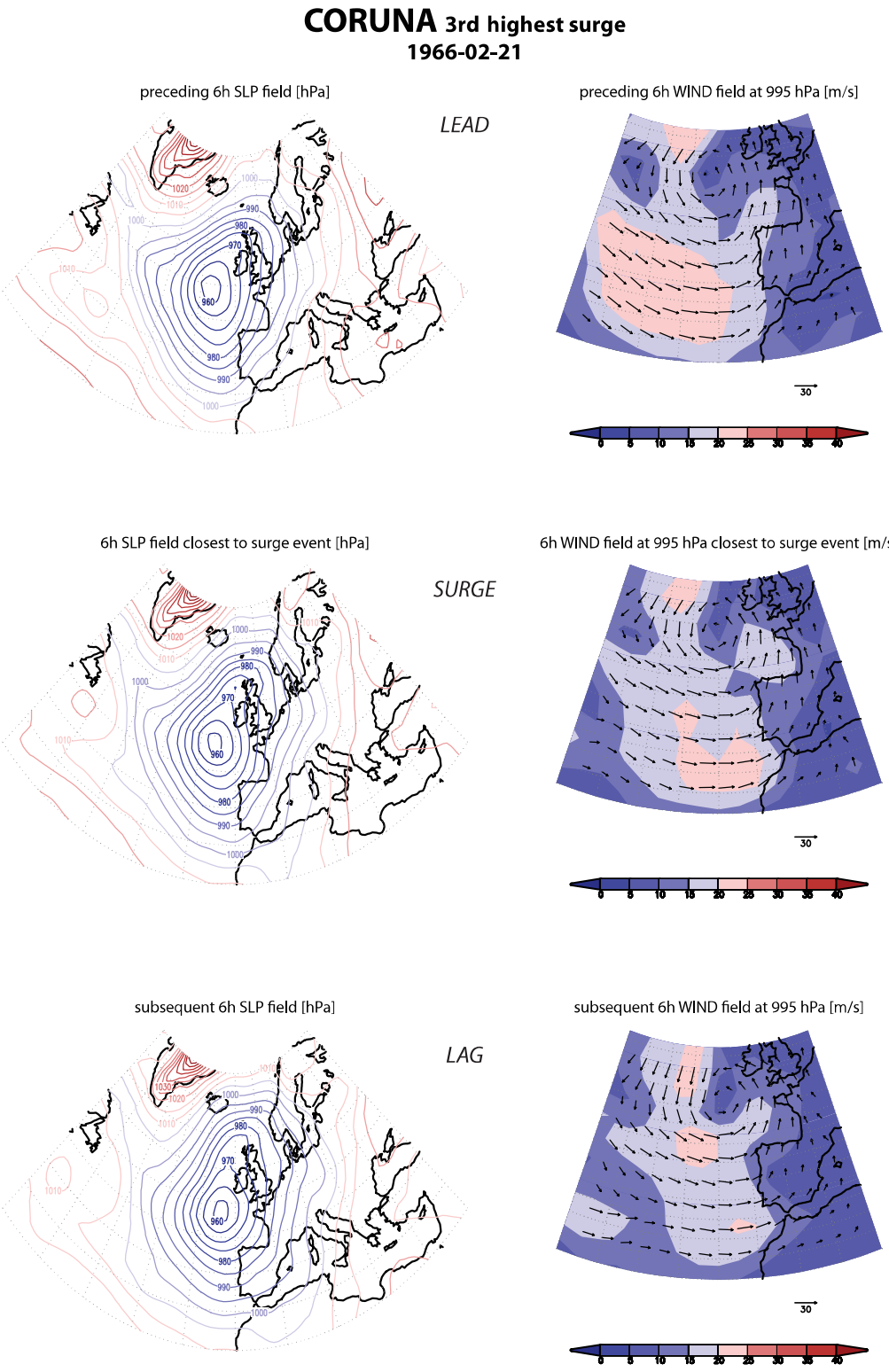

Figure A.3: *As Figure A.1 but for the third highest surge at Coruna.*

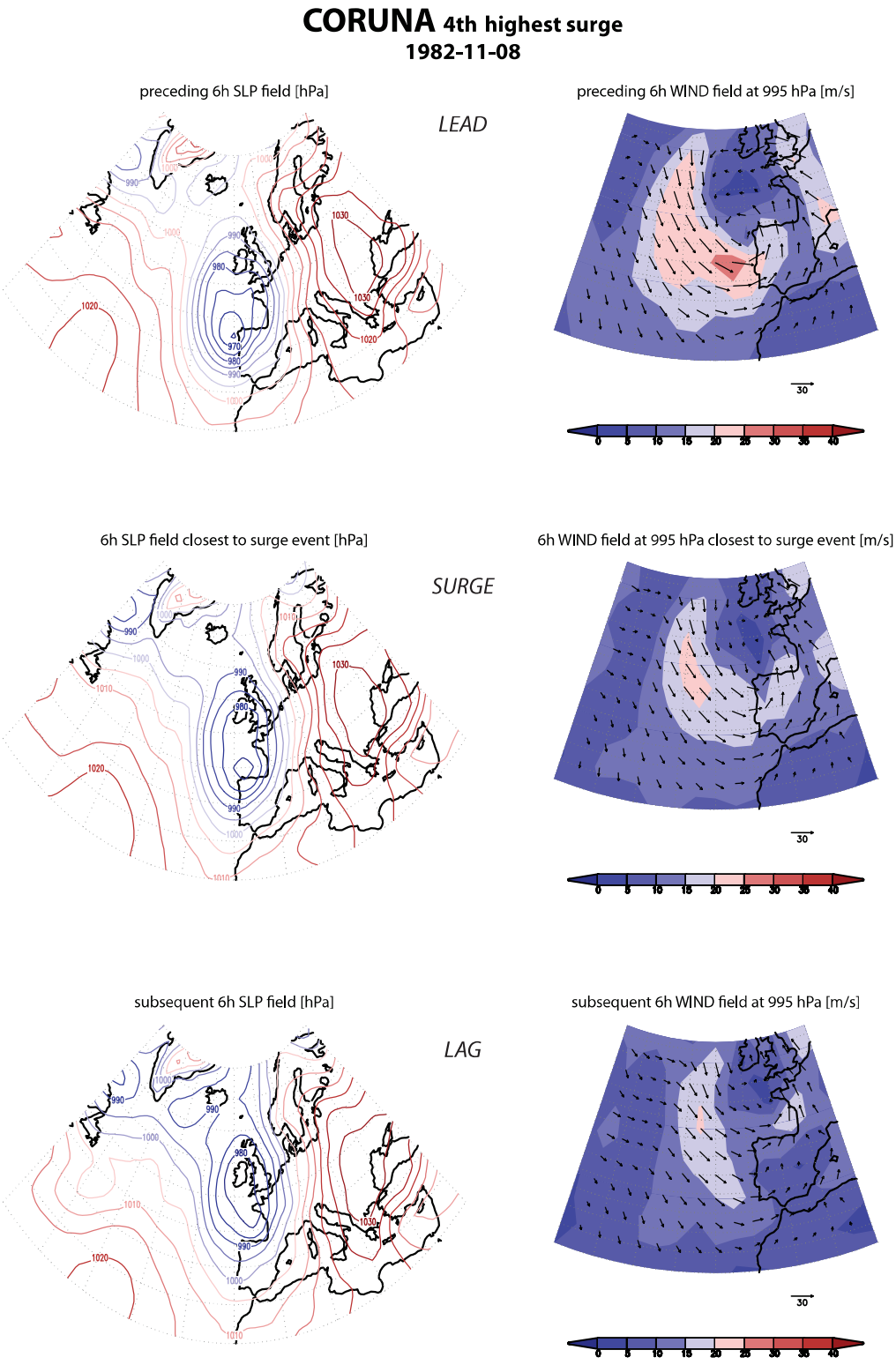

Figure A.4: *As Figure A.1 but for the fourth highest surge at Coruna.*

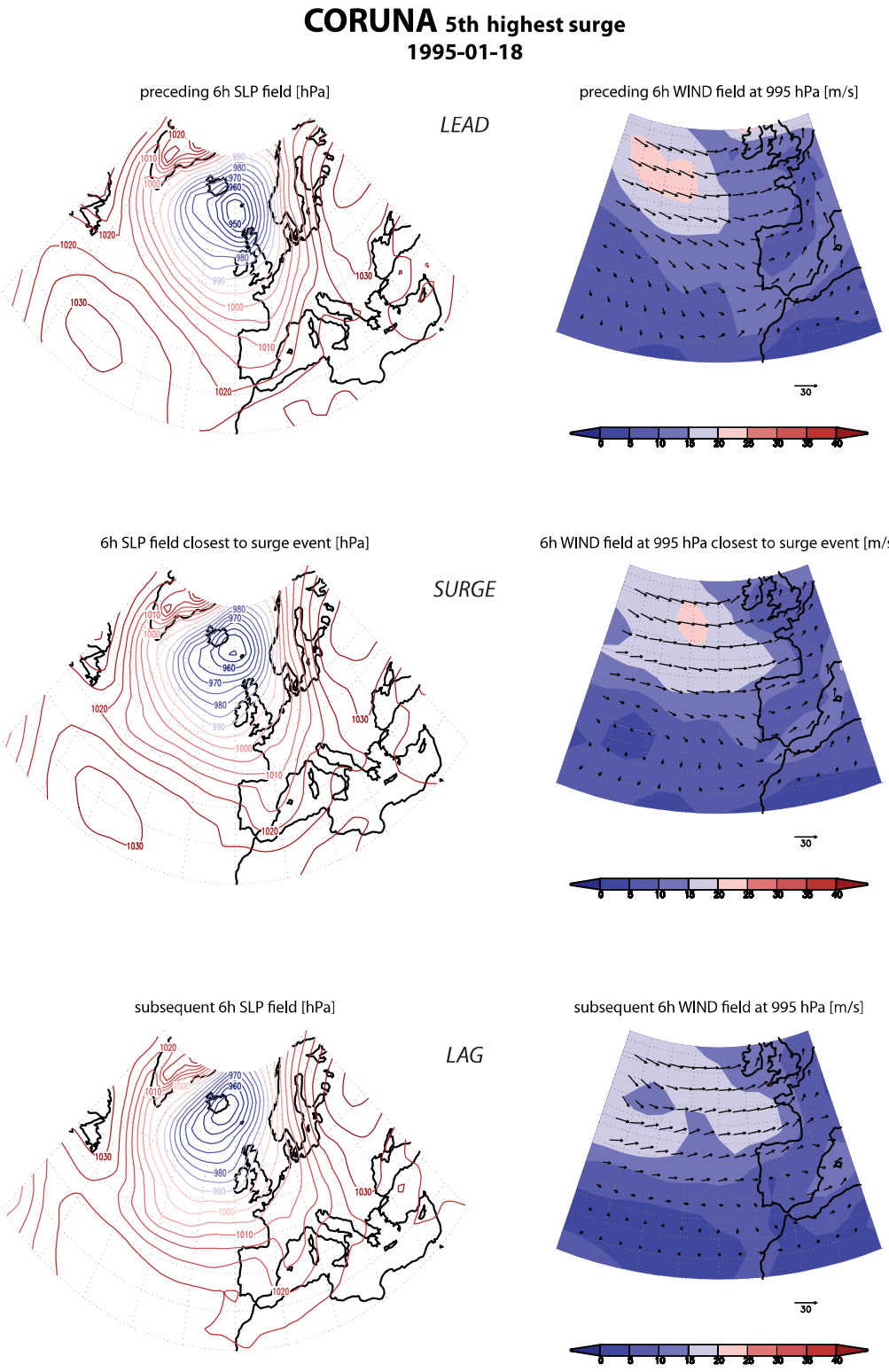

Figure A.5: *As Figure A.1 but for the fifth highest surge at Coruna.*

SANTANDER

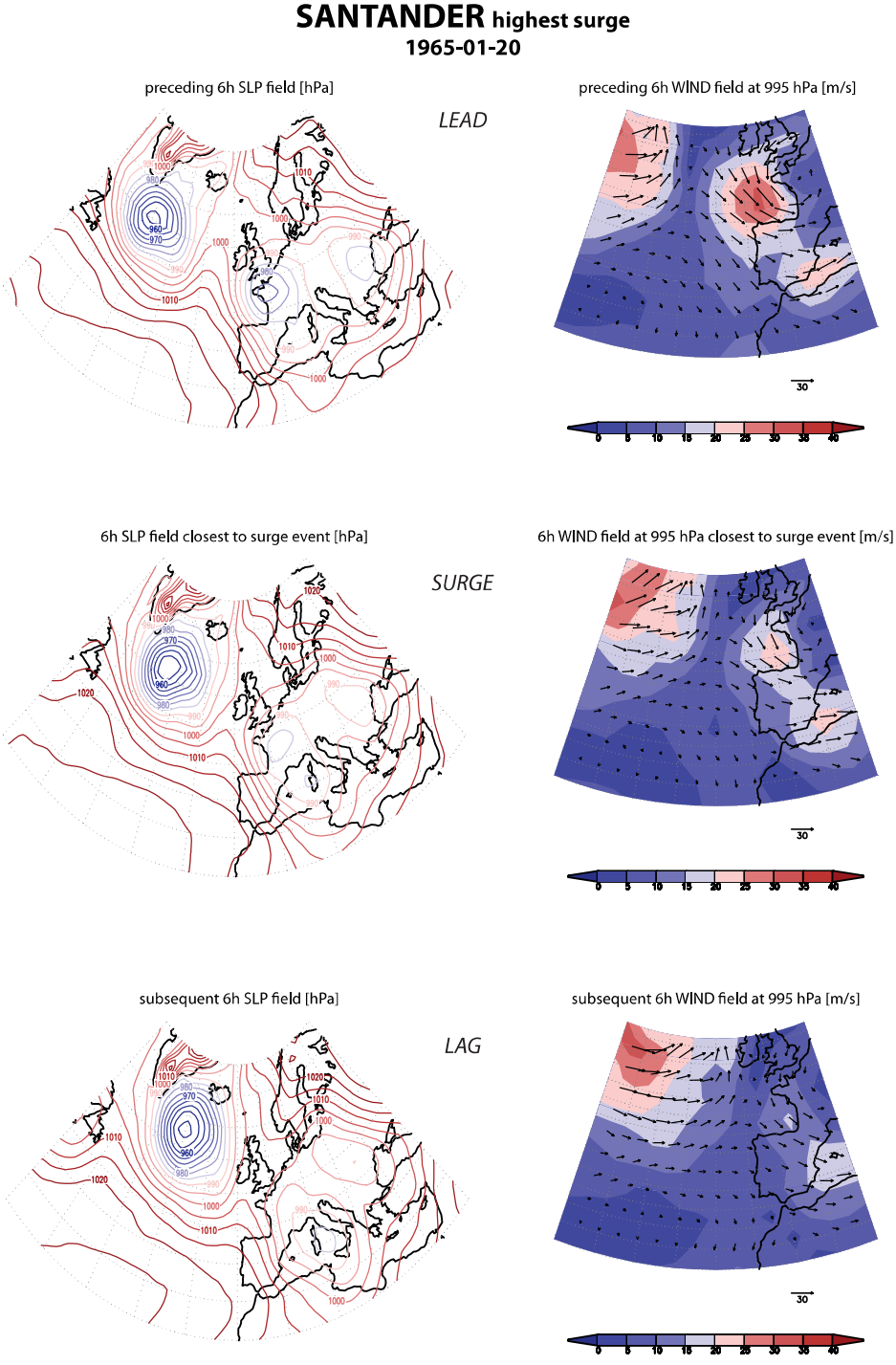

Figure A.6: *Large-scale 6h LEAD, SURGE and 6h LAG circulation patterns corresponding to the highest recorded surge at SANTANDER (1948-2001); left: NCEP/NCAR reanalysis 6h absolute SLP composites in hPa; date in YYYY-MM-DD; right: NCEP/NCAR reanalysis 6h wind field composites; arrows displaying direction and strength.*

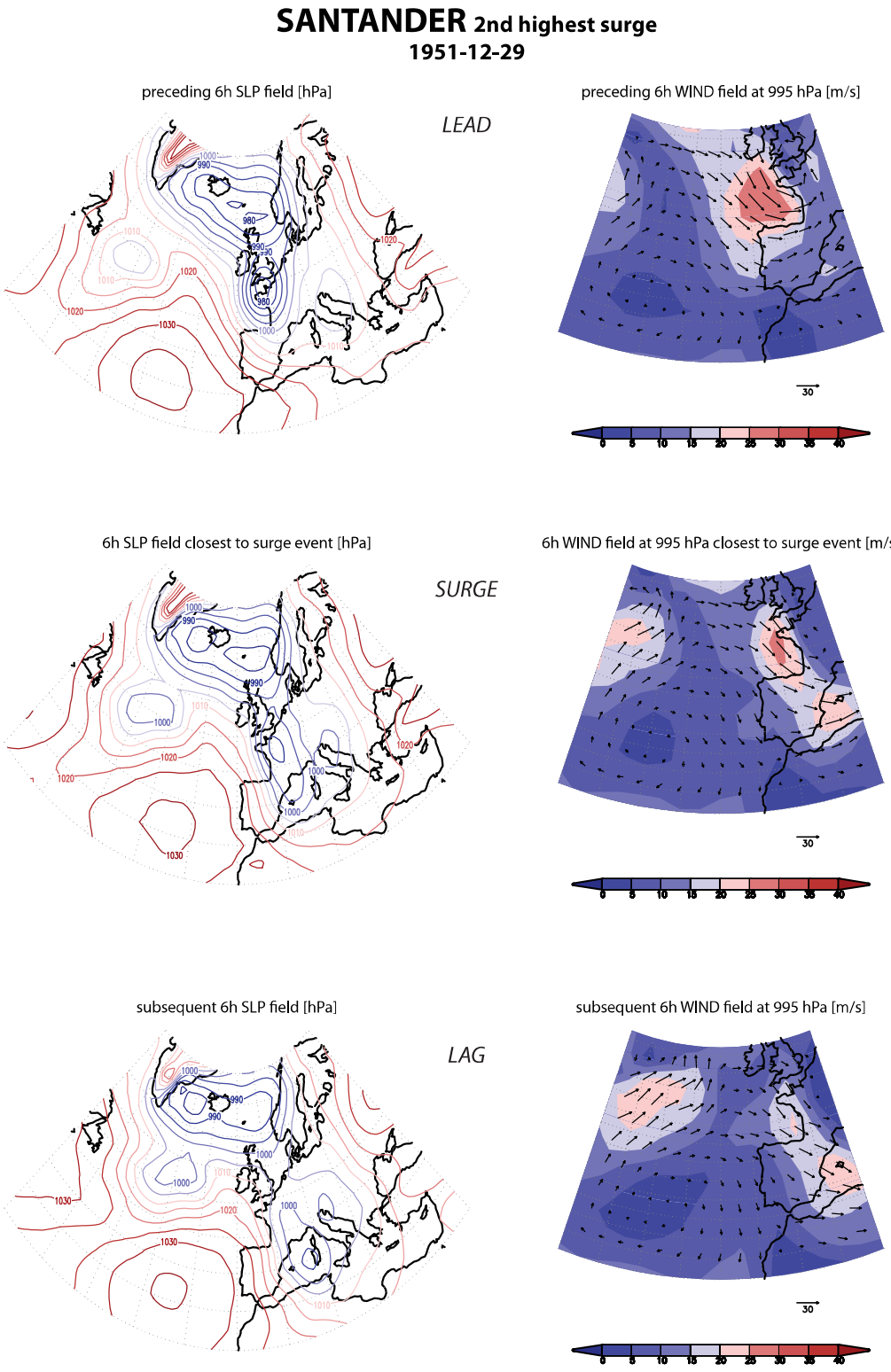

Figure A.7: *As Figure A.6 but for the second highest surge at Santander.*

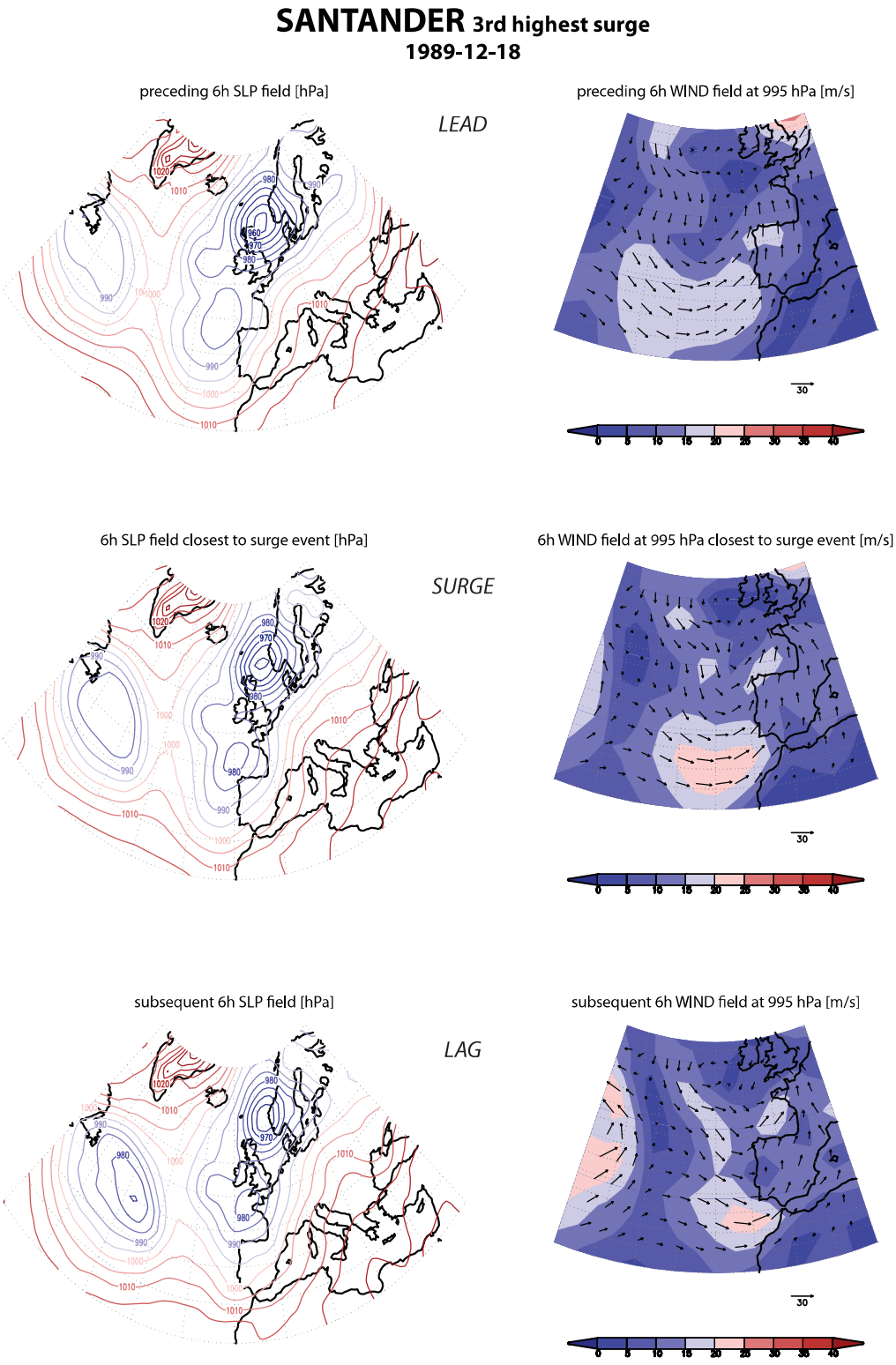

Figure A.8: *As Figure A.6 but for the third highest surge at Santander.*

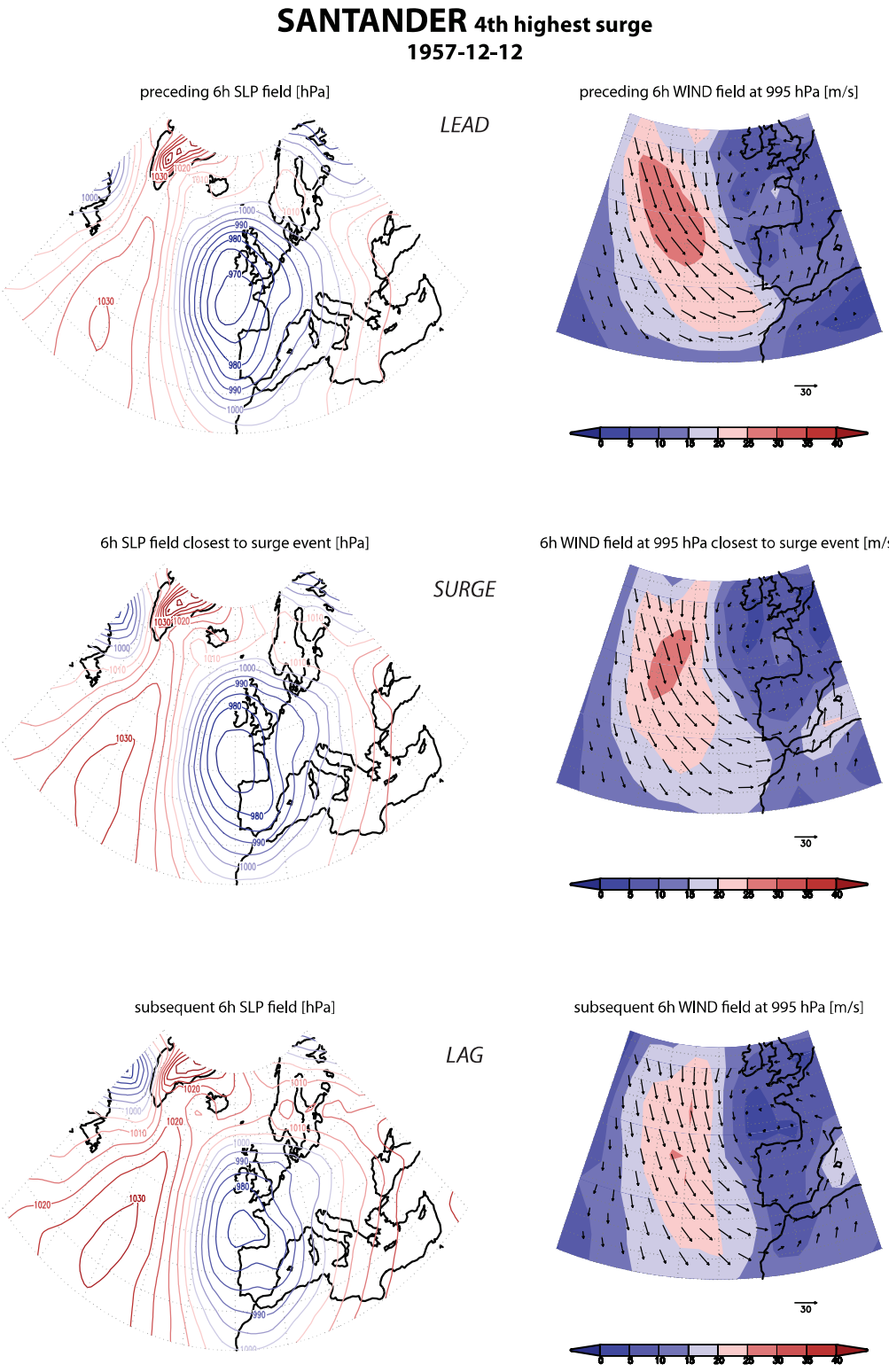

Figure A.9: *As Figure A.6 but for the fourth highest surge at Santander.*

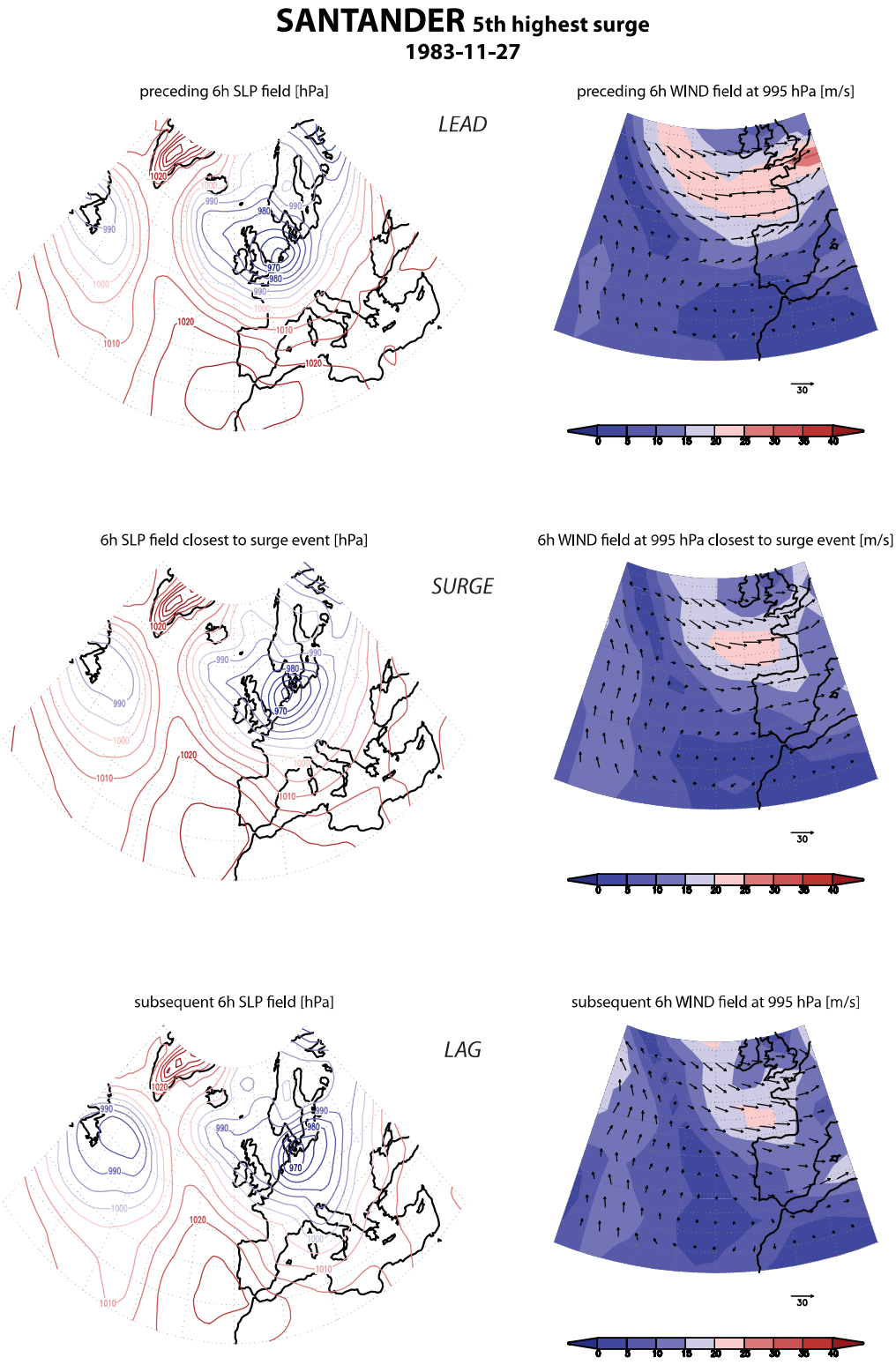

Figure A.10: *As Figure A.6 but for the fifth highest surge at Santander.*

VIGO

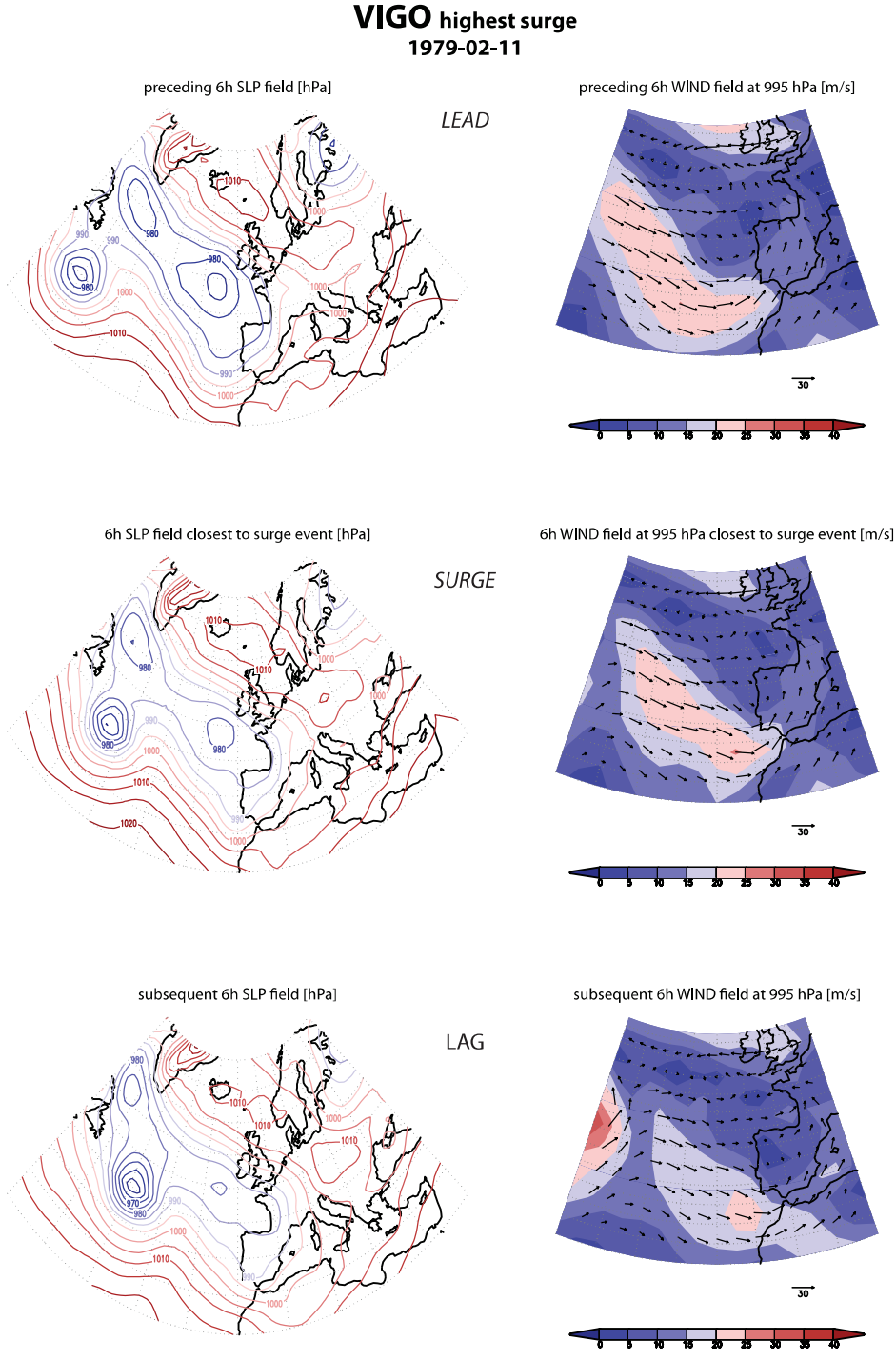

Figure A.11: *Large-scale 6h LEAD, SURGE and 6h LAG circulation patterns corresponding to the highest recorded surge at VIGO (1948-2001); left: NCEP/NCAR reanalysis 6h absolute SLP composites in hPa; date in YYYY-MM-DD; right: NCEP/NCAR reanalysis 6h wind field composites; arrows displaying direction and strength.*

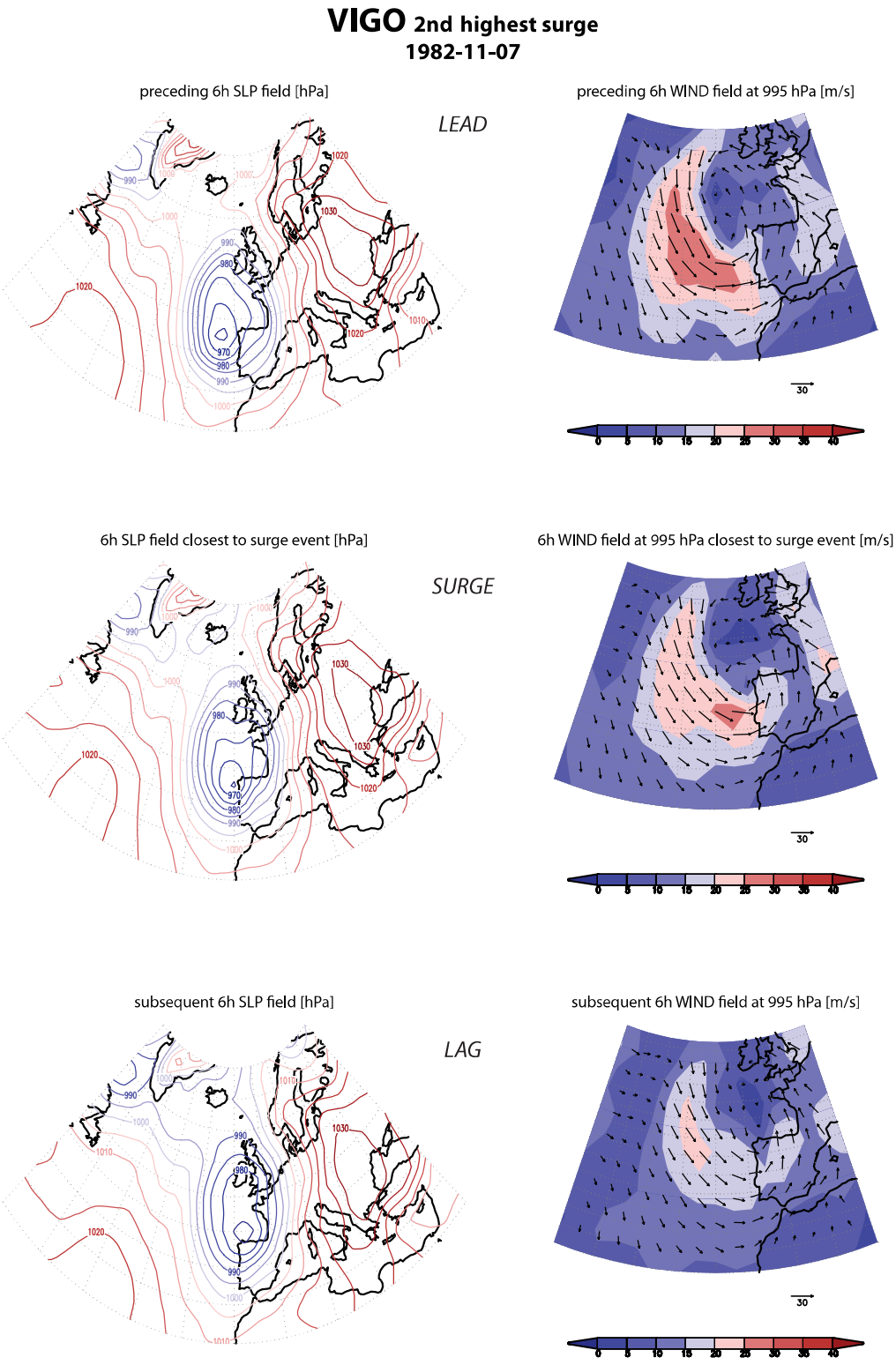

Figure A.12: *As Figure A.11 but for the second highest surge at Vigo.*

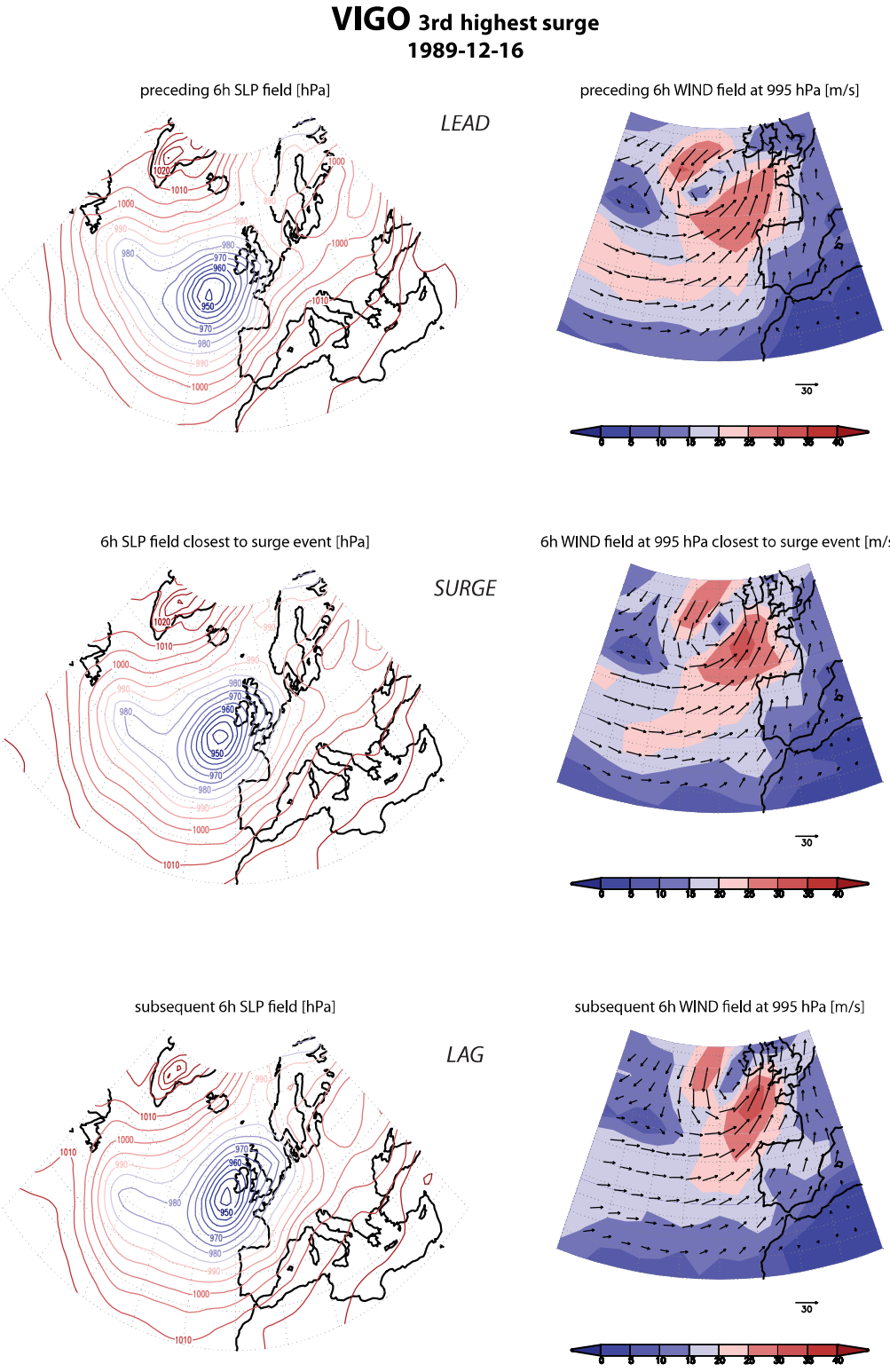

Figure A.13: *As Figure A.11 but for the third highest surge at Vigo.*

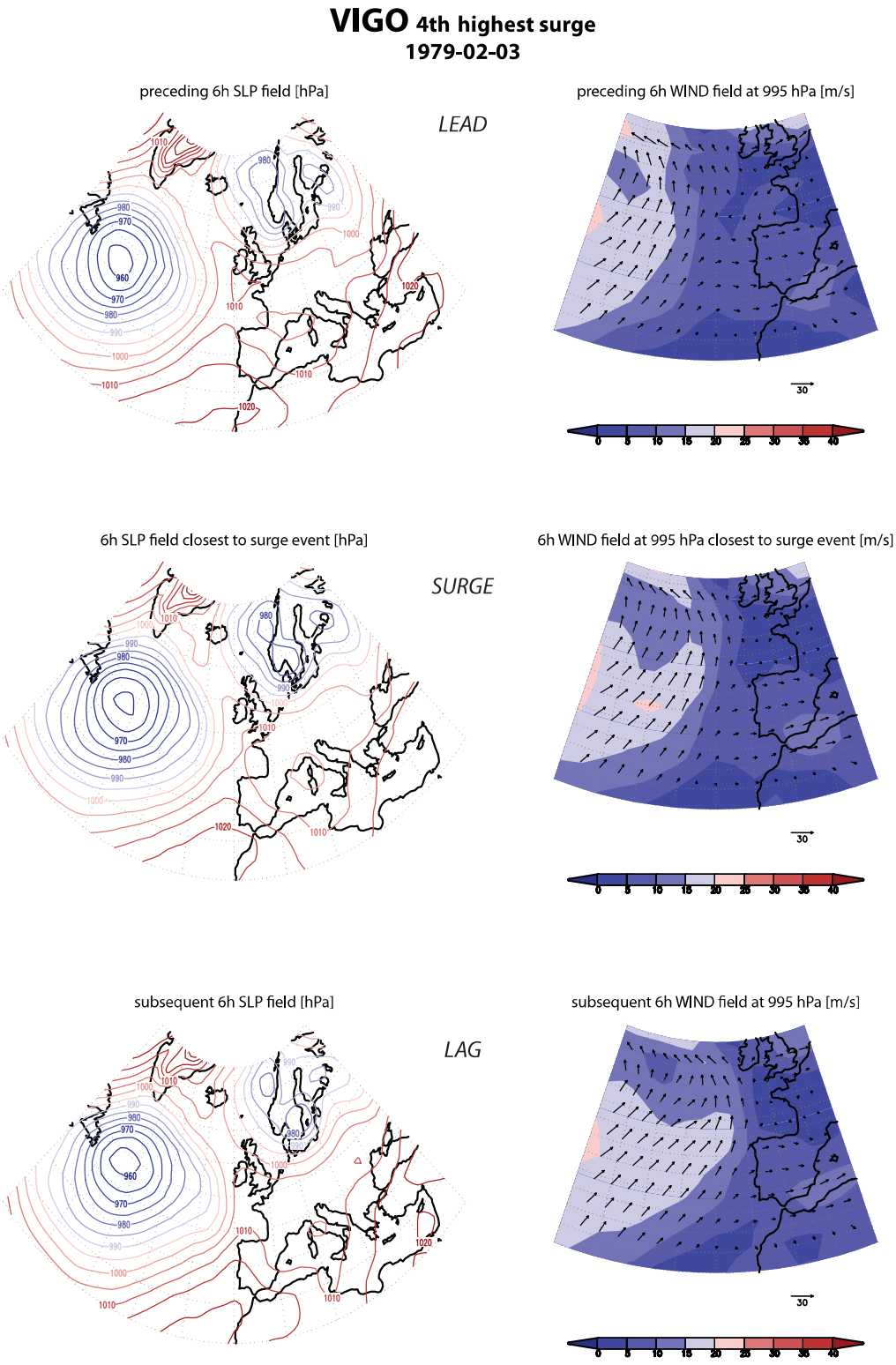

Figure A.14: *As Figure A.11 but for the fourth highest surge at Vigo.*

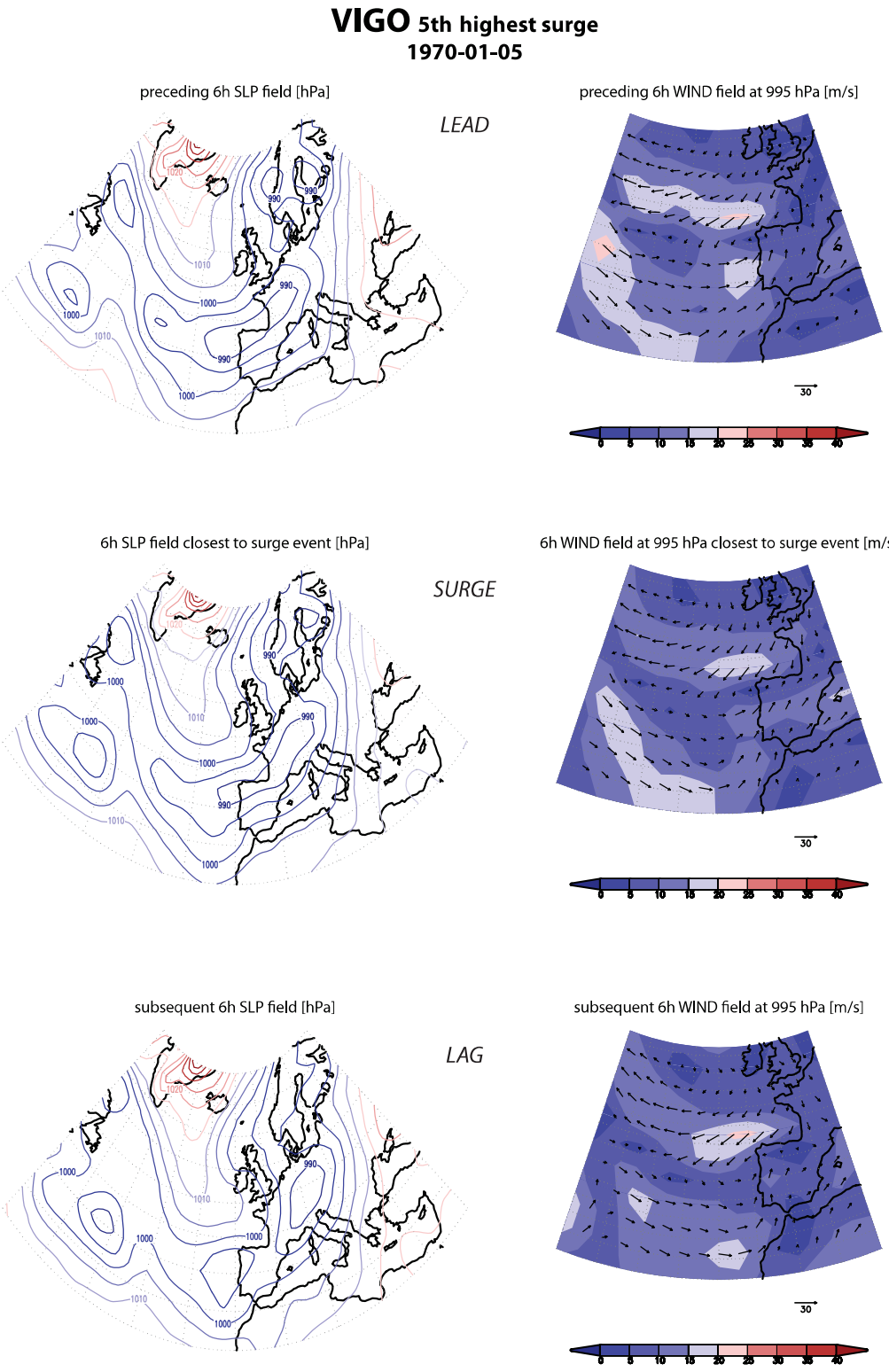

Figure A.15: *As Figure A.1 but for the fifth highest surge at Vigo.*

Appendix B

SANDRA clustering

Absolute SLP outputs

CORUNA

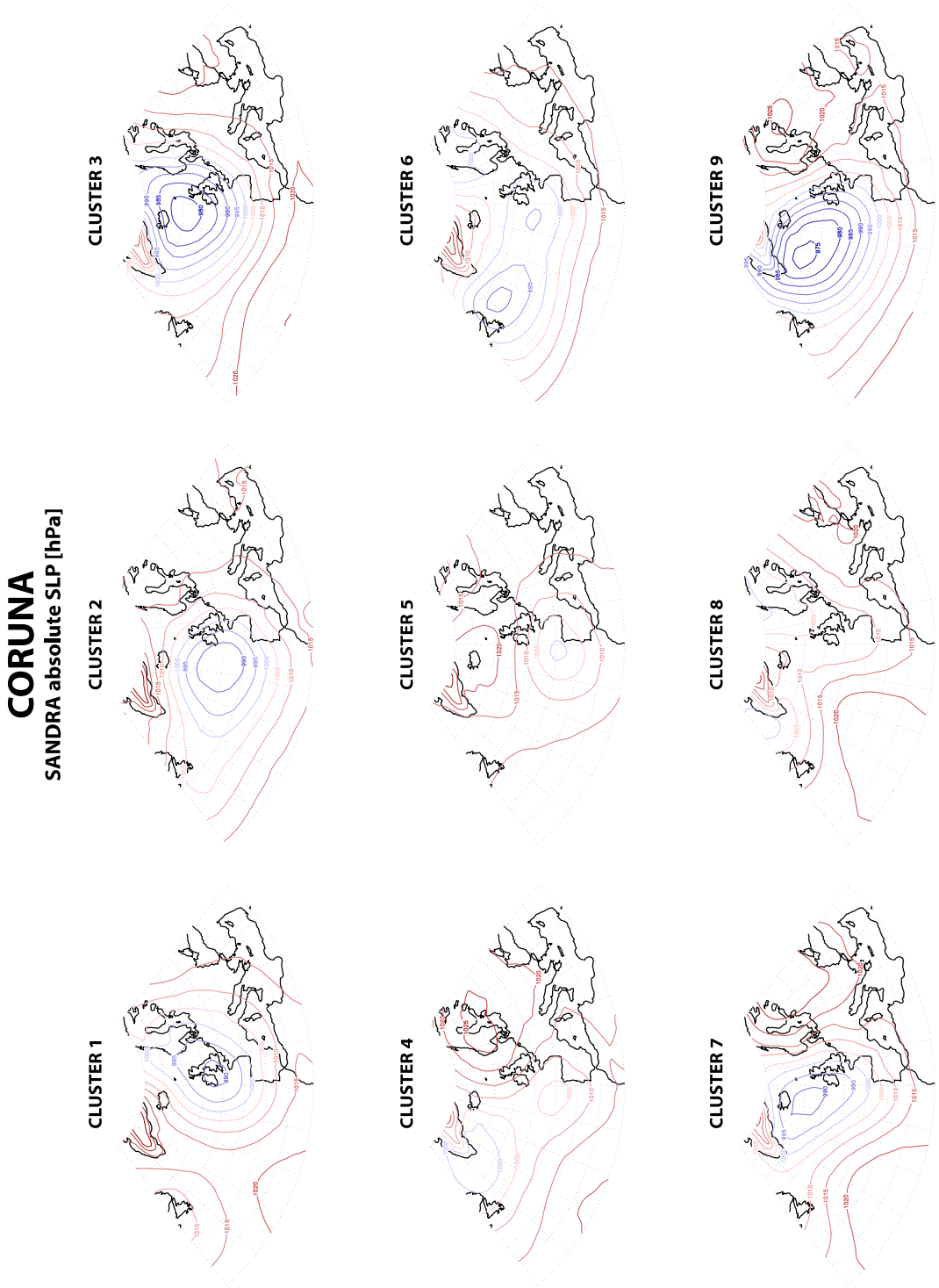

Figure B.1: *Results of the SANDRA cluster analysis for CORUNA; Clusters are displayed as absolute SLP composites (hPa); observation period 1948-2001.*

SANTANDER

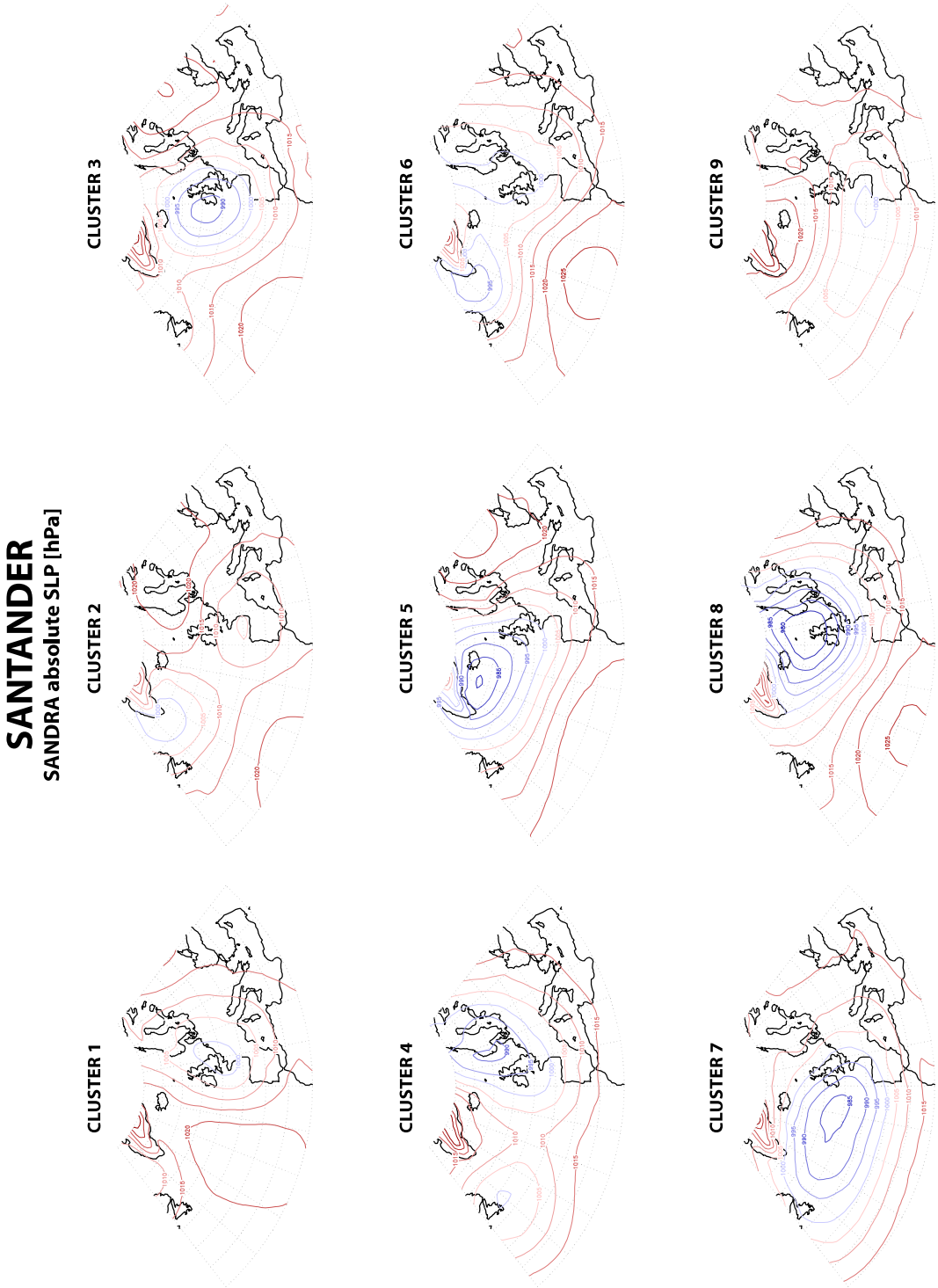

Figure B.2: *As Figure B.1 but for Santander.*

VIGO

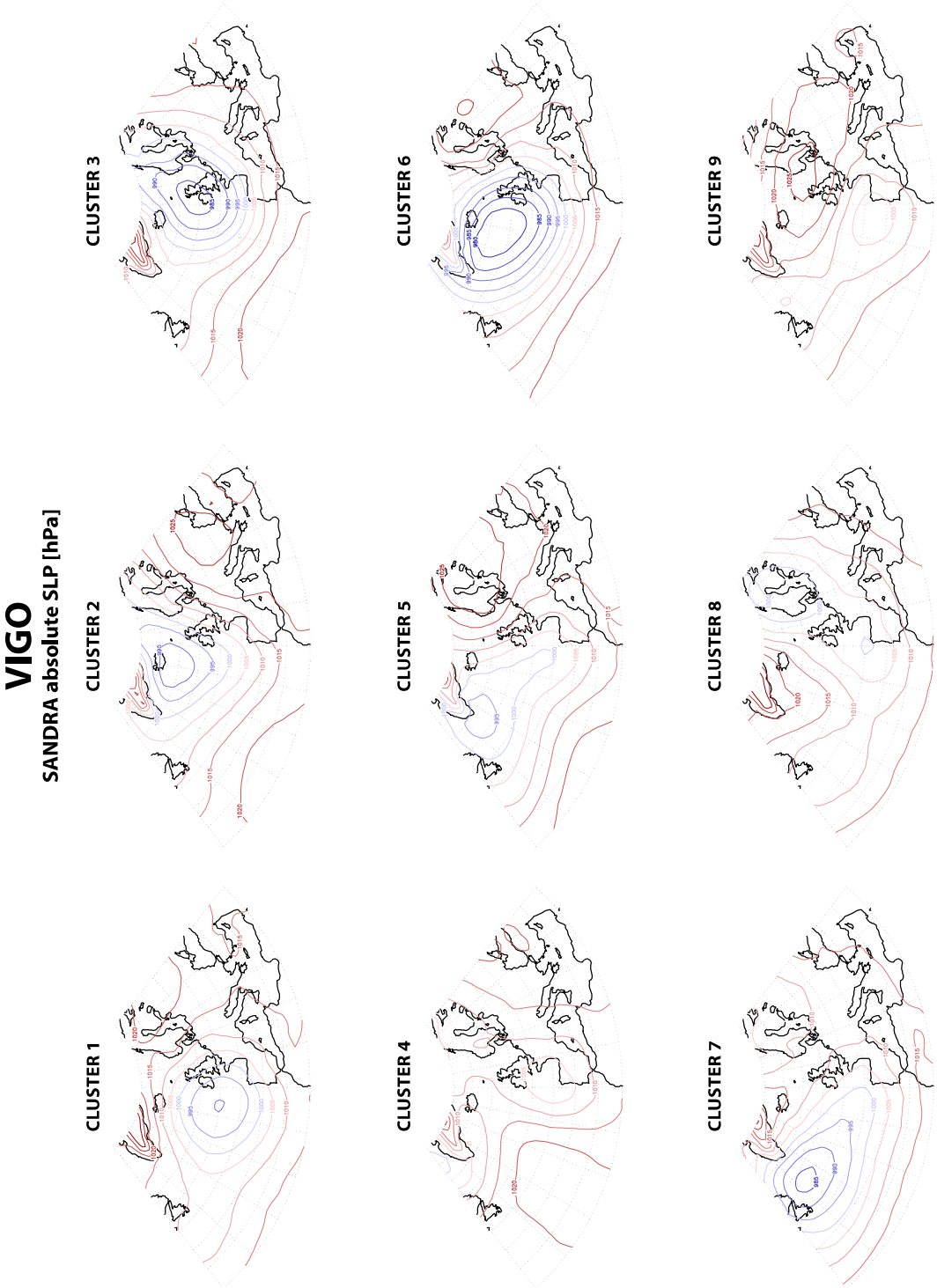

Figure B.3: *As Figure B.1 but for Vigo.*

Appendix C

ECHAM5-OM1

Simulated mean SLP

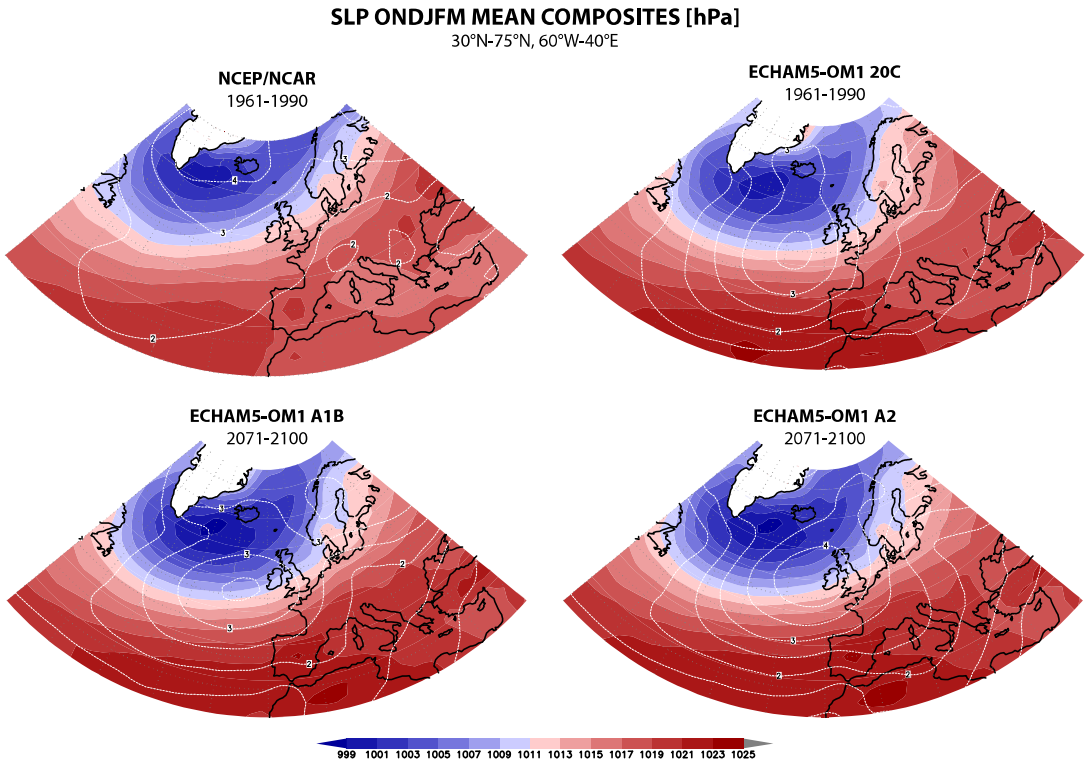

Figure C.1: *ONDJFM mean SLP [hPa] for NCEP/NCAR reanalysis (1961-1990) and ECHAM5-OM1 20C (1961-1990), A1B and A2 model outputs (2071-2100); standard deviation in dashes; values for Greenland are excluded due to mean land elevations >1500 m MSL.*

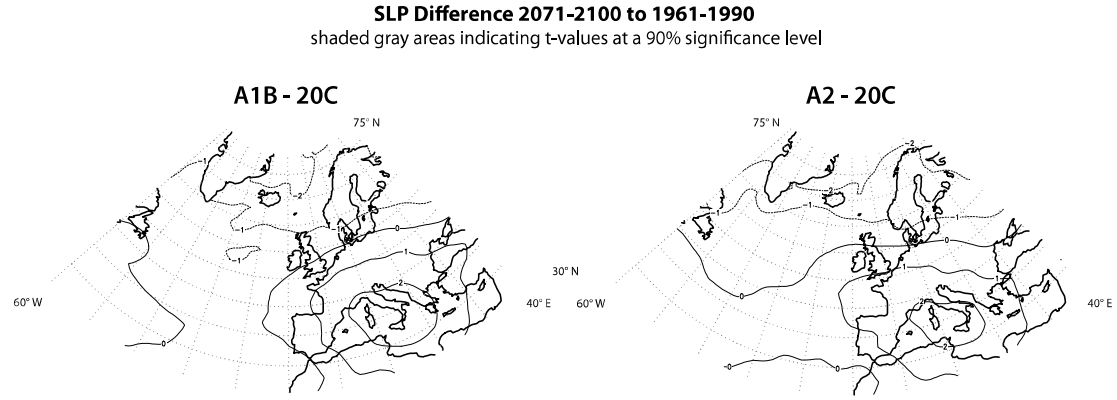

Figure C.2: *ECHAM5-OM1 SLP anomaly fields for SRES A1B and A2 forcing conditions; Scenario composites cover the period 2071-2100; The 20C control run is used as reference (1961-1990); shaded grey areas indicate t-values being significant at a 90% level; values for Greenland are excluded due to mean land elevations >1500 m MSL.*

Revised version

Minor corrections have been carried out which mainly improved the captions in the Appendix. There have been no modifications or changes regarding the applied datasets or results.

Berlin, *28.01.2010*